Université d'Ottawa · University of Ottawa

Université d'Ottawa · University of Ottawa

FACULTÉ DES ÉTUDES SUPÉRIEURES ET POSTDOCTORALES

FACULTY OF GRADUATE AND POSTDOCTORAL STUDIES

Amir Homayoun KAMKAR-PARSI

AUTEUR DE LA THÈSE - AUTHOR OF THESIS

M.A.Sc. (Electrical Engineering)

GRADE - DEGREE

Department of Electrical Engineering

FACULTÉ, ÉCOLE, DÉPARTEMENT - FACULTY, SCHOOL, DEPARTMENT

TITRE DE LA THÈSE - TITLE OF THE THESIS

ADSL-VDSL Interference Multigation for the Fiber-to-the-Cabinet Architecture using Adaptative Filtering and the Longitudinal Signal as a Reference

M. Bouchard

DIRECTEUR DE LA THÈSE - THESIS SUPERVISOR

T. Yeap

CO-DIRECTEUR DE LA THÈSE - THESIS CO-SUPERVISOR

EXAMINATEURS DE LA THÈSE - THESIS EXAMINERS

R. Goubran

E. Dubois

J.-M. De Koninck, Ph.D.

LE DOYEN DE LA FACULTÉ DES ÉTUDES SUPÉRIEURES ET POSTDOCTORALES

DEAN OF THE FACULTY OF GRADUATE AND POSTDOCTORAL STUDIES

ADSL-VDSL Interference Mitigation for the Fiber to the Cabinet Architecture using Adaptive Filtering and the Longitudinal Signal as a Reference

A. Homayoun Kamkar-Parsi, B. Eng.

Thesis submitted to the
Faculty of Graduate and Postdoctoral Studies
in partial fulfillment of the requirements for the degree of

Master of Applied Science

in Electrical Engineering

Ottawa-Carleton Institute for Electrical and Computer Engineering
School of Information Technology and Engineering

Faculty of Engineering
University of Ottawa

May 2004

Your file Votre référence
ISBN: 0-494-01507-1
Our file Notre référence
ISBN: 0-494-01507-1

UNIVERSITY OF OTTAWA
OTTAWA-CARLETON INSTITUTE FOR ELECTRICAL AND
COMPUTER ENGINEERING
SCHOOL OF INFORMATION TECHNOLOGY AND ENGINEERING

The undersigned hereby certify that they have read and recommend to the Faculty of Graduate Studies and Postdoctoral Studies for acceptance a thesis entitled "**ADSL-VDSL Interference Mitigation for the Fiber to the Cabinet Architecture using Adaptive Filtering and the Longitudinal Signal as a Reference**" by **A. Homayoun Kamkar-Parsi** in partial fulfillment of the requirements for the degree of **Master of Applied Science, Electrical Engineering**.

Dated: May 2004

Supervisor: _____
Dr. Martin Bouchard

Co-Supervisor: _____
Dr. Tet-Hin Yeap

Readers: _____
Dr. Eric Dubois

_____
Dr. Rafik A. Goubran

Abstract

With architectures such as fiber to the cabinet, the possible combination of shorter lines deployed from the cabinet with longer lines deployed from the Central Office in the same bundle can cause the far-end crosstalk from the transmitters located at the cabinet to severely degrade the performance of the long lines. External interference (including crosstalk) mostly couples to the twisted-pair line as a longitudinal signal, and then leaks to differential mode because of the lack of ideal line balance. This thesis offers a possible solution to mitigate crosstalk impairments worsened by the fiber to the cabinet architecture. This thesis uses the longitudinal signal as a reference to an adaptive wideband crosstalk canceller, aiming to decrease the crosstalk in the corrupted differential signal. Simulations show that the canceller can substantially reduce the crosstalk in the differential signal and evaluates three distinct adaptive algorithms for convergence speed and complexity.

Acknowledgments

I wish to acknowledge the School of Information Technology and Engineering (SITE) at the University of Ottawa for the motivating research environment, and excellent preparation of its graduates for leadership in the profession. I also had the opportunity to have completed my undergraduate work at this University.

I have had the pleasure and am grateful to my principal adviser, Professor Martin Bouchard, for his guidance. Throughout my graduate study, he has always been prompt and available in supporting whatever direction of research I decided to pursue, and offering me his effective insight whenever I needed it. He has been the person that I could always go to with ideas and have informative technical discussions.

I would also like to express my appreciation to my co-supervisor Professor Tet-Hin Yeap for his advice and encouragement. As well, thanks to my colleagues Gilles Bessens for the help with the simulation and Dave Fenton for sharing his background information and the useful tips.

Finally, I am grateful for the financial support of my graduate work, which was provided by The Natural Sciences and Engineering Research Council of Canada (NSERC) Postgraduate Scholarship and the University of Ottawa Excellence Postgraduate Scholarship.

Contents

List of Figures vii

List of Tables xii

List of Acronyms xiv

Chapter 1 Introduction 1

1.1 Thesis Motivation 1

1.2 Previous Work 2

1.3 Thesis Structure 4

1.4 Thesis Contributions 5

Chapter 2 Loop Plant DSL Network Architecture 7

2.1 Fiber to the Cabinet Architecture 8

2.2 ADSL 10

2.3 Considered Technologies Causing Crosstalk 14

2.3.1 ADSL Disturbers 15

2.3.2 VDSL Disturbers 15

Chapter 3 Quadrature Amplitude Modulation in Discrete Multitone 17

3.1 Single Carrier QAM Analysis 17

3.1.1 QAM Encoding and Modulation 18

3.1.2 QAM Demodulation, Decoding and Detection 19

3.1.3 Probability of Symbol Error 21

3.2 QAM Constellations Used in ADSL 22

3.3 QAM Constellation Energy 25

3.4 SNR Gap 26
3.5 Coding 29
3.5.1 Reed-Solomon Parameters 29
3.5.2 Reed-Solomon Coding Gain 31

Chapter 4 Discrete Multitone Modulation and Channel Equalization .33

4.1 Generalization of QAM to Several Subchannels 34
4.2 IDFT Modulator 36
4.3 Cyclic Prefix 40
4.4 DFT Demodulator 44
4.5 Channel Equalization 46
4.5.1 TEQ 46
4.5.2 FEQ 49

Chapter 5 Bitloading and Gain 52

5.1 Gain Scaling 52
5.2 Scrambler 57
5.3 Bitloading 59
5.3.1 SNR and Capacity 59
5.3.2 Bitloading Algorithm 61
5.3.3 Bitloading Gain Factor 64

Chapter 6 Twisted-Pair Transmission Line Modeling 66

6.1 Propagation Mode Introduction 66
6.2 Transmission Line Balance 70
6.3 Differential Mode Channel Model 72
6.3.1 Twisted-Pair Equivalent Circuit 72
6.3.2 Two-Port Model 74
6.3.3 *R*, *L*, *C*, *G* Parameters 77
6.3.4 Channel Transfer Function 80

6.4 Common Mode Channel Model 83
6.5 Velocity Difference between Differential and Common Mode Signals 85

Chapter 7 Crosstalk Model 90

7.1 Near-End Crosstalk 91
7.2 Far-End Crosstalk 92
7.3 DSL Architecture Considered 95
7.4 CO-RT Crosstalk Modeling 96
7.4.1 NEXT Time-Domain Signal in Differential Mode 96
7.4.2 NEXT Time-Domain Signal in Common Mode 98
7.4.3 FEXT Differential Mode Signal 100
7.4.4 FEXT Common Mode Signal 102
7.5 Resulting Design Model with only ADSL Disturbers 108
7.6 Resulting Design with ADSL and VDSL Lines in the Bundle 110

Chapter 8 Wideband Crosstalk Canceller 112

8.1 Convergence Level 113
8.2 Adaptive Noise Canceller Algorithm Comparisons 121
8.2.1 NLMS 125
8.2.2 Fast RLS Algorithm 128
8.2.3 Fast Affine Projection Algorithm 132

Chapter 9 Simulations 134

9.1 Complexity and Convergence Speed Comparisons 134
9.2 Crosstalk Canceller Performance 138
9.3 Simulation Environment 139
9.4 Results for Only ADSL Type Disturbers in the Remote Terminal 141
9.4.1 Remote Terminal at d_2 = 5kft 142
9.4.2 Remote Terminal at d_2 = 3kft 148
9.4.3 Remote Terminal at d_2 = 1kft 150

9.5 Results for Only VDSL Type Disturbers in the Remote Terminal 151
9.5.1 Remote Terminal at d_2 = 5kft 151
9.5.2 Remote Terminal at d_2 = 3kft 153
9.5.3 Remote Terminal at d_2 = 1kft 154
9.6 Results for Both ADSL and VDSL Disturbers in the Remote Terminal 155

Chapter 10 Conclusion 157

10.1 Primary Conclusion 157
10.2 Secondary Conclusions 157
10.3 Future Work 159

Appendix A: Results for d_2 = 3 kft, x=12 161

Appendix B: Results for d_2 = 1 kft, x=12 162

Appendix C: Results for d_2 = 3 kft, y=24 163

Appendix D: Results for d_2 = 1 kft, y=49 164

References 165

List of Figures

Figure 2-1: Example ADSL service delivery problem 7
Figure 2-2: FTTCab architecture 9
Figure 2-3: Upstream and Downstream FDD-ADSL PSD masks 12
Figure 2-4: DMT ADSL protocol stack 13
Figure 2-5: CO served customer receiving crosstalk interference from RT-served lines. 14
Figure 2-6: VDSL band allocation 15
Figure 2-7: Upstream and Downstream VDSL PSD mask 16
Figure 3-1: QAM transmitter system 18
Figure 3-2: Example of 16-QAM constellation 19
Figure 3-3: AWGN Channel 19
Figure 3-4: QAM demodulator, detector and decoder 20
Figure 3-5: Transmission and Reception of a QAM symbol over an AWGN channel 21
Figure 3-6: Constellation maps for b_i=2, b_i =3, b_i =4 and b_i =5 22
Figure 3-7: QAM cross constellation map for $b_i > 4$ and odd 23
Figure 3-8: 64-QAM square-constellation design 24
Figure 3-9: Resulting 64-QAM square-constellation corresponding to b_i = 6 bits 25
Figure 3-10: Q-function curve as a function of $20 \cdot \log(\frac{d_{\min}}{2\sigma})$ 27
Figure 4-1: DMT transmitter 34
Figure 4-2: DMT-QAM Encoder block 35
Figure 4-3: IDFT modulator 36
Figure 4-4: cyclic prefix added 40
Figure 4-5: DMT receiver 45
Figure 4-6: Magnitude frequency response of the linear convolution of $h(n)$ with $w_{TEQ}(n)$, with $\beta = 0$ 48
Figure 4-7: Example channel SNR 49

Figure 4-8: Example of a subchannel demodulator output before and after equalization with the corresponding complex coefficient. 50
Figure 4-9: FEQ 50
Figure 5-1: Gain Scaling 53
Figure 5-2: Simplified DMT modulation with initial PSD level output of – 40dbm/Hz.. 55
Figure 5-3: Signal PSD output from IDFT modulator with Cyclic Prefix added with PSD level set to – 40dBm/Hz 57
Figure 5-4: Scrambler for ADSL 58
Figure 5-5: Descrambler for ADSL 58
Figure 5-6: Bit allocation algorithm flow chart 62
Figure 5-7: SNR per subchannel ($SNR(i)$) 63
Figure 5-8: Bitloading allocation example for an FDD-ADSL transmission at 1.5Mb/s. 64
Figure 6-1: Simplified transmission system. 67
Figure 6-2: simplified circuit with crosstalk interference 68
Figure 6-3: Differential and common mode signal extractions 69
Figure 6-4: Magnitude of the balance function $B(f)$ 71
Figure 6-5: Equivalent twisted-pair transmission line 72
Figure 6-6: Two-Port Model 74
Figure 6-7: R vs frequency with 26-gauge wire 77
Figure 6-8: L vs frequency with a 26-gauge wire 79
Figure 6-9: Magnitude of the characteristic impedance Z_0 for 26 and 24 gauges 80
Figure 6-10: Insertion Losses for 26-gauge 5kft (left) and 24-gauge 15kft (right) differential channels 81
Figure 6-11: Differential Channel Impulse Responses for 26-gauge 5kft (left) and for 24-gauge 15kft (right) 82
Figure 6-12: Magnitude of the common mode characteristic impedance Z_{0_comm} for 26 and 24 gauges 85
Figure 6-13: Common mode Impulse response for a 5kft 26-gauge transmission line 87

Figure 6-14: 5kft 26-gauge Differential mode and Common mode channel impulse response 88
Figure 6-15: 1km 26-gauge Differential mode and Common mode channel Insertion loss 89
Figure 7-1: Illustration of NEXT 91
Figure 7-2: Illustration of attenuated NEXT 91
Figure 7-3: Illustration of FEXT 93
Figure 7-4: Illustration of amplified FEXT due to shorter distance 94
Figure 7-5: DSL architecture with a Central Office and a Remote Terminal (referred to as "CO-RT architecture"), with a shared bundle consisting of several ADSL and/or VDSL lines 95
Figure 7-6: NEXT differential time-domain model 97
Figure 7-7: NEXT common mode time-domain model 99
Figure 7-8: FEXT differential time-domain model 100
Figure 7-9: Channel transfer function definitions for the CO-RT architecture 101
Figure 7-10: FEXT common mode time-domain model 102
Figure 7-11: Resulting common mode signal in CO-served line at RX due to RT-served line causing crosstalk interference 104
Figure 7-12: Leakage from the FEXT common mode signal to the differential mode of the CO-served line 105
Figure 7-13: FEXT common mode signal and respective FEXT Differential signal traveling a distance of d_2 towards the receiver at different velocities 105
Figure 7-14: Differential and Common mode channel impulse responses and respective phase responses 107
Figure 7-15: Corresponding impulse response of $\phi_{Diff\ To\ Comm}(f)$ 108
Figure 7-16: Overall system representing the CO-RT architecture with only one type of disturber i.e. ADSL present in the bundle. 109
Figure 7-17: Overall system representing the CO-RT architecture with mixed technology disturbers i.e. ADSL and VDSL present in the bundle. 111

Figure 8-1: Crosstalk canceller implementation in the CO-RT system 112
Figure 8-2: Interference canceling system 114
Figure 8-3: Having access to different reference signals x_1 and x_2 separately for each source d_1 and d_2 respectively 116
Figure 8-4: Impulse response of $H_{BP}(n)$ 117
Figure 8-5: Impulse response of $H_{LP}(n)$ 118
Figure 8-6: Convergence plot 118
Figure 8-7: Adaptive noise cancellation filter obtained, $w(n)$ 119
Figure 8-8: x_1 (NEXT) and x_2 (FEXT) common mode PSDs 120
Figure 8-9: Frequency dependent achievable convergence 121
Figure 8-10: General structure of the adaptive crosstalk canceller 122
Figure 9-1: Selected scenario to evaluate the convergence speed 135
Figure 9-2: Simulated scenarios 140
Figure 9-3: General structure of the crosstalk canceller 141
Figure 9-4: SNR per tone (left) and corresponding bitloading allocation results for each tone (right) 142
Figure 9-5: Differential crosstalk PSDs (left) and Common mode crosstalk PSDs (right) 143
Figure 9-6: Crosstalk canceller convergence vs frequency shown for 15 dB convergence over the frequency band of interest and the maximum convergence achievable curve. 144
Figure 9-7: QAM data samples received for the tone number 95 (representing a constellation size of M=16) with the crosstalk canceller OFF (left) and the improved QAM data samples with the crosstalk canceller ON at 15 dB of convergence (right) 146
Figure 9-8: Adaptive crosstalk canceller impulse response obtained with 15 dB of convergence 146

List of Tables

Table 5-1: Gain scaling for 2 to 8-bit constellations.....54
Table 5-2: Gain scaling for 9 to15-bit constellations.....54
Table 8-1: NLMS Algorithm.....127
Table 8-2: Fast RLS algorithm.....131
Table 8-3: FAP algorithm.....133
Table 9-1: Order of complexity of the three considered adaptive algorithms for L=90 filter taps.....135
Table 9-2: Convergence speed comparisons for L=90 filter taps and 40 causality delays.....136
Table 9-3: Power received for NEXT/FEXT.....137
Table 9-4: Power levels at CO-served customer receiver for 49 FDD-ADSL disturbers with d_2 = 5kft.....145
Table 9-5: Results with d_2 = 5 kft and the considered crosstalk is Self-NEXT and Self-FEXT from x= 49 FDD-ADSL at the Remote Terminal DSLAM.....145
Table 9-6: Results with d_2 = 5 kft and the considered crosstalk is NEXT and FEXT from 12 FDD-ADSL at the Remote Terminal DSLAM.....147
Table 9-7: Power levels at CO-served customer receiver for 12 FDD-ADSL disturbers with d_2 = 5kft.....147
Table 9-8: Results with d_2 = 3 kft and the considered crosstalk is Self-NEXT and Self-FEXT from x= 49 FDD-ADSL at the Remote Terminal DSLAM.....148
Table 9-9: Power levels at CO-served customer receiver for 49 FDD-ADSL disturbers with d_2 = 3kft.....148
Table 9-10: Results with d_2 = 1 kft and the considered crosstalk is Self-NEXT and Self-FEXT from x=49 FDD-ADSL at the Remote Terminal DSLAM.....150
Table 9-11: Power levels at CO-served customer receiver for 49 FDD-ADSL disturbers with d_2 = 1kft.....150

Table 9-12: Results with d_2 = 5 kft and the considered crosstalk is NEXT and FEXT from y=49 VDSL at the Remote Terminal DSLAM 152

Table 9-13: Power levels at CO-served customer receiver for 49 VDSL disturbers with d_2 = 5kft 152

Table 9-14: Results with d_2 = 3 kft and the considered crosstalk is NEXT and FEXT from y=49 VDSL at the Remote Terminal DSLAM 153

Table 9-15: Power levels at CO-served customer receiver for 49 VDSL disturbers with d_2 = 3kft 153

Table 9-16: Results with d_2 = 1 kft and the considered crosstalk is NEXT and FEXT from y=12 VDSL at the Remote Terminal DSLAM 154

Table 9-17: Power levels at CO-served customer receiver for 12 VDSL disturbers with d_2 = 1kft 154

Table 9-18: Results with d_2 = 1 kft and the considered crosstalk is NEXT and FEXT from x=24 VDSL and y=24 ADSL at the Remote Terminal DSLAM 155

Table 9-19: Power levels at CO-served customer receiver for 24 VDSL and 24 ADSL disturbers with d_2 = 1kft..... 156

List of Acronyms

ADSL	Asymmetric Digital Subscriber Line
ANSI	American National Standards Institute
APA	Affine Projection
AWGN	Additive White Gaussian Noise
BER	Bit Error Rate
CAP	Carrierless Amplitude Modulation / phase modulation
CO	Central Office
CO-RT	Central Office-Remote Terminal
CPE	Customer Premise Equipment
DFT	Discrete Fourier Transform
DMT	Discrete Multitone
DSL	Digital Subscriber Line
DSLAM	Digital Subscriber Line Access Multiplexer
DSM	Dynamic Spectrum Management
FAP	Fast Affine Projection
FDD	Frequency-Division Duplexing
FEC	Forward Error Correction
FEQ	Frequency-Domain Equalizer
FEXT	Far-End Crosstalk
FFT	Fast Fourier Transform
FIR	Finite Impulse Response
f_s	Sampling Frequency
FTTCab	Fiber To The Cabinet
FTTEx	Fiber To The Exchange
IDFT	Inverse Discrete Fourier Transform
IFFT	Inverse Fast Fourier Transform
ISI	Inter-Symbol Interference

ISDN	Integrated Services Digital Network
ITU	International Telecommunications Union
LMS	Least-Mean-Square
MSE	Mean-Squared Error
NEXT	Near-End Crosstalk
NLMS	Normalized Least Mean Square
POTS	Plain Old Telephone Service
PSD	Power Spectral Density
QAM	Quadrature Amplitude Modulation
RFI	Radio-Frequency Interference
RLS	Recursive Least Squares
RT	Remote Terminal
RX	Receiver
RS FEC	Reed Solomon Forward Error Correction
TX	Transmitter
TEQ	Time-Domain Equalizer
SNR	Signal-to-Noise Ratio
SSM	Static Spectrum Management
UTP	Unshielded Twisted Pair
VDSL	Very-High-Speed Digital Subscriber Line

Chapter 1

Introduction

1.1 Thesis Motivation

A major impairment in Digital Subscriber Line (DSL) technology is crosstalk interference. With architectures such as Fiber to the Cabinet (FTTCab), the lines deployed from the central office can share the same bundle as the shorter lines deployed from a remote terminal located near the customer premises. Far-End Crosstalk (FEXT) originating from the remote terminal transmitters becomes the major performance-constraining factor as the transmission lines from the remote terminal become shorter. This is due to the fact that when signal sources are originating at different physical locations such as a Central Office versus a Cabinet (also referred to as a Remote Terminal), the transmitted signals enter the final shared bundle at significantly different levels. The useful signal of the long line is much more attenuated due to a longer propagation distance to reach the customer. Therefore, the resulting higher level far-end crosstalk caused by the shorter lines can severely interfere with the attenuated downstream signal at the receiver of the longer line, implying a significant performance degradation.

This situation will be analyzed with the deployment of ADSL or VDSL services from a remote terminal and their detrimental effect on the long line deployed from the central office carrying ADSL that shares the same final distribution bundle. Due to the nature of twisted pairs, external interferences (including crosstalk) mostly couple to the twisted-pair line as a longitudinal signal, and then leak to differential mode because of the lack of

ideal line balance. Throughout the course of this thesis, the longitudinal signal will be also referred to as the "common mode" signal.

This thesis offers a possible solution to mitigate crosstalk impairments worsened by the FTTCab architecture. This thesis uses the common mode signal as a reference to an adaptive wideband crosstalk canceller. The output of the canceller should produce a signal similar to the crosstalk signal. The output signal is subtracted from the received signal to reduce the actual crosstalk that is originating from the lines deployed from the remote terminal, corrupting the downstream differential signal of the line deployed from the central office. Simulations will be performed to evaluate the performance of the canceller, to assess if it can substantially reduce the crosstalk in the differential signal. The adaptive filtering performed by the crosstalk canceller will be implemented using different adaptive filtering algorithms including the normalized least-mean-squares (NLMS) algorithm, a fast implementation of the recursive-least-squares algorithm (Fast-RLS), and the fast affine projection algorithm (FAP). The three algorithms will be compared in terms of complexity and convergence speed.

1.2 Previous Work

Current DSL technologies, under the Static Spectrum Management (SSM) rule described by the American National Standard Institute (ANSI) [SML01], are designed under the assumption of worst case crosstalk scenarios leading to overly conservative DSL deployments. DSL lines from Central Offices or Remote Terminals transmit signals using only a fixed Power Spectral Density mask imposed by SSM. Enforcing the maximum power level imposed by the mask on all the DSL lines limits the performance of all future lines or new generation DSLs due to severe estimated crosstalk levels. Future DSL deployments, under SSM rules, become excessively restrictive in terms of coverage and data rate.

To compensate for the SSM overly restrictive deployments, Dynamic Spectrum Management (DSM) [SON02] specifies that DSL modems should not transmit more power than necessary to achieve their target data rates and should not transmit more bandwidth than necessary for communication. DSM can be categorized into two modes: autonomous or collaborative. Collaborative mode implies the presence of a central control unit coordinating all the lines.

Autonomous DSM [SON02] [YU01] allows each modem to dynamically optimize its transmitted power allocation (iterative water-filling), depending on the transmission line (channel) and the crosstalk level on the line. Minimizing the transmitted power on each line will allow a reduction of the crosstalk level emitted. However, the performance is bounded since the crosstalk level, although minimized, is still a remaining factor and therefore presents a limitation.

Collaborative DSM is much more complex as it requires knowledge of many of the channel parameters of each line, and where each modem's transmission parameters are coordinated by a central processing unit. From [SON02], the autonomous DSM will give a global performance essentially equivalent to the use of a complex central unit.
However, the knowledge of each line's transmission characteristics, including cross-coupling functions, allows a crosstalk cancellation for each line, also called Vectored Discrete Multitone (Vectored DMT) [GIN02]. Vectored DMT uses a Multi-Input Multi-Output (MIMO) interference identification technique [CIO01] to perform crosstalk cancellation.

This prior technique is very interesting, but requires a major change in current DSL topologies to incorporate a global central processing unit and each modem should return extensive information to the processing unit.

Another interesting technique using an electronic device aimed at cancellation of Radio Frequency Interference (RFI) is presented in [COM98]. The device is implemented to

nullify any common mode signal but permits the differential signal to propagate. The reasoning behind this technique is that RFI couples to the twisted pair line initially in common mode and then leaks to the differential mode, corrupting the useful differential signal. The drawback of using this technique is that it requires the knowledge of the exact locations of the common mode leakage along the line and it requires personnel to be deployed.

Previous work has been done using the common mode signal for RFI cancellation. The cancellation has been done by several narrowband filters[YEA], each canceling a single narrow band radio interferer. The simulations were performed using a CAP modulation technique for VDSL [YEA03] [LEF00].

1.3 Thesis Structure

Chapter 2 will present the loop plant DSL network architecture that will be considered in this thesis and introduces the considered impairments associated with this architecture.

Chapters 3, 4 and 5 will describe the Discrete Multitione (DMT) modulation in ADSL. Chapter 3 will detail QAM for DMT and the Reed-Solomon coding used in the simulation. Chapter 4 expands the QAM technique to several parallel QAM encoders for equally spaced narrowband subchannels and discusses the equalization of the transmission channel. Chapter 5 will conclude the DMT discussion by explaining the algorithm that decides the number of bits to be assigned to each subchannel (Bitloading algorithm) and also how the power of each subchannel is adjusted.

Chapter 6 details the model for the differential mode propagation using two-port theory, and follows by elaborating a common-mode model derived from the differential mode model.

Chapter 7 presents the modeling of crosstalk signals in differential and common modes as well as the approach taken to model them for the considered DSL architecture.

Chapter 8 describes the adaptive wideband crosstalk canceller, discusses the measure to evaluate the performance of the canceller, and briefly introduces and compares three adaptive algorithms.

Chapter 9 evaluates the performance of the crosstalk canceller under different conditions using simulations of the considered architecture.

Chapter 10 provides the general conclusions from the previous chapter and discusses any possible future work.

1.4 Thesis Contributions

The original research work is located mainly at the end of the thesis. The main contributions are:

- in Chapter 5, the bitloading algorithm developed from an adapted version of a known algorithm for the simulation;
- the mathematical model of the gain scaling applied to each tone for power adjustment;
- in Chapter 7, a novel model of the crosstalk in differential and common modes created for the FTTCab architecture, more specifically, the generation of NEXT and FEXT time domain signals in common mode and the transfer to differential mode;
- in Chapter 8, the integration of the crosstalk canceller as an attempt to solve the specific problem caused by the FTTCab architecture;

- in Chapter 9, the convergence speed of each algorithm evaluated for the FTTCab architecture;
- and also the evaluation of the canceller's ability to reduce the effect of the crosstalk interference;

Chapter 2

Loop Plant DSL Network Architecture

The following chapter will present the loop plant DSL overlay network architecture that will be considered in this thesis and introduces the considered impairments associated with a particular architecture. The first section will cover the Fiber to the Cabinet (FTTCab) architecture, including the deployment of DSL services from a cabinet also referred to as a Remote Terminal. The second section will cover the DSL technologies considered in this thesis that are deployed from the cabinet.

DSL technology transforms an ordinary telephone twisted pair line into a broadband communications link. The loop plant refers to the twisted-pair infrastructure connecting, for example, customers to the telephone company's central office (CO) network.

The most easily recognized deployment for ADSL services is from the Central Office and can be seen in the following example, where Customers C_1 and C_2 have DSL services, and Customer C_3 is located at a distance that precludes DSL service. This example is represented in Figure 2-1:

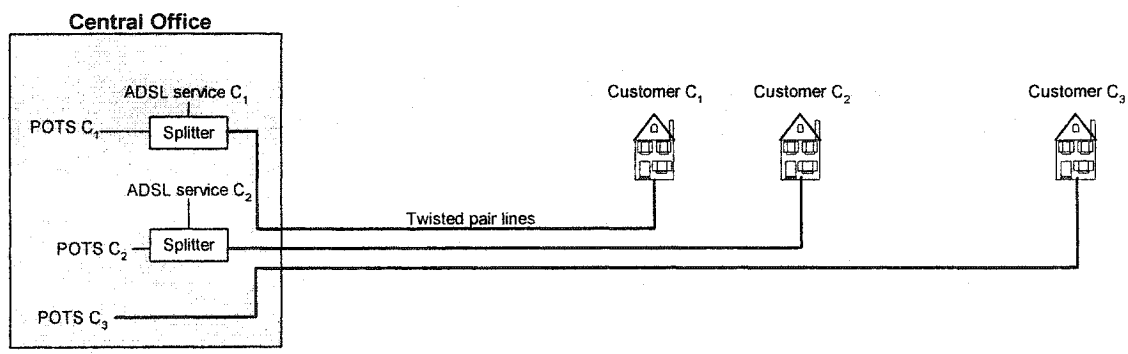

Figure 2-1: Example ADSL service delivery problem

This situation occurs most often in rural areas where customer's premises are sparsely located and therefore the loop length differences between customers can be substantial. When a significant number of customers are located at a distance precluding the delivery of data services, the construction of a Remote Terminal (i.e. Cabinet) along the bundle, containing ADSL line cards, might be warranted. To minimize the cost of the transitional infrastructure, the POTS delivery is sometimes kept at the CO. Other reasons could require the installation of a cabinet in the field, like the development of new housing too far to be serviced from the CO. The POTS for these new houses would most likely be serviced from the cabinet, and the existing customers would still be serviced from the CO, but going through a cabinet, which is covered in the next section.

2.1 Fiber to the Cabinet Architecture

A Cabinet (remote terminal) enables an easy access point to the loop plant in the field, offering the possibility to place equipment inside it that would have normally been at the Central Office. To resolve the issue stated above to reach outlying customers, the Fiber to the Cabinet (FTTCab) architecture was devised. The device housing the DSL line card modems (for Customer C_3 in the example of Figure 2-2) is connected to a device called a DSLAM (Digital Subscriber Line Access Multiplexer) also located in the cabinet. The DSLAM is a device, which takes a number of DSL subscriber lines and concentrates these to a single ATM line, i.e. a fiber optical line that connects to the Central Office equipment. The DSLAM can drive several ADSL line cards, including VDSL line cards. The deployment of DSL technologies from the Cabinet allows the delivery of higher bit rates due to shorter loops, implying lower signal attenuation. Thus, this is another driving force of a FTTCab architecture.

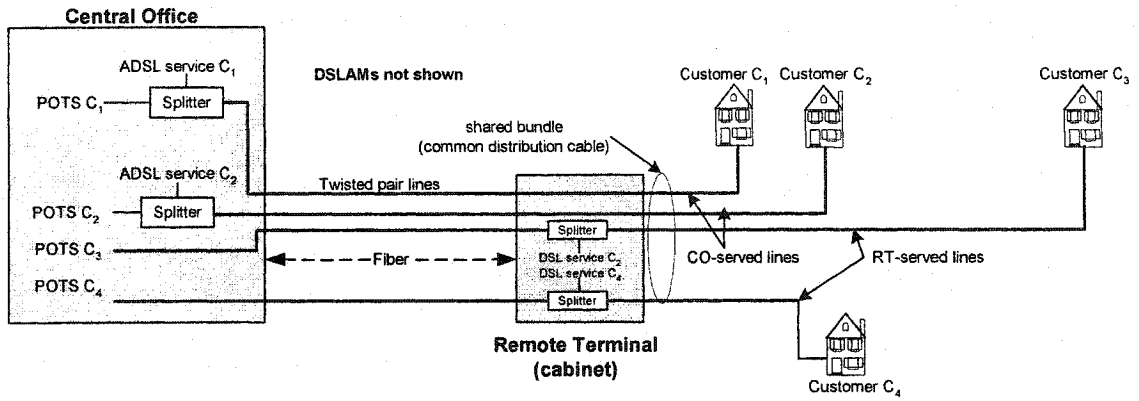

Figure 2-2: FTTCab architecture

As mentioned previously, the addition of DSL services from a Remote Terminal does not preclude DSL services delivery from the Central Office. As space is often limited in the Remote Terminal, DSL service delivery from the remote terminal is often reserved to customers requiring it, either due to distance limitations (i.e. out of reach), or because the customer demands a higher bit rate not available if the DSL service is deployed from the Central Office as demonstrated with customer C_4 in Figure 2-2.

However, deploying DSL services from a remote terminal and still having services from the Central Office present challenges when it comes to interference, that is when both the twisted pair lines deployed from the Central Office and the twisted pair lines deployed from the Remote Terminal are sharing the same bundle (i.e. common distribution cable). The signals transmitted from the Central Office to the CO-based customers will experience stronger attenuation due to longer loops. The signals originating from the transmitters located in the remote terminal radiate onto the CO-served lines in proximity causing some interference since all the twisted pair lines are sharing the same bundle. This interference, also called crosstalk, presents serious problems to the receivers (customers) that have their DSL service from the Central Office since the radiated interference is relatively strong (i.e. not negligible) in comparison to their weakened received signal, thus resulting in possibly serious performance degradation. The exact manner in which the interference occurs when Central Office based DSLs and Remote

Terminal based DSLs are co-existing in the same bundle will be covered in greater detail in Chapter 8.

Several DSL literatures [RIC03] [CRT02] [SON02] [JAC99], recognize that DSL systems deployed from both a Central Office and a Remote Terminal in a common distribution cable can increase the likelihood of crosstalk interference. The deployment issues faced by carriers today are for instance ADSL services from Remote Terminals and their detrimental effect on CO-served ADSL services sharing the same bundle and also the same issue is present when VDSL services are deployed from Remote Terminals.

2.2 ADSL

From Figure 2-2, the CO-served lines (i.e. the long lines deployed from the Central Office to the customers) are serviced with Asymmetric Digital Subscriber Line (ADSL) technology. The data-rate of ADSL strongly depends on the transmission line characteristics connecting the end-user to the central office such as the length, the noise level including crosstalk and background noise and impulse noise etc. Typically, the upstream data flow is up to 640 kb/s while the downstream data flow is between 1.5 and 8 Mb/s for shorter loops.

The standard [ITU99] specifies that the asymmetrical full duplex transmission can be done using frequency division duplexing or by frequency overlap with echo canceling.
In this thesis, the FDD-ADSL (Frequency Division Duplexing ADSL) technology has been covered in the presence of disturbers from the Remote Terminal i.e. the lines deployed from the Remote Terminal carrying either FDD-ADSL or VDSL services.
The upstream signal occupies a frequency range from 25kHz to 138kHz and the downstream signal is from 138kHz to 1.104MHz. To limit the interference with other services, the PSD Mask (Power Spectral Density) defines the absolute upper bound

power for spectrum management compliance. The upstream and downstream PSD masks are defined by equation 2.1. These are taken from "Test procedures for digital subscriber line (DSL) transceivers" [ITU02] and plotted in Figure 2-3 for a frequency range from 0 to 1.104 MHz.

$$PSD_{ADSL} = K_{ADSL} \times \frac{2}{f_0} \times \frac{\left[\sin\left(\pi \frac{f}{f_0}\right)\right]^2}{\left(\pi \frac{f}{f_0}\right)^2} \times \frac{1}{1+\left(\frac{f}{f_{LP3dB}}\right)^{12}} \times \frac{1}{1+\left(\frac{f_{HP3dB}}{f}\right)^{N}}, \qquad (2.1)$$

$(0 \le f < \infty)$

where:

-For downstream transmission:

f in Hz, f_0 =2.208 × 10^6 Hz, $f_{LP3dB} = \frac{f_0}{2}$, f_{HP3dB} =138 × 10^3 Hz,

$N = 16$, $K_{ADSL,ds} = 0.1104$ Watts

-For upstream transmission:

f in Hz, $f_0 = 276 \times 10^3$ Hz, $f_{LP3dB} = 138 \times 10^3$, $f_{HP3dB} = 25.875 \times 10^3$ Hz,

N =8, $K_{ADSL,us} = 0.02187$ Watts

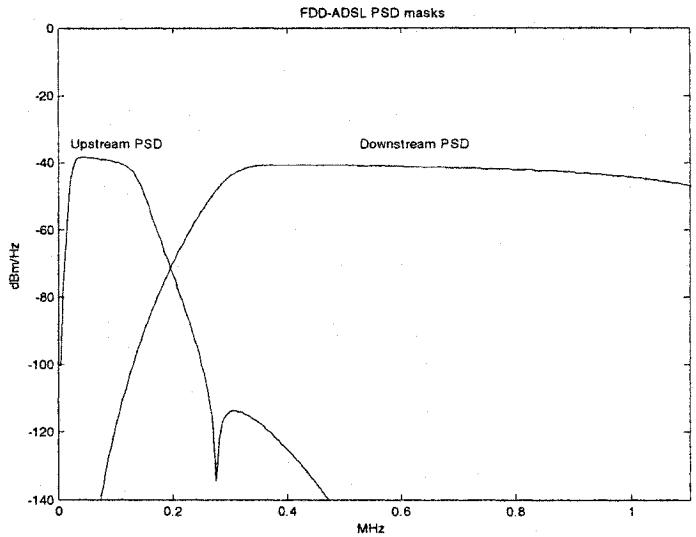

Figure 2-3: Upstream and Downstream FDD-ADSL PSD masks

Any transmitted signal must respect either one of these PSDs depending on the data stream direction. FDD-ADSL transmitted signals have been modeled using the ADSL protocol stack with Discrete Multitone (DMT) modulation presented in Figure 2-4. To create the transmitted signal, *Transmitted Output Signal*, a Matlab program has been written to simulate the ADSL protocol stack as in Figure 2-4. Each block of the ADSL protocol stack has been programmed and will be explained in chapters 3, 4, 5 giving the literature background and the implementation. The twisted-pair channel modeling and the crosstalk canceller will be explained in chapters 6 and 8.

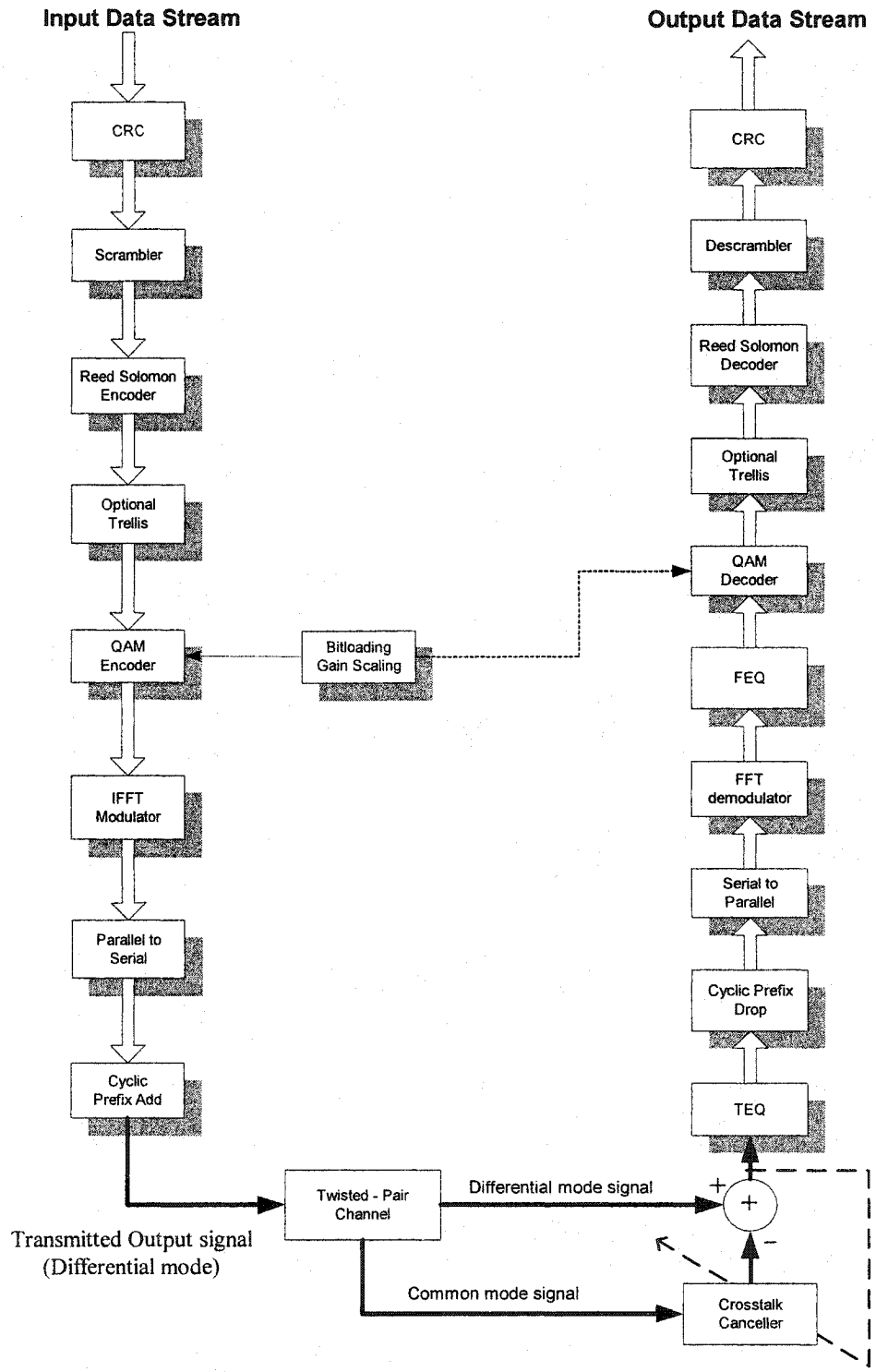

Figure 2-4: DMT ADSL protocol stack

2.3 Considered Technologies Causing Crosstalk

As briefly explained in section 2.1, when a remote terminal is present in the architecture sharing a common distribution cable, it causes an increase of crosstalk interference corrupting the signals received by the CO-served customers. The crosstalk interference signals are categorized into two types, namely NEXT and FEXT (explained in Chapter 7). When all the twisted pair lines in the distributions carry the same DSL technology, the originating crosstalk signals are referred to as Self-NEXT and Self-FEXT.

In this thesis, the two technologies that are considered to cause crosstalk interference are ADSL and VDSL. This thesis focuses on the performance degradation to the CO-served customer when ADSL and VDSL are deployed from the Remote Terminal. The situation is better illustrated in Figure 2-5.

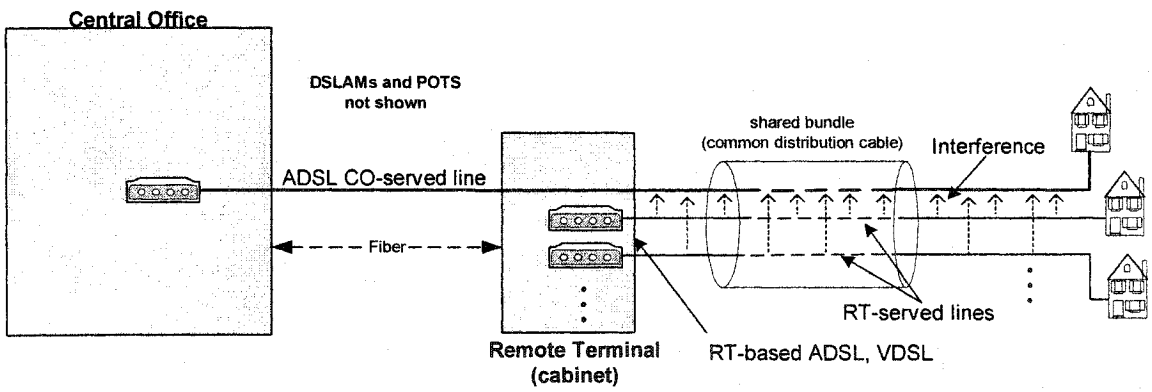

Figure 2-5: CO served customer receiving crosstalk interference from RT-served lines

For the simulation, the important information required regarding the disturbers is primarily their respective emitted PSDs depending on their transmission direction. Therefore, the two following subsections cover only the essential details required as part of the modeling of the disturbance signals (i.e. crosstalk interference signals) as explained in chapter 8.

2.3.1 ADSL Disturbers

The standard specifies when ADSL is deployed from the Remote Terminal, the transmitted PSDs are the same as those deployed from the central office. Therefore, this thesis considers the PSD masks specified in equation 2.1 is what is emitted from the respective transmitters. This assumes full-rate ADSL on all Remote Terminal served lines causing crosstalk interference.

2.3.2 VDSL Disturbers

The standard for Very high bit rate Digital Subscriber Line (VDSL) is not definitive yet (draft). It does not reflect a consensus of Committee T1-Telecommunications and it may be changed or modified.

Similar to ADSL, VDSL is designed to operate on a single twisted pair. It offers downstream data rates up to 52 Mbps and up to 6 Mbps upstream on shorter lines and can operate on loops up to 6000ft at lower data rates.

VDSL transceivers also use frequency division duplexing to separate the upstream and downstream transmissions. Figure 2-6 illustrates the VDSL band allocation for upstream and downstream transmissions [ITU03].

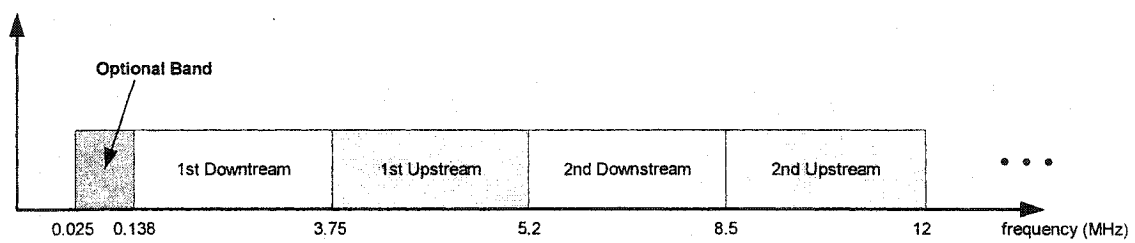

Figure 2-6: VDSL band allocation

The use of the optional band shall be either for the upstream transmission, the downstream transmission or not used. However, it is reasonable that for spectral compatibility with FDD-ADSL, the VDSL optional band shall not be allocated for the downstream transmission to reduce crosstalk interference with upstream ADSL transmission. For the simulations, the optional band from 25kHz to 138kHz has been chosen for the upstream transmission in order to have an identical frequency band allocation for upstream and downstream transmissions as ADSL for common frequencies that is between 0 and 1.104MHz. However, in contrast to ADSL, the VDSL standard specifies different PSD levels for deployment of VDSL from a central office (FTTEx) or from a cabinet (FTTCab). For VDSL deployed from the cabinet, the downstream PSD level at the frequencies common with ADSL is subject to further study for spectral compatibility and management. For the frequencies common to ADSL and VDSL, -60 dBm/Hz (instead of – 40dBm/Hz for ADSL) is a provisional value pending future specification in spectrum management standard [ITU03]. Figure 2-7 illustrates the PSD masks for VDSL deployed from a cabinet (remote terminal). It should be noted that the PSD levels are shown just up to 1.104 MHz since ADSL does not transmit at higher frequencies.

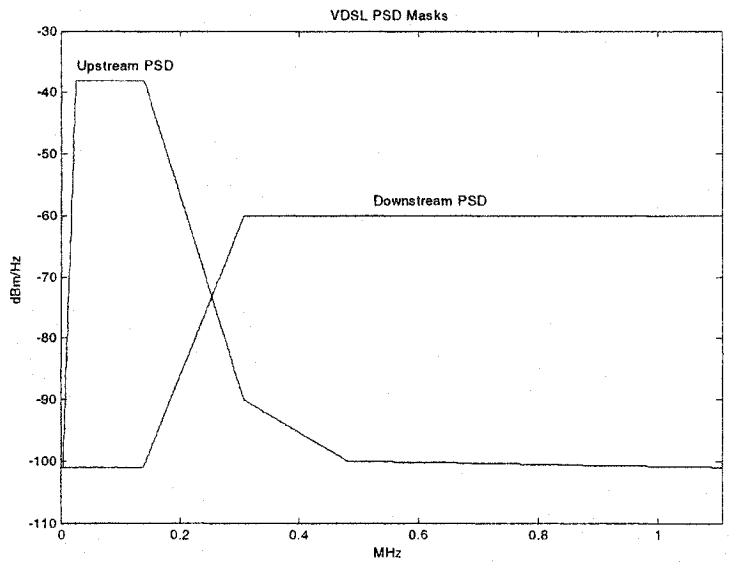

Figure 2-7: Upstream and Downstream VDSL PSD mask

Chapter 3

Quadrature Amplitude Modulation in Discrete Multitone

The ANSI T1E1.4 committee has standardized Discrete Multitone (DMT) modulation as the line code to be used for ADSL transmission system [ITU99]. This chapter will detail QAM for DMT and the Reed-Solomon coding used in the simulation. The two subsequent chapters will complete the discussion of DMT modulation.

DMT is a form of multicarrier system that is a set of independent single carrier Quadrature Amplitude Modulation (QAM) subchannels, and is based on the discrete Fourier transform. A DMT system transmits data in parallel over several equally spaced narrowband subchannels, also called tones. Each subchannel is QAM-encoded and uses different carrier frequencies. The main advantage of multicarrier modulation is that it is able to adapt fairly easily to the system environment, the noise environment or other technology design limitations, such as permitting other telephone services like Basic Rate ISDN and POTS to be used on the same twisted pair line as DSL.

3.1 Single Carrier QAM Analysis

The analysis of a single QAM encoded channel is important to understand the intricacies of the modulation, most notably how to calculate the capacity of one QAM encoded channel (i.e. tone).

3.1.1 QAM Encoding and Modulation

In a QAM digital transmission system, the input bit stream is partitioned into blocks of b bits. Each block represents a message m that can then have values from 0 to 2^b-1. The encoder maps each message, m, into a constellation point. Each constellation point represents a QAM encoded data symbol, x_m. Each data symbol is a two-dimensional vector. A message, m, can then be mapped to one of the $M = 2^b$ possible constellation points (i.e. one of M vector assignments) after encoding. Following the encoding is the modulation process, which converts successive encoded data, x_m, into continuous analog signals, $x_m(t)$. This overall structure can be illustrated as in Figure 3-1.

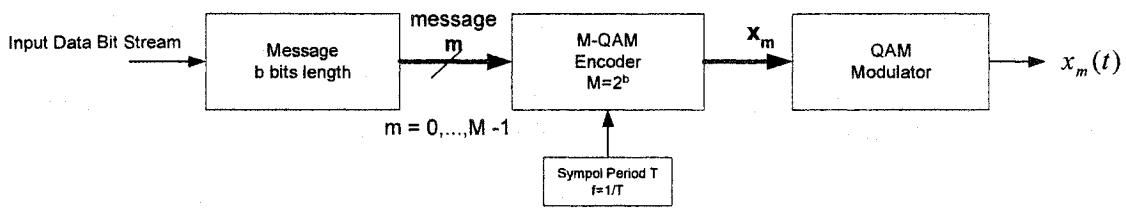

Figure 3-1: QAM transmitter system

The QAM modulator consists of two orthogonal unit-energy basis functions as the following:

$$\text{Quadrature function: } \varphi_1(t) = \sqrt{\frac{2}{T}}\cos(2\pi f_c t) \quad 0 \le t \le T$$

$$\text{In-phase function: } \varphi_2(t) = \sqrt{\frac{2}{T}}\sin(2\pi f_c t) \qquad 0 \le t \le T$$

where T is the symbol period and f_c is the carrier frequency. The transmitted signal has the form [PRO01]:

$$x_{m,k}(t) = \sqrt{\frac{2E_0}{T}}\left(x_{1,k}\cos(2\pi f_c t) - x_{2,k}\sin(2\pi f_c)\right) \qquad 0 \le t \le T$$

where $x_{1,k}\sqrt{E_0}$ and $x_{2,k}\sqrt{E_0}$ are the magnitude components of the QAM encoded data x_m for the k^{th} message m (ie. the k^{th} symbol period T) and E_0 is the energy over one symbol of the signal with lowest amplitude. Figure 3-2 shows as an example the 16-QAM constellation where d is the minimum distance between 2 constellation points and $\frac{d}{2} = \sqrt{E_0}$.

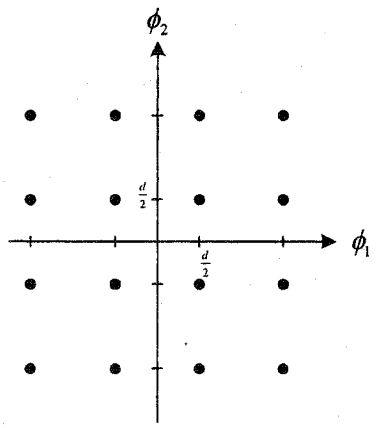

Figure 3-2: Example of 16-QAM constellation

3.1.2 QAM Demodulation, Decoding and Detection

Considering the typical case with an additive white Gaussian noise (AWGN) channel as in Figure 3-3:

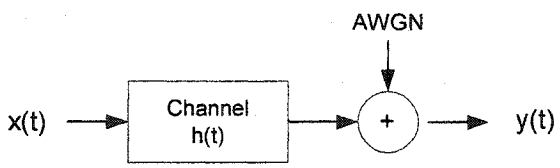

Figure 3-3: AWGN Channel

If the channel $h(t)$ is ISI free with $|H(f)| = 1$ and zero phase, the use of equalization is not required. But with nonzero channel noise, the demodulator and detection can be implemented as in Figure 3-4. The QAM demodulator uses N=2 parallel matched filters with impulse responses $\varphi_1^*(-t)$ and $\varphi_2^*(-t)$. The demodulator outputs are sampled at time $= T$ giving the output vector $\mathbf{y} = [y_1 \quad y_2]$. Since $\mathbf{y}$ does not necessarily equal the data symbol vector $\mathbf{x}$ sent because of the noise disturbance, a symbol-to-symbol detector has to be implemented. The optimum detection is the maximum likelihood detector where the decision is made by taking the demodulator output vector $\mathbf{y}$ and by comparing it with the closest symbol vector $\mathbf{x}_m$ with $m = 0, \ldots, M\text{-}1$ in the *M-QAM* constellation. The term "closest" is referred to the smallest vector length, which verifies the following conditional equation:

$$\text{If } \| \mathbf{y} - \mathbf{x}_i \| \leq \| \mathbf{y} - \mathbf{x}_j \| \text{ for all } j \neq i,\ j = 0, \ldots, M-1\ ;\ i = 0, \ldots, M-1$$
$$\text{then the index is } m = i, \text{ giving the detection } \mathbf{x}_m = \mathbf{x}_i$$

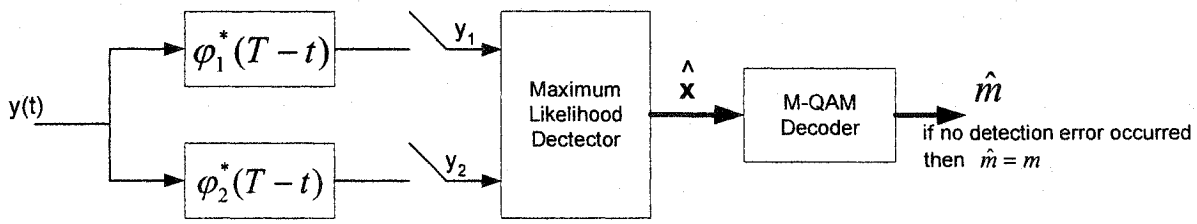

Figure 3-4: QAM demodulator, detector and decoder

The decoder block does exactly the reverse of the encoder mapping. It takes the detected QAM encoded data vector received and converts it back to the corresponding message m or the associated group of bits.

3.1.3 Probability of Symbol Error

The probability of symbol error on the previous AWGN channel (ISI-free) can be approximated with the following example: the QAM encoded message x_0 is sent as in Figure 3-5.

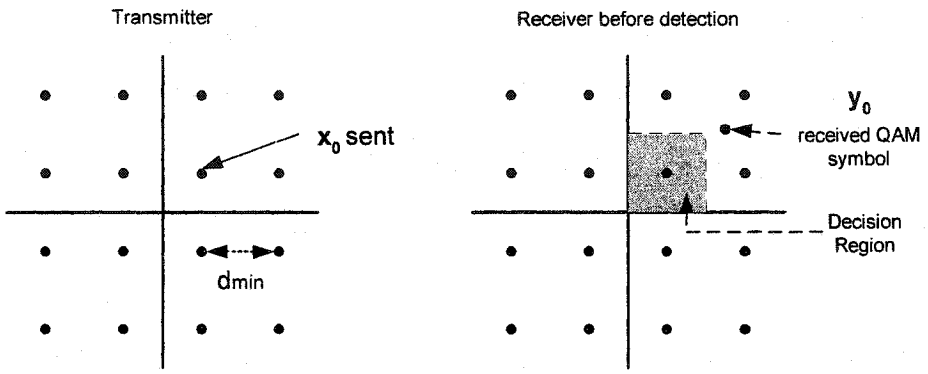

Figure 3-5: Transmission and Reception of a QAM symbol over an AWGN channel

An error will not occur if the received symbol, y_0, was lying inside the decision region of x_0 and the Maximum Likelihood Detector would have made the correct corresponding detection. Since the received signal lies outside the decision region due to the fact that the noise is greater than half of the distance between the closest two constellation points (d_{min} as in Figure 3-5 for example), then the detection fails and a symbol error will occur. On an AWGN channel with noise variance σ^2 and with zero mean, the probability that the noise is greater than $d_{min}/2$ can be approximated by [STA99]:

$$P_e \cong N_e Q(\frac{d_{\min}}{2\sigma}) \tag{3.1}$$

where N_e is average number of nearest neighbours, and the Q-function Q(x) is the probability that a zero-mean Gaussian random variable with variance $\sigma^2 = 1$ is greater than x given by:

$$Q(x) = \int_{x}^{\infty} \frac{1}{\sqrt{2\pi}} e^{-\frac{v^2}{2}} dv$$

Equation (3.1) will be useful to calculate the SNR gap in section 3.4.

3.2 QAM Constellations Used in ADSL

Each subchannel can use different QAM-constellation sizes depending on the bitloading algorithm (refer to Chapter 5 for more details). The ADSL standard [ITU99] specifies the constellation mapping and shape to employ.

For b_i = 2, 3, 4 and 5 bits, the constellations have the shapes represented in Figure 3-6 [ITU99]. The decimal value numbers represented in the graphs are the mapping of the corresponding binary messages of size b_i bits, for a given constellation size of $M = 2^{b_i}$.

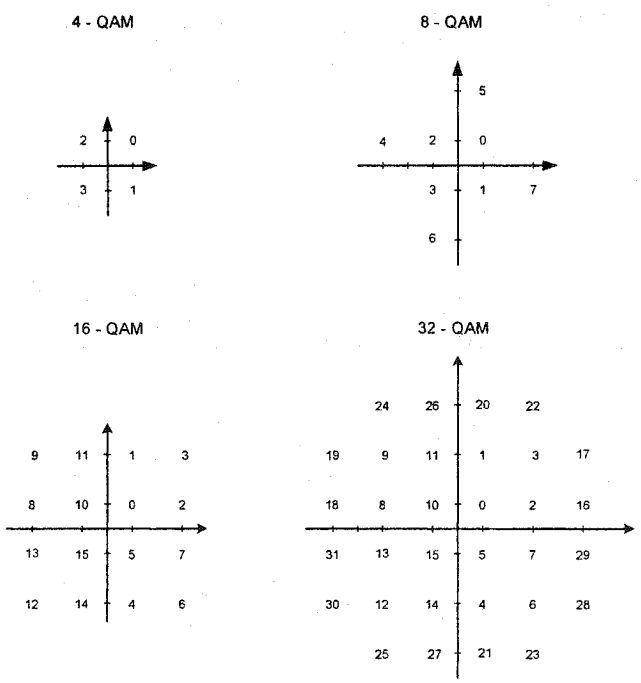

Figure 3-6: Constellation maps for b_i=2, b_i =3, b_i =4 and b_i =5

For $b_i > 4$ and odd, ADSL uses the cross QAM constellation as in Figure 3-7.

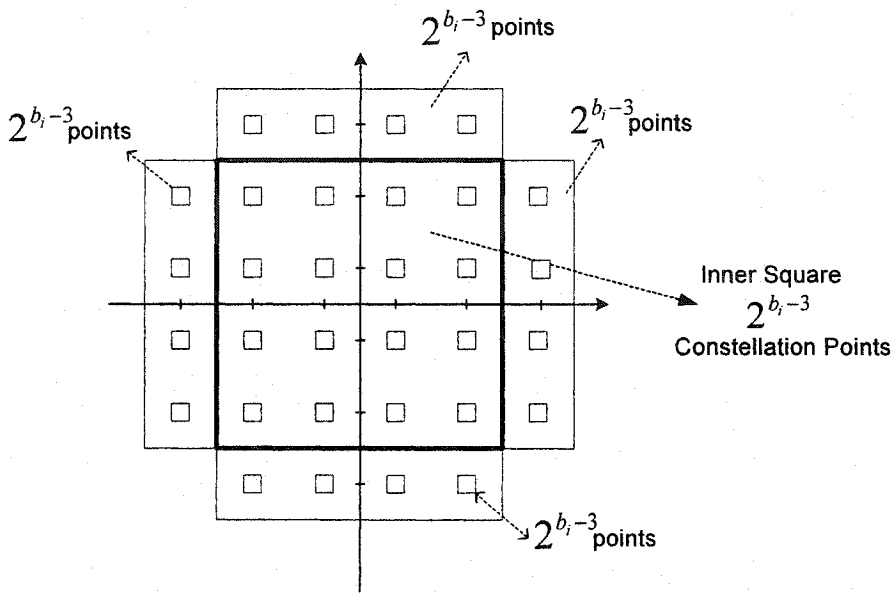

Figure 3-7: QAM cross constellation map for $b_i > 4$ and odd

However, for $b_i > 5$, the next odd-bit cross QAM constellation can be found by replacing each constellation point represented by a decimal value of the previous odd-bit cross-constellation with the following 2x2 block:

$4m+1$	$4m+3$
$4m$	$4m+2$

where m represents the decimal value encoded

The same procedure is applied to construct larger square expansions for even-bit square QAM constellations, for $b_i > 4$ from the previous even-bit QAM constellations.

An example of a QAM square constellation with $b_i = 6$ (64-QAM) obtained by transforming the 16-QAM constellation using the 2x2 block is shown in Figure 3-8.

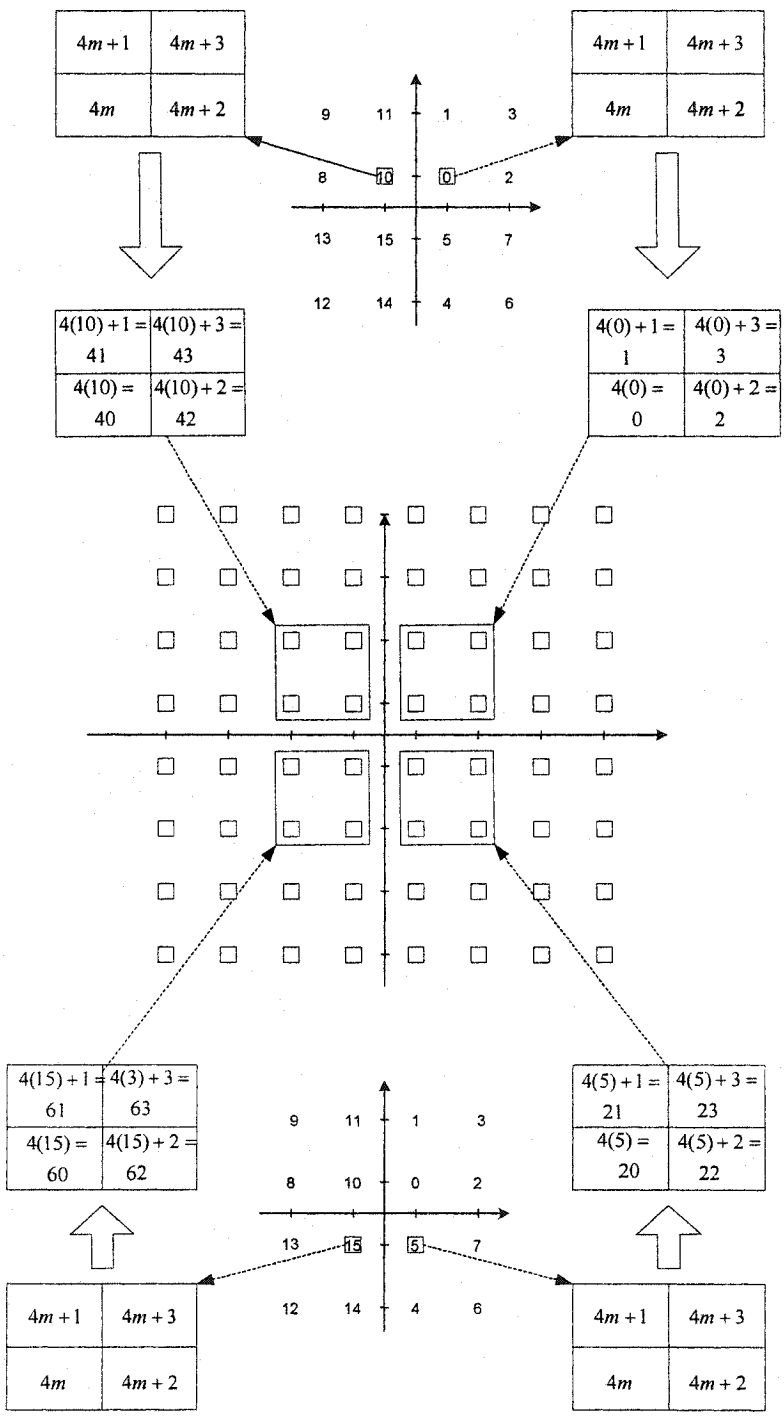

Figure 3-8: 64-QAM square-constellation design

The resulting 64-QAM constellation by using the 2x2 block expansion is shown in Figure 3-9.

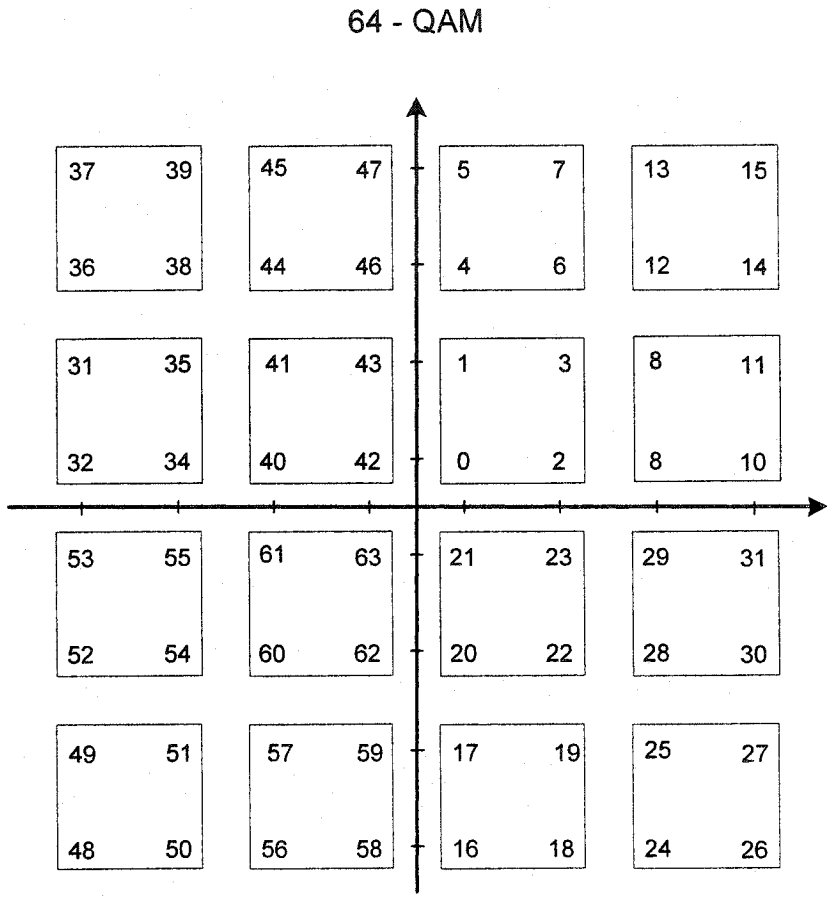

Figure 3-9: Resulting 64-QAM square-constellation corresponding to $b_i = 6$ bits

Note that for all the QAM constellations, the X and Y values are on $\pm 1, \pm 3$ ... grid [ITU99]. Thus, the distance between two closest constellation points is $d = 2$.

3.3 QAM Constellation Energy

The average energy of the transmitted signal can be calculated in two ways [PRO01]:
1) in the continuous time domain as the average integrated squared value of $x(t)$ over all the possible signals:

$$E_x = \frac{1}{M}\sum_{m=0}^{M-1}\int_{-\infty}^{\infty} |x_m(t)|^2 \, dt \tag{3.2}$$

2) in the discrete time domain as the average squared length of the data symbol vectors $\boldsymbol{x_m}$ in the M-QAM constellation:

$$E_x = \frac{1}{M}\sum_{m=0}^{M-1} \| \vec{x}_m \|^2 \tag{3.3}$$

3.4 SNR Gap

The ANSI T1 committee for ADSL [ITU99] requires that the BER should not exceed 10^{-7} for DSL applications. Taking equation (3.1) and assuming the number of nearest neighbours to be 4 [STA99], then the probability of symbol error in QAM is closely approximated by:

$$P_s \leq 4 \cdot Q\left(\frac{d_{\min}}{2\sigma}\right) \tag{3.4}$$

A symbol error occurs when a single bit or more in the symbol is wrong. Since equation (3.4) gives the probability of symbol error for any QAM constellation size *M*, then one should consider all the sizes allowed for ADSL by [ITU99]. The standard allows constellation sizes from 2^2 to 2^{15}. All the constellation sizes should have the same probability of symbol error. Taking the worst case, as a 2-bit or 4-QAM constellation , the probability of symbol error is then:

$$P_s = \sum_{i=1}^{2}\binom{2}{i} P_b{}^i (1-P_b)^{2-i} = 2P_b\left(1-\frac{1}{2}P_b\right) \cong 2P_b \tag{3.5}$$

Equating equations (3.4) and (3.5) gives $Q(\frac{d_{\min}}{2\sigma}) = \frac{1}{2}P_b$ where P_b is the probability of bit error that should not exceed 10^{-7}[ITU99][STA99]. Consequently, by looking at the Q-function curve of Figure 3-10,

$$20 \cdot \log\left(\frac{d_{\min}}{2\sigma}\right) = 14.5 \text{ dB} \tag{3.6}$$

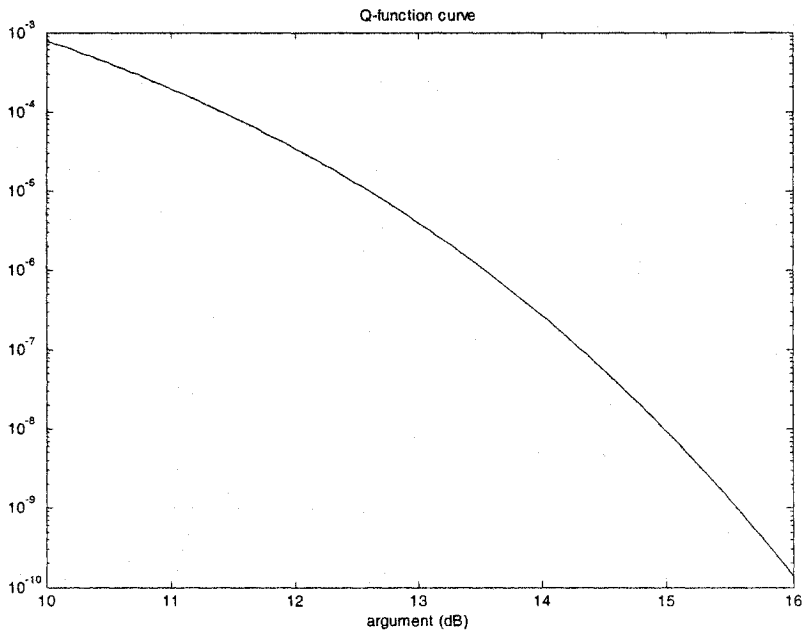

Figure 3-10: Q-function curve as a function of $20 \cdot \log(\frac{d_{\min}}{2\sigma})$

With an AWGN channel with a channel gain $|H|$ (the assumption taken here is that the channel has a constant gain |H| over the operating transmission frequency band).

$$d_{\min}^2 = d^2 \mid H \mid^2 \tag{3.7}$$

where d is the Euclidean distance between constellation points at the input of the channel (transmitter side). Defining a convenient quantity, the SNR gap Γ[CIO91] as

$$3\Gamma = \left(\frac{d_{\min}}{2\sigma}\right)^2 \tag{3.8}$$

giving then:

$$10\cdot\log(3\Gamma) = 14.5 \text{ dB} \quad => \quad \Gamma\text{dB} = 9.8 \text{ dB} \tag{3.9}$$

As mentioned previously in section 3.3, the average energy shown in equation (3.3) for a QAM system can be simplified with [PRO01]:

$$E_x = \frac{M-1}{6}d^2 \tag{3.10}$$

This simplification is accurate for QAM systems with a number of bits $b \geq 2$ and even, and is also a quite good approximation when b is odd [CIO91].

Re-arranging the equations 3.7, 3.8 and 3.10 => $M = 1 + \frac{E_x |H|^2}{2\sigma^2 \cdot \Gamma}$

and taking the log base 2 gives:

$$b = \log_2(M) = \log_2\left(1 + \frac{SNR}{\Gamma}\right) \tag{3.11}$$

where $SNR = \frac{E_x |H|^2}{2\sigma^2}$ [CIO91].

Hence, equation 3.11 provides the QAM constellation size M (i.e. $M=2^b$) that can be used to transmit over the channel with a respective SNR to ensure a BER of 10^{-7}. Also, the SNR gap is then an important factor that varies in regards of the coding and modulation methods as represented in equation (3.12).

$$\Gamma = 9.8 \text{ dB} + \gamma_m \text{ dB} - \gamma_c \text{ dB} \quad (3.12)$$

γ_c is the coding gain of any applied code such as Reed-Solomon or trellis, and γ_m is referred to as the margin, which is the amount of extra performance to make sure to have the required performance in the presence of unexpected channel impairments such as crosstalk, extra attenuations etc. With an uncoded QAM system (γ_c = 0) and with no margin (γ_m = 0), equation 3.12 becomes Γ = 9.8 dB.

A good coding gain can reduce the gap of 9.8 dB to 3 to 5 dB, consequently increasing the capacity.

3.5 Coding

Forward error correction is employed in communication systems to achieve a coding gain in order to increase the system margin and the maximum achievable data rate [ZHA01].

There are typically two coding methods implemented in ADSL: Reed-Solomon forward error correction (RS-FEC) and trellis coded modulation (TCM). The optional Trellis coded modulation of the ADSL standard was not implemented in this simulation, but it is used to increase the coding gain to maintain a given data rate at a lower SNR. Typically, the combination of Reed-Solomon coding with Trellis would provide a coding gain of approximately 5 dB [STA99].

3.5.1 Reed-Solomon Parameters

Reed-Solomon FEC increases the coding gain, but when combined with the interleaving, it permits the correction of large error bursts caused by impulse noise. Interleaving is

optional in the ADSL standard and it has not been implemented since the simulation does not consider impulse noise but crosstalk noise. Also, it is mentioned in [STA02] that major service providers have 99% of their ADSL lines operating without interleaving.

In ADSL systems, Reed-Solomon code words can be up to 255 bytes long. The exact amount of overhead and code word length depends on several factors, including the transmission direction and the target bit rate. Unfortunately, the simulation using Matlab does not permit highly variable code word length since the Matlab RS encoder function used to achieve the coding allows only code word lengths of 2^M-*1*. Therefore, a fixed value of 255 bytes has been chosen for the code word length, with 22 bytes of overhead giving an overhead percentage of about 8.6%. This percentage falls within the 6 to 10 % given for a maximum error-correcting protection against Gaussian noise when the system is operating near capacity [STA02], therefore the chosen values are reasonable for ADSL simulation.

The RS decoder is able to correct error bytes up to half the length of the overhead in the entire code word. Assuming that the most probable case is when only one bit is likely to be wrong per byte error, then with the parameters chosen, the RS scheme used can correct a probability of bit error up to $\frac{22/2}{255 \cdot 8} = 5.39 \cdot 10^{-3}$ in the code word. Also, this value falls within the range of the ADSL allowed bit error rate per code word given with 6 to 10% of overhead, since with 6% of overhead the RS can correct up to a probability of $\frac{6\%/2}{8} = 3.75 \cdot 10^{-3}$ bit error in the code word, and with 10% a correction up to $\frac{10\%/2}{8} = 6.25 \cdot 10^{-3}$ bit error rate in the code word.

3.5.2 Reed-Solomon Coding Gain

Using [STA02], an approximation of the Reed-Solomon coding gain and the BER before and after RS coding can be estimated. Assuming that the probability of byte error, P_{byte}, is small, then for the chosen parameters, the probability of code word error is closely approximated by the probability that 22/2 +1 = 12 byte errors occur [STA02]. When 12 byte errors occur, the RS decoder will declare a failure giving then a probability of bit error in the code word of $\frac{12}{255 \cdot 8} = 5.9 \cdot 10^{-3}$, assuming again a single bit error per byte error.

Since the standard specifies a maximum BER of 10^{-7} for an ADSL system after all error correction schemes used (here it is assumed that only RS coding has been used), then the required probability of code word error is: $\frac{10^{-7}}{5.9 \cdot 10^{-3}}$.

In backwards reasoning, the probability of code word error is approximated by the probability of having 12 bytes in error in the code word, thus:

$$\binom{255}{12} P_{byte}{}^{12} (1 - P_{byte})^{255-12} = \frac{10^{-7}}{5.9 \cdot 10^{-3}}$$

Solving the equation iteratively gives: $P_{byte} \cong 0.00105$

Therefore, a system with a probability of byte error of $P_{byte} \cong 0.00105$ would give an overall probability of bit error of 10^{-7} with an RS coding of 22 bytes overhead and 255 bytes word length.

For an uncoded system, a probability of byte error of 0.00105 would give a probability of bit error (BER), P_b, of:

$$P_{byte} = \binom{8}{1} P_b^{1}(1-P_b)^{8-1} = 8 \cdot P_b(1-P_b)^7 = 0.00105$$

Solving this equation gives as a result: $P_b \cong 1.4 \cdot 10^{-3}$.

Consequently, the SNR Gap for a QAM system as explained in section 3.4 for $P_b \cong 1.4 \cdot 10^{-3}$ is determined by finding the argument in the Q-function, which verifies:

$$Q(x) = \frac{1}{2} P_b = 7.0 \cdot 10^{-4}$$

Looking at the Q-function curve, the argument is $x \cong 10.9dB$. Therefore, instead of requiring 14.5 dB as in section 3.4 for an uncoded system to get a BER of 10^{-7}, the system, with coding would require only 10.9 dB resulting in a coding gain of:

$$14.5\text{dB} - 10.9\text{dB} = 3.6 \text{ dB}$$

The SNR Gap would be then reduced to:

$$\Gamma = 9.8 \text{ dB} - \gamma_c \text{ dB} = 6.2 \text{ dB}$$

The coarse calculations done to get the coding gain are in fact an upper bound result since the extra parity overhead was not taken into account [STA02]. The coding gain should be slightly less.

Also, with chosen parameters, the Reed-Solomon scheme is then capable of correcting BER in the order of 10^{-3} before correction and can reduce it to at most 10^{-7} after correction as required by DSL standards [ITU99].

Chapter 4

Discrete Multitone Modulation and Channel Equalization

The previous chapter presented the necessary basics in QAM to pursue the study of DMT. This chapter will expand the QAM technique to several parallel QAM encoders for equally spaced narrowband subchannels, and then modulate each QAM symbol at its own respective carrier frequency by the use of the inverse discrete Fourier transform. In the following sections, a detailed DMT transmitter implemented as in Figure 4-1 will be described.

The first section generalizes the use of QAM to several parallel subchannels, followed by the description of the IDFT modulation block in more detail, and its corresponding DFT demodulation block. The second part of the chapter discusses the equalization of the channel, and how to counteract the effect of inter-symbol interference (ISI). The next chapter will conclude the DMT discussion by explaining the algorithm that decides the number of bits to be assigned to each subchannel (Bitloading algorithm) and also how the power of each subchannel is adjusted to get the desired overall transmitted Power Spectral Density (PSD).

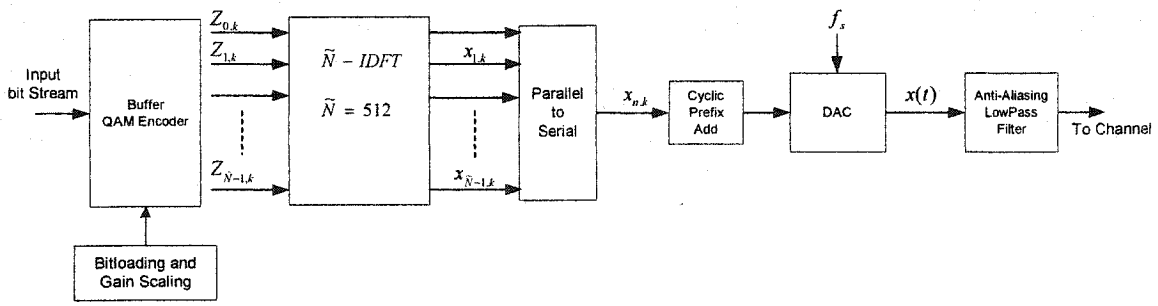

Figure 4-1: DMT transmitter

4.1 Generalization of QAM to Several Subchannels

One can re-write the capacity per subchannel equations in section 3.4 for each subchannel with corresponding index i as:

$$b_i = \log_2(1 + \frac{SNR_i}{\Gamma}) \tag{4.1}$$

$$E_i = \frac{M_i - 1}{6} d_i^2 \tag{4.2}$$

Each subchannel i, is characterized by a corresponding SNR_i and a corresponding total of number of bits b_i that can be supported. Therefore, each subchannel can have different QAM constellation sizes. DMT modulates the QAM encoded data using the Inverse Discrete Fourier Transform (IDFT) and demodulates it using the DFT. For a given subchannel (subcarrier), the ADSL standard [ITU99] specifies 0 or 2 to 15 bits for QAM constellation sizes and 256 tones from 0 to 1.104 MHz. Each subchannel has then a 4.3125 kHz bandwidth. The downstream system uses a sampling rate of 2.208 MHz. A more detailed QAM encoder block is represented in Figure 4-2.

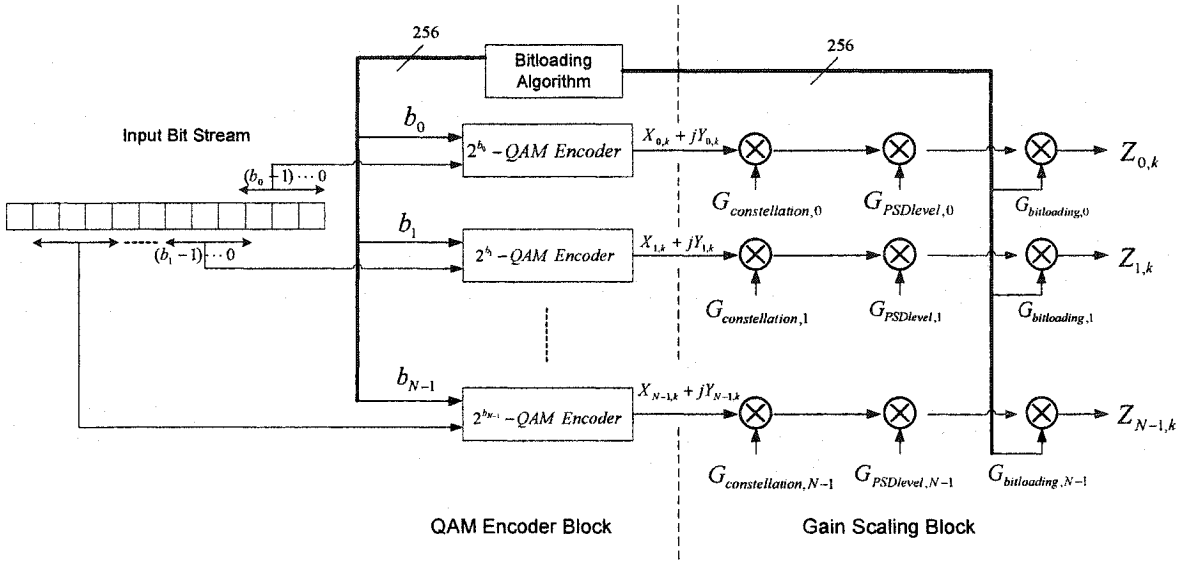

Figure 4-2: DMT-QAM Encoder block

As illustrated in Figure 4-2, the input bit stream is partitioned. The partition size depends on b_i and represents the input of each QAM encoder for each subchannel *i*. The encoding process is similar for the single QAM encoder as explained in section 3.1.1 but applied for each subchannel *i*. Each subchannel (i = 0 to 255) is QAM encoded using M = 2^{b_i}-QAM constellation. The QAM constellation size chosen for each subchannel represented by b_i is set by the bitloading algorithm (refer to section 5.3) during initialization. The total number of bits transmitted corresponding to each k^{th} instant or the k^{th} symbol is given by:

$$b_{Total} = \sum_{i=0}^{N-1} b_i \tag{4.3}$$

The output of the encoder for each subchannel is represented by a complex value, $X_{i,k} + jY_{i,k}$. $X_{i,k}$ and $Y_{i,k}$ are the magnitude component of the encoded data for each subchannel *i* combined into a single complex element instead of a 2-D vector.

In addition, Figure 4-2 also shows the product of three gain factors $G_{constellation,i}$, $G_{PSDlevel,i}$ and $G_{bitloading,i}$ that represents the gain scaling g_i, that is applied to each complex encoded data prior to the IFFT modulation block. The gain scaling will be explained in more detail in Chapter 5.

4.2 IDFT Modulator

Figure 4-3 illustrates a more detailed IDFT modulator block implemented.

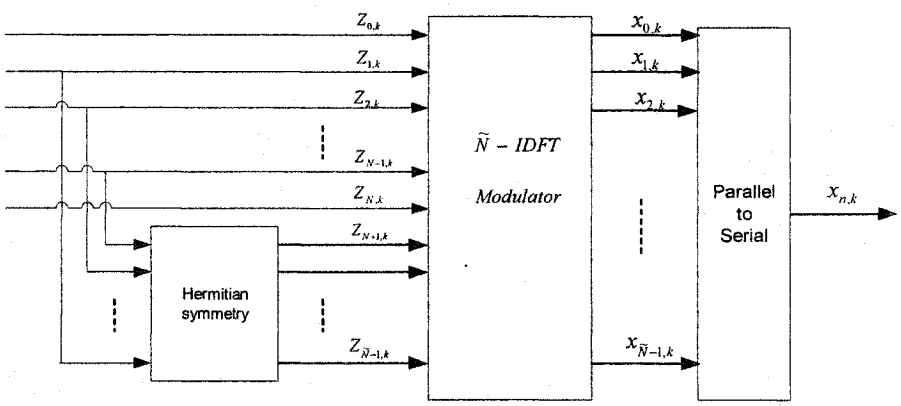

Figure 4-3: IDFT modulator

The constellation encoder of the previous section generates QAM-encoded data symbols for each of the N = 256 subchannels. The input to the IDFT modulator can be represented by a series of complex values, $Z_{i,k}$, where the real part is the scaled X-coordinate and the imaginary part is the scaled Y-coordinate of the QAM-encoded data giving:

$$Z_{i,k} = g_i \left(X_{i,k} + j\, Y_{i,k} \right) \tag{4.4}$$

The index i represents the respective subchannel and g_i is the scaling factor applied to all the constellation points for i^{th} subchannel (see section 5.1 for more details). The subscript k indicates the k^{th} IDFT symbol transmitted that will be explained shortly.

DMT modulation is performed in the discrete-domain instead of the continuous-time domain. The modulation is produced by the Inverse Discrete Fourier Transform (IDFT):

$$x_k(n) = \frac{1}{\widetilde{N}} \cdot \sum_{i=0}^{\widetilde{N}-1} e^{\frac{j2\pi \cdot n \cdot i}{\widetilde{N}}} \cdot Z_{i,k} \qquad \text{for } n = 0 \text{ to } \widetilde{N}-1 \tag{4.5}$$

In practice, the IDFT is replaced by the Inverse Fast Fourier Transform (IFFT). The constellation encoder combined with gain scaling generates only 255 complex values $Z_{i,k}$. In order to generate real time-domain output values $x_k(n)$ after modulation, the number of input values Z_i is increased to $\widetilde{N} = 2N$ by taking the complex conjugate of the N -1 previous input values, placed in mirrored positions to produce Hermitian symmetry in the following manner:

$$Z_i = \begin{cases} Z_i & i = 0,\ldots,N-1 \\ Z^*_{\widetilde{N}-i} & i = N+1,\ldots,\widetilde{N}-1 \end{cases} \tag{4.6}$$

Note that the Nyquist frequency at i = 256 should not be used and should be real valued for $Z_N = Z_{256}$. Also, i = 0 (i.e. DC) should not carry any information so Z_0 is set to 0, (no input bits should be assigned [ITU99] at DC since QAM modulation cannot transmit using DC). The set of $\widetilde{N}$ real time-domain samples at the output of the $\widetilde{N} - Point\ IDFT$: $x_{i,k}$ for i =0 to $\widetilde{N}-1$ represents the k^{th} symbol, sometimes called the k^{th} IDFT symbol. The $\widetilde{N}$ samples representing a IDFT symbol are serialized to produce x_k(n) and then applied to a Digital-to-Analog converter (DAC) giving the continuous time signal x_k(t). It can be proven with the following calculations that DMT is a form of

multicarrier modulation. Note that the calculations have been undertaken for a single IDFT symbol transmission, thus, the subscript k has been purposely omitted.

Using equation (4.5):

$$x(n) = \frac{1}{\tilde{N}} \cdot \sum_{i=0}^{\tilde{N}-1} e^{\frac{j2\pi \cdot n \cdot i}{\tilde{N}}} \cdot Z_i \quad \text{for} \quad n = 0 \; to \; \tilde{N}-1$$

$$= \frac{1}{\tilde{N}} \cdot \left\{ \begin{array}{l} e^{\frac{j2\pi \cdot n \cdot 0}{\tilde{N}}} \cdot Z_0 + e^{\frac{j2\pi \cdot n \cdot 1}{\tilde{N}}} \cdot Z_1 + e^{\frac{j2\pi \cdot n \cdot 2}{\tilde{N}}} \cdot Z_2 + \cdots + e^{\frac{j2\pi \cdot n \cdot (\frac{\tilde{N}}{2})}{\tilde{N}}} \cdot Z_{\frac{\tilde{N}}{2}} + \cdots + \\ + e^{\frac{j2\pi \cdot n(\tilde{N}-2)}{\tilde{N}}} \cdot Z_{\tilde{N}-2} + e^{\frac{j2\pi \cdot n(\tilde{N}-1)}{\tilde{N}}} \cdot Z_{\tilde{N}-1} \end{array} \right\}$$

Regrouping the subchannels together and simplifying:

$$= \frac{1}{\tilde{N}} \cdot \left\{ \begin{array}{l} e^{\frac{j2\pi \cdot n \cdot 0}{\tilde{N}}} \cdot Z_0 + \left[e^{\frac{j2\pi \cdot n \cdot 1}{\tilde{N}}} \cdot Z_1 + e^{\frac{j2\pi \cdot n\tilde{N}}{\tilde{N}}} e^{\frac{-j2\pi \cdot n}{\tilde{N}}} \cdot Z_{\tilde{N}-1} \right] + \\ \left[e^{\frac{j2\pi \cdot n \cdot 2}{\tilde{N}}} \cdot Z_2 + e^{\frac{j2\pi \cdot n\tilde{N}}{\tilde{N}}} e^{\frac{-j2\pi \cdot n \cdot 2}{\tilde{N}}} \cdot Z_{\tilde{N}-2} \right] + \cdots + e^{\frac{j2\pi \cdot n \cdot (\frac{\tilde{N}}{2})}{\tilde{N}}} \cdot Z_{\frac{\tilde{N}}{2}} \end{array} \right\}$$

$$= \frac{1}{\tilde{N}} \cdot \left\{ Z_0 + \left[e^{\frac{j2\pi \cdot n \cdot 1}{\tilde{N}}} \cdot Z_1 + e^{\frac{-j2\pi \cdot n}{\tilde{N}}} \cdot Z_{\tilde{N}-1} \right] + \left[e^{\frac{j4\pi \cdot n}{\tilde{N}}} \cdot Z_2 + e^{\frac{-j4\pi \cdot n}{\tilde{N}}} \cdot Z_{\tilde{N}-2} \right] + \cdots + (-1)^n \cdot Z_{\frac{\tilde{N}}{2}} \right\}$$

(4.7)

Since the Hermitian symmetry has been applied, then each complex element Z_i has a corresponding complex conjugate as indicated by equation 4.6:

$$Z_i = Z^*_{\tilde{N}-i} \quad \text{equivalent to} \quad Z^*_i = Z_{\tilde{N}-i} \tag{4.8}$$

Re-writing the complex element in their polar form:

$$Z_i = |Z_i| e^{j\angle Z_i} \quad \text{and} \quad Z_{\tilde{N}-i} = |Z_{\tilde{N}-i}| e^{j\angle Z_{\tilde{N}-i}} \tag{4.9}$$

and using equation 4.8, then $Z_{\tilde{N}-i} = |Z_i| e^{-j\angle Z_i}$ (4.10)

Note that the frequency 0 Hz, or DC (the subchannel at index i=0), should not be used, and no energy is allocated, then $Z_0 = 0$. Also, at the Nyquist Frequency at $i = \frac{\tilde{N}}{2}$, the input value should be real or null, the value was chosen as $Z_{\frac{\tilde{N}}{2}} = 0$. Using the relation found in (4.10), equation 4.7 is simplified further:

$$= \frac{1}{\tilde{N}} \cdot \left\{ \left[|Z_1| e^{j\angle Z_1} \cdot e^{\frac{j2\pi \cdot n}{\tilde{N}}} + |Z_1| e^{-j\angle Z_1} \cdot e^{\frac{-j2\pi \cdot n}{\tilde{N}}} \right] + \left[\cdot |Z_2| e^{j\angle Z_2} e^{\frac{j4\pi \cdot n}{\tilde{N}}} + |Z_2| e^{-j\angle Z_2} e^{\frac{-j4\pi \cdot n}{\tilde{N}}} \right] + \cdots \right\}$$

$$= \frac{1}{\tilde{N}} \cdot \left\{ |Z_1| (e^{j(\frac{j2\pi \cdot n}{\tilde{N}} + \angle Z_1)} + e^{-j(\frac{j2\pi \cdot n}{\tilde{N}} + \angle Z_1)}) + |Z_2| (e^{j(\frac{4\pi \cdot n}{\tilde{N}} + \angle Z_2)} + e^{-j(\frac{4\pi \cdot n}{\tilde{N}} + \angle Z_2)}) + \cdots + \right\}$$

Using the identity: $\cos(\theta) = \frac{e^{j\theta} + e^{-j\theta}}{2}$ gives

$$= \frac{2}{\tilde{N}} \left\{ |Z_1| \cdot \cos(\frac{2\pi \cdot n}{\tilde{N}} + \angle Z_1) + |Z_2| \cdot \cos(\frac{4\pi \cdot n}{\tilde{N}} + \angle Z_2) + \cdots \right\}$$

To generalize:

$$x(n) = \frac{2}{\tilde{N}} \cdot \sum_{i=1}^{\frac{\tilde{N}}{2}-1} |Z_i| \cdot \cos(\frac{2\pi \cdot n \cdot i}{\tilde{N}} + \angle Z_i) \qquad \text{for} \quad n = 0 \text{ to } \tilde{N} - 1$$

From this result, it can be seen that the modulation using IDFT corresponds to a multicarrier modulation since the information carried by each subchannel i is modulated by a cosine with a specific distinct frequency $w = \frac{2\pi \cdot i}{\widetilde{N}}$ and a phase of $\angle Z_i$, and all the carriers are summed together. The frequency spacing between subcarriers is $\Delta f = \frac{2\pi}{\widetilde{N} \cdot f_s \cdot 2\pi} = 4.3125\ kHz$ since the sampling frequency, f_s, is 2.208 MHz and $\widetilde{N} = 512$. In addition, the result $x(n)$ is real as expected since the Hermitian symmetry has been applied, and considering the properties of the IDFT.

4.3 Cyclic Prefix

The IDFT modulator outputs a symbol block k of $\widetilde{N}$ real samples, which will be serialized. Each symbol block is added a Cyclic Prefix (CP). The ADSL standard [ITU99] specifies a cyclic prefix length, v, of 32 samples. The last v samples of each IDFT symbol are taken and copied to the beginning of the symbol block forming a DMT symbol as in Figure 4-4.

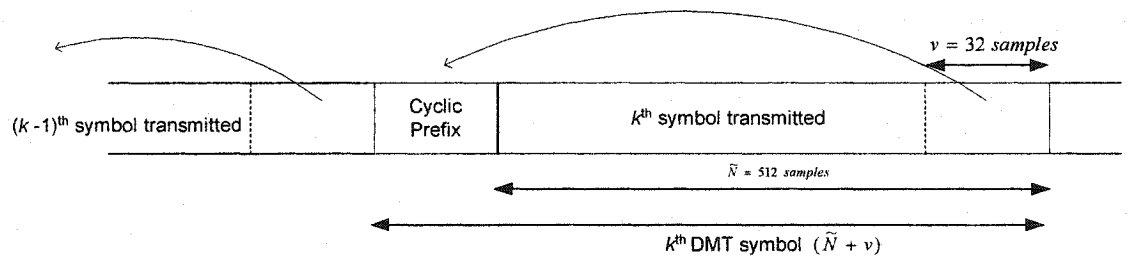

Figure 4-4: cyclic prefix added

The cyclic prefix is considered as guard band to combat ISI introduced by the channel. If the channel memory (length of the channel impulse response) is less than the guard band,

v, then the ISI would corrupt only the cyclic prefix samples, which will be discarded (Cyclic Prefix Drop as in Figure 4-5) at the receiver side before the DFT demodulation.

Considering an AWGN channel as in equation 4.11,

$$\boldsymbol{y} = \boldsymbol{H}\boldsymbol{x} + \boldsymbol{n} \tag{4.11}$$

the transmitted samples are indexed $x_{-v},\ldots,x_0,x_1,\ldots,x_{\tilde{N}-1}$, the corresponding outputs are $y_0,y_1,\ldots,y_{\tilde{N}-1}$ and the channel $\boldsymbol{H}$ in a convolution matrix form is defined as:

$$H = \begin{bmatrix} h_0 & h_1 & \ldots & h_v & 0 & 0 & 0 & 0 & 0 & 0 \\ 0 & h_0 & h_1 & \ldots & h_v & 0 & 0 & 0 & 0 & 0 \\ \ddots & \ddots & \ddots & \ddots & \ddots & \ddots & \ddots & \ddots & \ddots & \ddots \\ 0 & 0 & 0 & h_0 & h_1 & \ldots & h_v & 0 & 0 & 0 \\ 0 & 0 & 0 & 0 & h_0 & h_1 & \ldots & h_v & 0 & 0 \\ \ddots & \ddots & \ddots & \ddots & \ddots & \ddots & \ddots & \ddots & \ddots & \ddots \\ 0 & 0 & 0 & 0 & 0 & 0 & h_0 & h_1 & \ldots & h_v \end{bmatrix}$$

The dimension of the channel in matrix form $\boldsymbol{H}$ is $\tilde{N}$ by $\tilde{N}+v$ which corresponds to outputs $\boldsymbol{y}$ of length $\tilde{N}$, meaning that the receiver ignores the guard band samples because they contain interference from previous DMT symbols.

However, the use of a cyclic prefix as a guard period in Discrete Multitone (DMT), that is $x_{-i} = x_{\tilde{N}-i}$ for $i = 1,\ldots,v$ leads to an important observation. When a cyclic prefix is used, the matrix $\boldsymbol{H}$ becomes a square "circulant" matrix as the following:

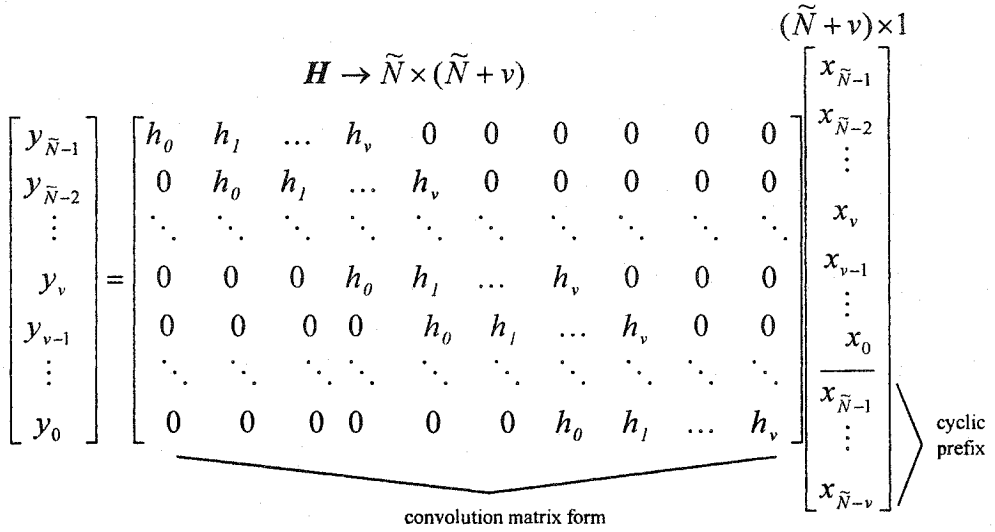

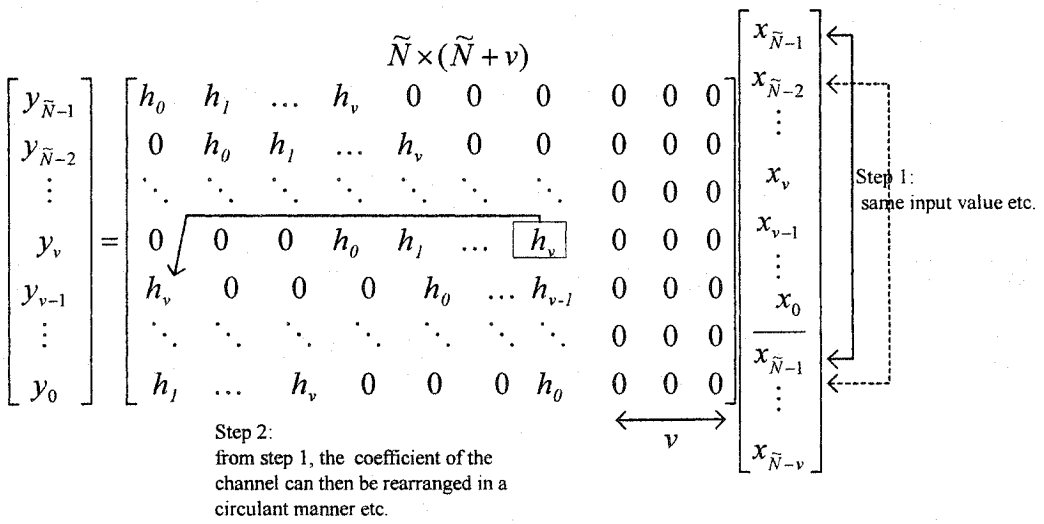

After rearranging all the coefficients of the channel, the matrix $\boldsymbol{H}$ becomes circulant and the size of the matrix can be decreased to an $\tilde{N}$ by $\tilde{N}$ matrix:

$$\begin{bmatrix} y_{\tilde{N}-1} \\ y_{\tilde{N}-2} \\ \vdots \\ y_v \\ y_{v-1} \\ \vdots \\ y_0 \end{bmatrix} = \begin{bmatrix} h_0 & h_1 & \dots & h_v & 0 & 0 & 0 \\ 0 & h_0 & h_1 & \dots & h_v & 0 & 0 \\ \ddots & \ddots & \ddots & \ddots & \ddots & \ddots & \ddots \\ 0 & 0 & 0 & h_0 & h_1 & \dots & h_v \\ h_v & 0 & 0 & 0 & h_0 & \cdots & h_{v-1} \\ \ddots & \ddots & \ddots & \ddots & \ddots & \ddots & \ddots \\ h_1 & \dots & h_v & 0 & 0 & 0 & h_0 \end{bmatrix} \begin{bmatrix} x_{\tilde{N}-1} \\ x_{\tilde{N}-2} \\ \vdots \\ x_v \\ x_{v-1} \\ \vdots \\ x_0 \end{bmatrix}$$

$$\boldsymbol{H} = \tilde{N} \times \tilde{N} \textit{ circulant Matrix}$$

It should be noted that the first v output samples of each transmitted DMT symbol are ignored. Circulant matrices have the property that they can be decomposed as [STA99]:

$$\boldsymbol{H} = \boldsymbol{Q}^* \Lambda \boldsymbol{Q} \tag{4.12}$$

where $\boldsymbol{Q}$ is a matrix corresponding to the discrete Fourier transform (DFT) and Λ is a diagonal matrix containing the $\tilde{N}$ Fourier transform values for the sequence h_n that characterizes the channel.

In DMT, the transmit symbol vectors are generated by $\boldsymbol{x} = \boldsymbol{Q}^* \boldsymbol{X}$ where $\boldsymbol{X}$ is a frequency domain vector. The vector $\boldsymbol{X}$ corresponds to the vector $\boldsymbol{Z}$, which is the input of the IDFT modulator as explained in the previous section, but for convenience the variable name $\boldsymbol{X}$ has been used here instead and the complex elements of the vector $\boldsymbol{X}$ corresponds then to the QAM encoded data of each respective subchannel.

At the receiving end, the received symbol vector y (channel output) is demodulated by taking the Discrete Fourier Transform (which will be also explained in the next section) giving:

$$\boldsymbol{Y} = \boldsymbol{Q}\boldsymbol{y} = \boldsymbol{Q}(\boldsymbol{H}\boldsymbol{x} + \boldsymbol{n}) = \boldsymbol{Q}\boldsymbol{H}\boldsymbol{Q}^* \boldsymbol{X} + \boldsymbol{N} = \Lambda \boldsymbol{X} + \boldsymbol{N} \tag{4.13}$$

From the result obtained in equation 4.13, it can be seen that in the DMT system (as long as the length of the channel is less than the guard period), the channel output vector y behaves in the frequency domain as a simple element-by-element product of the DFT of the channel represented by the diagonal matrix Λ and the DFT of the transmitted signal X. Each DFT element (complex number) of the channel corresponds to a gain and phase distortion that would be then directly applied to the corresponding subchannel. In order to reverse the effect of the channel, a single coefficient equalizer per subchannel (FEQ) can then resolve the issue as explained in the following section.

However, in ADSL systems, the transmission channel length is higher than the guard period v. It can easily be over hundreds of coefficients depending of the loop length etc. (refer to section 4.5 for details). Consequently, the need of an equalizer such as a TEQ as explained in section 4.5.1 is required to shorten the length of channel to less than or equal to the length of the cyclic prefix. In practice, decreasing the length of the channel with a time-domain equalizer (TEQ) is simpler than trying to achieve an ISI-free channel.

4.4 DFT Demodulator

On the receiver side, the channel time-domain output samples are equalized with the time-domain equalizer, TEQ (refer to section 3.4). Each block of 544 samples ($\widetilde{N}+v$) is reduced to $\widetilde{N}=512$ samples by discarding the cyclic prefix represented by the CP Drop block as in Figure 4-5. Taking the output of the serial to parallel block, the demodulation is produced by the Discrete Fourier Transform (DFT):

$$Y_{i,k}=\sum_{n=0}^{\widetilde{N}-1} e^{\frac{-j2\pi\cdot n\cdot i}{\widetilde{N}}}\cdot y_k(n) \text{ for } i=0 \text{ to } \widetilde{N}-1 \tag{4.14}$$

In practice, the DFT is replaced by the Fast Fourier Transform (FFT). The DMT receiver has been implemented as in Figure 4-5. The sampling frequency (f_s) is at 2.208 MHz.

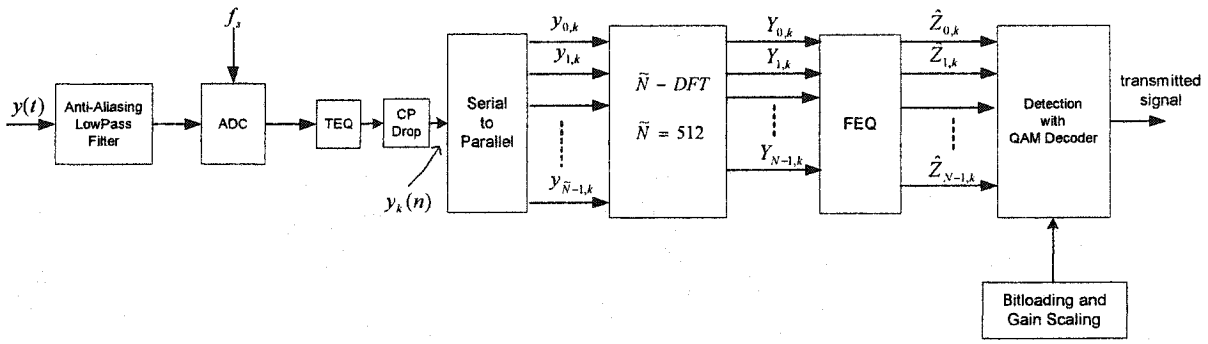

Figure 4-5: DMT receiver

The DFT of the time-domain samples brings back the frequency domain output $Y_{i,k}$. Only the first N=256 outputs (i = 0 to N) are kept due to the Hermitian symmetry as explained in section 4.2. $Y_{i,k}$ corresponds to the complex element of the respective subchannel i for the k^{th} DMT symbol transmitted. Each complex element of each subchannel is fed to the frequency-domain equalizer, FEQ (refer to section 4.5.2) giving $\hat{Z}_{i,k}$ followed by the detection module. The detection module is implemented with a maximum likelihood detector as in section 3.1.2. Once the detection has been completed, the inverse mapping is performed by the QAM decoder to recover the initial message transmitted. It should be noted that both the receiver and transmitter must have prior knowledge of the bitloading used as well as the gain scaling (refer to section 5.1) applied on each subchannel i during the data transmission.

4.5 Channel Equalization

In practice, the AWGN channel is not ideal and causes different attenuation and phase distortions over the frequency spectrum. As a result, successive symbol transmissions would most likely interfere with one another. The interference between successive transmissions is called Inter-symbol Interference (ISI). ISI can severely complicate the implementation of an optimum decoder. Therefore, the use of an equalizer will help combat ISI to obtain an AWGN channel that exhibits no ISI and, for instance, a lower complexity decoder as in section 3.1.2 can be implemented. ADSL DMT systems require some kind of equalization. The ADSL standard [ITU99] does not provide a specific implementation of the Time-domain Equalizer (TEQ) or the Frequency-domain Equalizer (FEQ) as in Figure 4-5.

4.5.1 TEQ

As mentioned previously in section 4.3, a cyclic prefix is used to eliminate inter-symbol interference between successive DMT symbols. The purpose of the equalizer, TEQ, is to shorten the length of the channel impulse response to less than or equal to the length of the guard period v, the cyclic prefix, before demodulation. Increasing the length of the cyclic prefix instead would perhaps help but meanwhile the channel throughput will be then reduced by a factor of $\widetilde{N} / (\widetilde{N} + \mathrm{v})$. One can also raise the number of subchannels N, and thus increase v to maintain the same performance loss. However, with larger N, the system would need more memory allocation, more delay and also additional coefficients for the Frequency-domain Equalizer (FEQ) (refer to section 4.5.2).

For the simulation, a non-adaptive FIR equalizer has been designed since prior knowledge of the channel impulse response is already known and the channel characteristics for the simulation have been kept constant over time. This thesis

emphasizes crosstalk cancellation (Chapter 8) and the need for an adaptive equalizer is not really necessary. The TEQ implemented as shown in equation 4.15 is a modified frequency inverse of the channel.

$$W_{TEQ}(f) = \frac{H^*(f)}{|H(f)|^2 + \beta} \tag{4.15}$$

β is a very small valued parameter to help compensate when $|H(f)|$ is near the noise floor. On longer loop lengths, at higher frequencies, the attenuation can be very high ($|H(f)|$ is small) and the output signal would be comparable to the noise floor, and therefore inverting $|H(f)|$ would be a pointless exercise. At those higher frequencies, the inverse $|W_{TEQ}(f)|$ would have a very high gain, which would in turn amplify unwanted noise. Its effect can be better seen when equation 4.15 is rearranged as follows:

$$W_{TEQ}(f) = \frac{1}{|H(f)| + \dfrac{\beta}{|H(f)|}} e^{j\angle H^*(f)} \tag{4.16}$$

In the equation above, if at a given frequency f_0, $|H(f)|$ is small and in the same range as β, then the denominator will be in the range of unity, and consequently $|H(f)|$ would remain approximately at unity. Therefore, at frequency f_0, no magnitude equalization would be performed.

Once $W_{TEQ}(f)$ has been designed, the IDFT has been performed on it to get the corresponding impulse response $w_{TEQ}(n)$. To equalize the channel distortion, the optimum theoretical equalizer impulse response should be non-causal. Hence, a causality delay has been introduced to make the TEQ equalizer causal and practical.

Theoretically, the product of $W_{TEQ}(f)$ with $H(f)$ should a give a unity magnitude frequency spectrum. However, the procedure of inverting the channel directly in the discretized frequency domain corresponds to a circular convolution in the time domain and not a linear convolution. Thus, only the circular convolution of $w_{TEQ}(n)$ with h(n) results to a unity magnitude in the frequency domain if β =0. When the linear convolution is taken, the magnitude frequency response is not totally flat because the equalizer $w_{TEQ}(n)$ obtained does not fully invert the channel as shown in Figure 4-6. Consequently, the design parameters for $w_{TEQ}(n)$ such as β, the numbers of coefficients, the delay, have to be chosen to produce an appropriate inverse at the frequencies where the transmitted signal has been distorted. The channel SNR has been calculated using equation 4.17 to verify the quality of the equalizer. It refers to the squared difference between a signal of unit magnitude and zero phase across the entire frequency band and the frequency response of the equalized channel obtained by the linear convolution of $h(n)$ and $w_{TEQ}(n)$. For this example, the equalizer has been adapted for a 15kft, 24-gauge twisted-pair channel and the channel SNR obtained is shown in Figure 4-7.

$$Channel\ SNR(i) = -10 \cdot \log(\{| FFT(Id(i)) - WH(i) |\}^2) \tag{4.17}$$

where the vector ***Id*** is the ideal delayed Dirac impulse response and $|WH(i)|$ represents the magnitude frequency response for the i^{th} tone (subchannel) of the equalized channel.

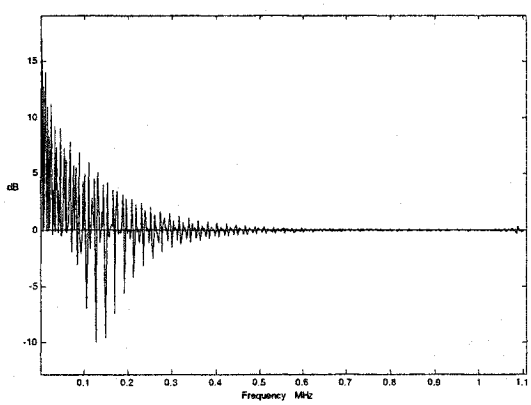

Figure 4-6: Magnitude frequency response of the linear convolution of $h(n)$ with $w_{TEQ}(n)$, with $\beta = 0$

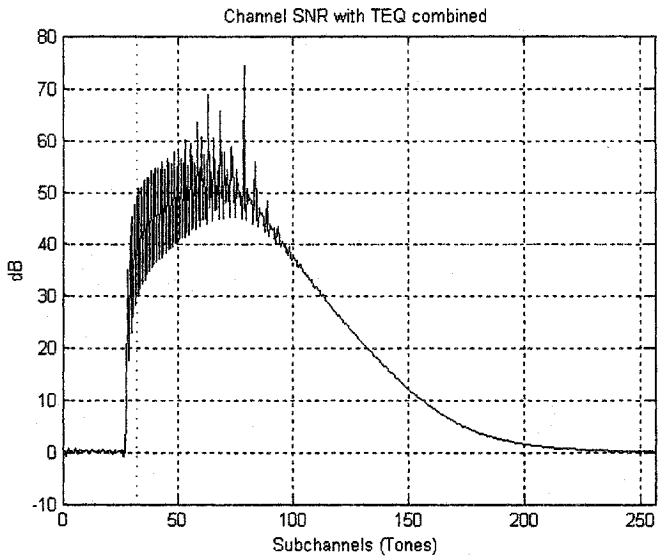

Figure 4-7: Example channel SNR

A high channel *SNR* is required at the frequencies (tones) assigned by the bitloading since only those tones have been used to transmit the information signal. For this example, tones from 35 to 113 have been assigned by the bitloading algorithm. Also, the lower frequencies have a low channel SNR because the equalizer has been purposely designed not to efficiently invert the lower frequencies for this example, therefore reducing the noise enhancement, since the equalizer increases the gain of the frequencies that have been attenuated by the channel but also simultaneously increases the noise at those same frequencies.

4.5.2 FEQ

The frequency-domain equalizer, FEQ, is performed after the FFT demodulation. If the guard period was sufficiently large (i.e. greater than the duration of the channel impulse response), then the FEQ would be only a single complex coefficient on each subchannel output after the demodulator. The FEQ deals with the different gains and phase delays

that the channel introduces over the different subchannels. Therefore, equalizing each subchannel output sample by multiplying with the corresponding complex coefficient will re-adjust the magnitudes and phase positions as in Figure 4-8.

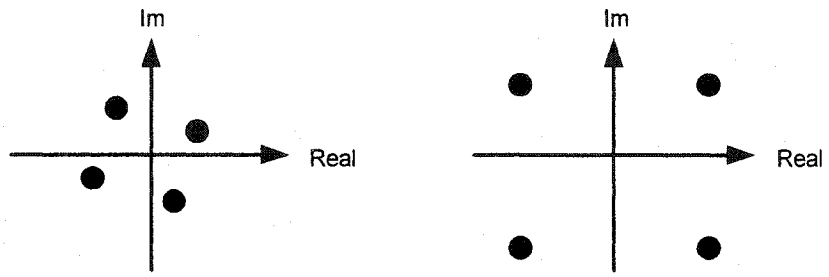

Figure 4-8: Example of a subchannel demodulator output before and after equalization with the corresponding complex coefficient.

The FEQ can be combined with the TEQ if needed to shorten the channel impulse response. If the TEQ is necessary, then the FEQ coefficients are the inverse of the equalized channel frequency response at tone i, $WH(i)$, as shown in equation 4.18.

$$W_{FEQ}(i) = \frac{1}{WH(i)} \tag{4.18}$$

where $W_{FEQ}(i)$ is the complex gain of the equalized channel frequency response for the i^{th} subchannel. The FEQ will be then applied as in Figure 4-9.

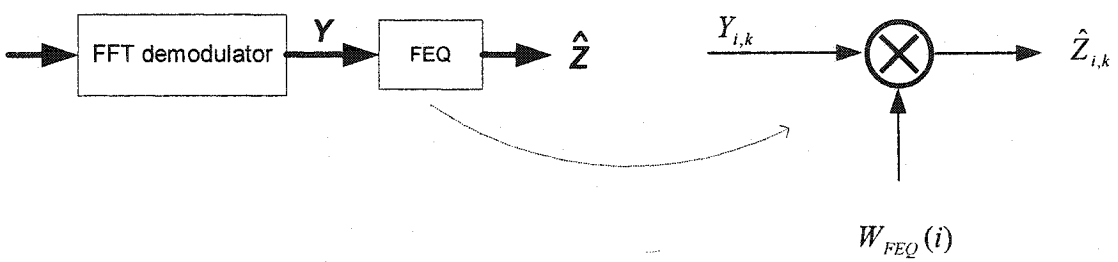

Figure 4-9: FEQ

If the channel SNR is quite high over the transmission tones, implying that the TEQ has reduced the channel memory substantially, then the combination of the implemented TEQ with the FEQ will only provide a slight improvement over the use of the TEQ alone.

Chapter 5

Bitloading and Gain

The two previous chapters discussed important aspects of the DMT modulation; this chapter concludes the discussion of DMT by explaining the gain scaling that can be applied to each tone individually, briefly talking about the scrambler and lastly describing the bitloading algorithm. The bitloading algorithm allocates the number of bits to assign to the available subchannels and consequently determining the QAM constellation size for each subchannel.

5.1 Gain Scaling

The simulation undertaken for this thesis considers the gain scaling as being the product of three gain factors: $G_{constellation,i}$, $G_{PSDlevel,i}$ and $G_{bitloading,i}$, hence,

$$g_i = G_{constellation,i} \times G_{PSDlevel,i} \times G_{bitloading,i} \tag{5.1}$$

The QAM encoder output of each subchannel i for the k^{th} DMT symbol is represented by a complex element $X_{i,k} + jY_{i,k}$ and adjusted via the gain scaling, g_i, resulting: $Z_{i,k}$ as shown in Figure 5-1.

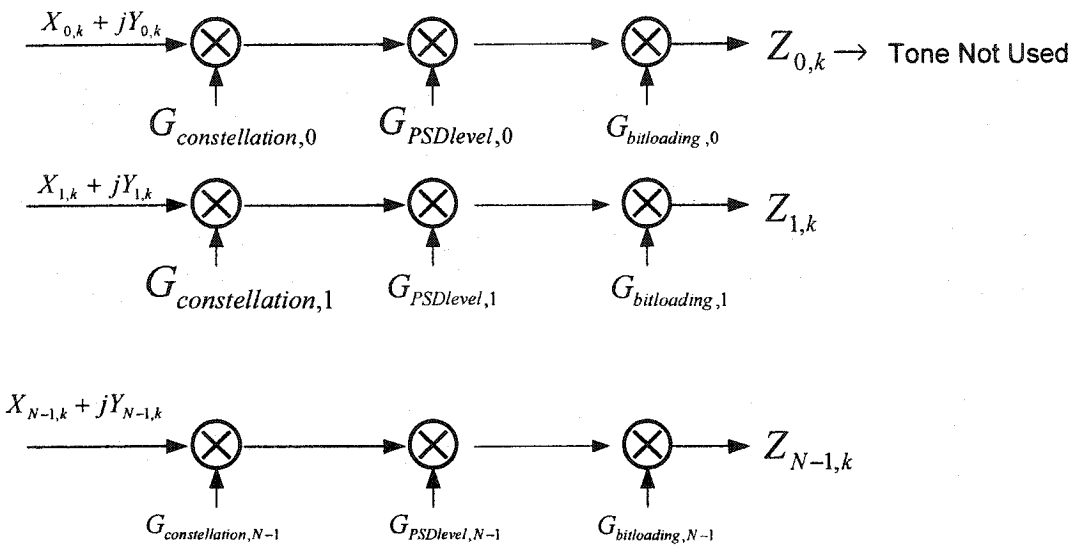

Figure 5-1: Gain Scaling

Each gain factor: $G_{constellation,i}$, $G_{PSDlevel,i}$ or $G_{bitloading,i}$, has a particular purpose:

- For $G_{constellation,i}$:

All QAM constellations regardless of their size have to be normalized to the same average energy. Each subchannel is assigned a constellation size set by the bitloading algorithm. $G_{constellation,i}$ is the gain factor to normalize the complex value to the same average energy of a reference constellation size. The average energy of each constellation for M = 2^2 to 2^{15} has been evaluated accurately using equation 3.3 in section 3.3 or equation 3.10 when b_i>2 and even. Also, the symmetry for odd-bit constellation for ADSL eases the calculations. The reference constellation taken is the 4-QAM constellation which has an average energy of 2. The normalization gain factor, $G_{constellation,i,}$ for all the ADSL constellation sizes has been calculated and shown in tables 5-1 and 5-2.

Table 5-1: Gain scaling for 2 to 8-bit constellations

#bits/const.	2	3	4	5	6	7	8
Avg. Energy (multiple of $d^2/2$)	1	3	5	10	21	41	85
$G^2_{constellation}$	1	1/3	1/5	1/10	1/21	1/41	1/85

Table 5-2: Gain scaling for 9 to15-bit constellations

#bits/const.	9	10	11	12	13	14	15
Avg. Energy (multiple of $d^2/2$)	165	341	661	1365	2645	5461	10581
$G^2_{constellation}$	1/165	1/341	1/661	1/1365	1/2645	1/5461	1/10581

- For $G_{PSDlevel,i}$:

During initialization, the ADSL standard [ITU99] specifies that the transmitted training sequence should have a power spectral density (PSD) of about – 40 dbm/Hz as shown in Figure 5-2.

In order to set the training sequence to have the specified PSD level, the following calculations have been made to find the magnitude of $G_{PSDlevel,i}$:

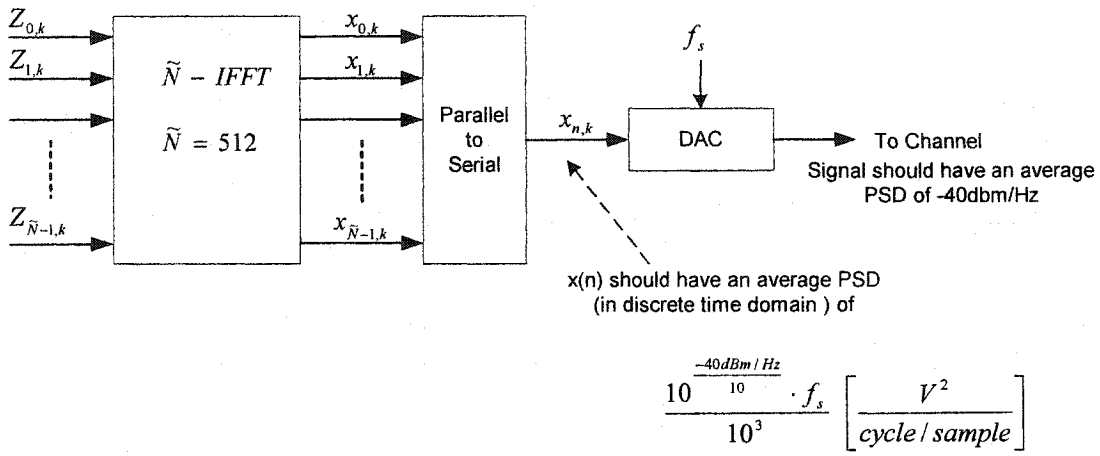

Figure 5-2: Simplified DMT modulation with initial PSD level output of – 40dbm/Hz

In order to have a power spectral density (PSD) output of – 40 dbm/Hz, with a sampling frequency, $f_s = 2.208\ MHz$, the sequence at the output of the IFFT modulator should also have a PSD of -40 dBm/Hz i.e. in discrete time domain of

$$\frac{10^{\frac{-40dBm/Hz}{10}} \cdot f_s}{10^3} \quad in \left[\frac{V^2}{cycle/sample}\right]$$

$$\text{with } PSD\ of\ x_{i,k} = \frac{|FFT(x_{i,k})|^2}{\tilde{N}}\ in \frac{V^2}{cycles/sample} \tag{5.2}$$

And considering that $FFT(x_{i,k}) = Z_{i,k}$ then,

$$Average\left\{\frac{|Z_{i,k}|^2}{\tilde{N}}\right\} = \frac{10^{\frac{-40dBm/Hz}{10}} \cdot f_s}{10^3} \quad in \left[\frac{V^2}{cycle/sample}\right]$$

and

$$\underbrace{Average\left\{G^2_{constellation,i}(X^2_{i,k}+Y^2_{i,k})\right\}}_{E_i}\cdot\frac{G^2_{PSDlevel,i}}{\widetilde{N}}=\frac{10^{\frac{-40\,dBm/Hz}{10}}\cdot f_s}{10^3}$$

From which, it can be found that:

$$G^2_{PSDlevel,i}\cdot E_i=\widetilde{N}\cdot\frac{10^{\frac{-40\,dBm/Hz}{10}}\cdot f_s}{10^3}$$

As a result:
$$G^2_{PSDlevel,i}=\widetilde{N}\cdot\frac{10^{\frac{-40\,dBm/Hz}{10}}\cdot f_s}{10^3\cdot E_i} \qquad (5.3)$$

Since all the QAM constellation sizes have already been normalized by $G_{constellation,i}$ then E_i in equation 5.3 can be replaced by the average energy of the reference QAM constellation (which is $E_i = 2$).

Figure 5-3 shows the PSD output from the IDFT modulator including the cyclic prefix (for more detail refer to section 4.3) generated by the simulation program. The transmitted signal was set to – 40dBm/Hz i.e. $Z_i = G_{constellation,i}\cdot G_{PSDlevel,i}\cdot(X_i + Y_i)$ with a PSD_{level} = - 40dBm/Hz.

The signal is defined only over a certain range of frequencies since for instance some the tones (subchannels) have not been used.

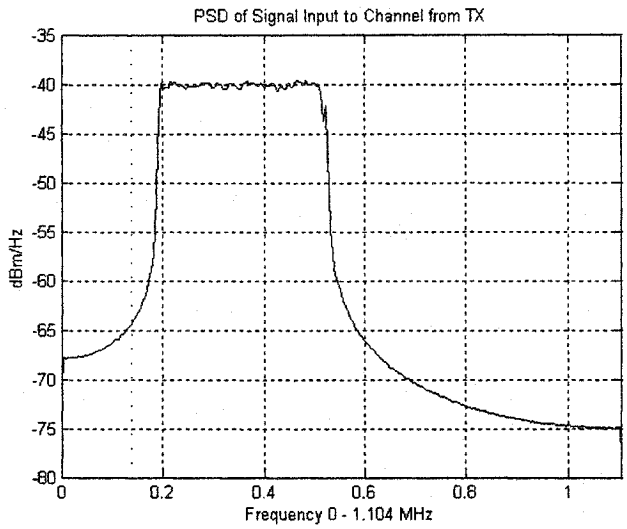

Figure 5-3: Signal PSD output from IDFT modulator with Cyclic Prefix added with PSD level set to – 40dBm/Hz

- $G_{bitloading,i}$ is the gain applied to adjust the power level of the transmitted signal using the bitloading algorithm (refer to section 5.3).

5.2 Scrambler

The scrambler is used to randomize the input bit stream in order to achieve an almost continuous spectrum and continuous spread of energy at the output [FER97]. Since binary sequences of zeros, ones or alternating sequences may occur in realistic data transfer more often that other sequences, it is convenient to make those events less probable because they may generate concentration of energy at a particular frequency causing interference problems. Equalizers and echo-cancellers often benefit from the use of a scrambler [STA99]. Also, for instance, the scrambler makes the data carried by each subchannel to be different (randomized) each time i.e. each subchannel will eventually carry data that cover all the possible constellation points with respect to the QAM constellation size assigned. Thus, an average PSD level of - 40dBm/Hz via the gain factor

$G_{PSDlevel,i}$ can be achieved since $G_{PSDlevel,i}$ is derived using the average energy of the QAM constellation for each subchannel i as shown in equation 5.3.

Figure 5-4 and Figure 5-5 show the scrambler [ITU99] and corresponding descrambler for ADSL used in the simulation. The descrambler was not provided by the ADSL standard but it was derived using a similar descrambler found in [FER97].

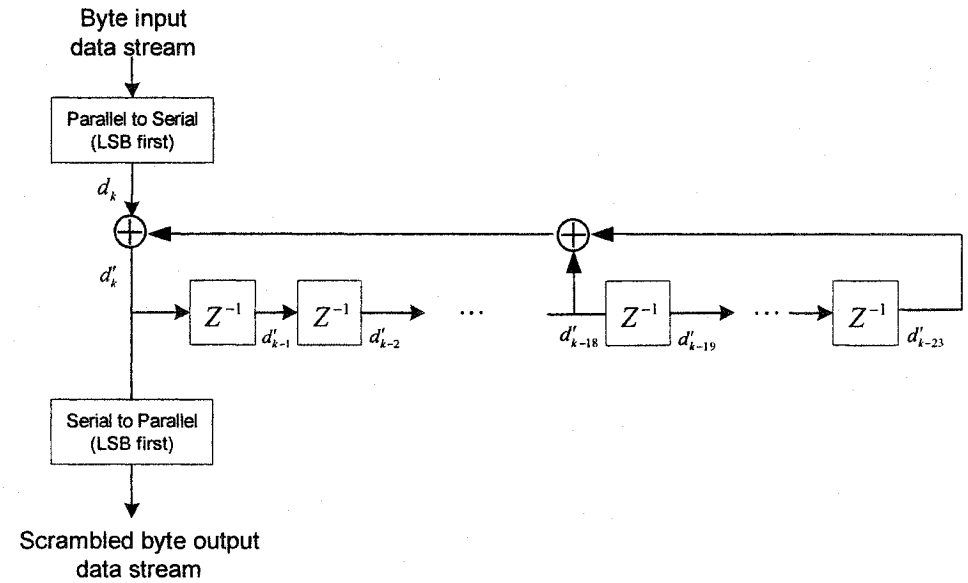

Figure 5-4: Scrambler for ADSL

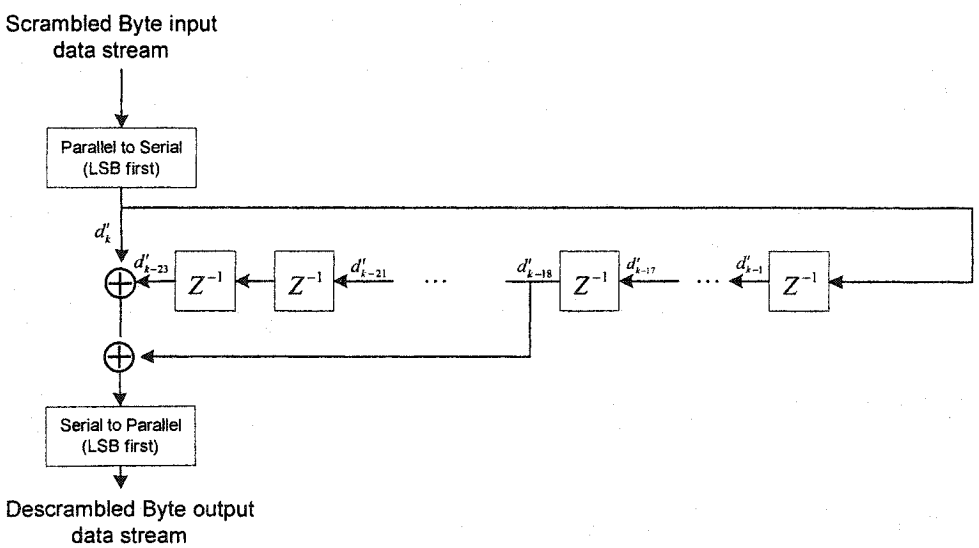

Figure 5-5: Descrambler for ADSL

5.3 Bitloading

A bitloading algorithm is the process of assigning the appropriate number of bits to each subchannel efficiently in a multichannel transmission such as DMT. The ADSL standard does not specify a bitloading algorithm. There are several approaches for bit loading algorithms for DMT applications found in [SONG02] [CAM99]. The choice of the appropriate algorithm depends on whether the transmission technology is total power limited or PSD limited [BIN00]. However, ADSL systems are PSD limited because it is necessary to limit the crosstalk (refer to Chapter 7) induced to other adjacent pairs in the same telephone bundle. PSD limitation implies that the maximum power used on each subchannel is restricted to the PSD mask imposed by the standardization committee. On the other hand, the total power limitation is the overall power allowed over all the carriers i.e. the entire available bandwidth.

For any of the two constraints, the number of bits allocated in each subchannel is chosen to achieve either a maximum data rate at a fixed BER or at a minimum BER for a defined data rate.

The bit loading algorithm chosen for the simulation is a modified version found in [KOU99], which introduces an iterative algorithm for assigning the appropriate number of bits b_i for each subchannel i, with the PSD limitation constraint.

5.3.1 SNR and Capacity

Since the transmission technology is FDD-ADSL and the downstream case is only considered in this thesis, the FDD-ADSL downstream PSD as in Chapter 2 has been used for the Power Spectral Density Mask (PSD).

Knowing the maximum allowable PSD for each subchannel, considered constant over the subchannel bandwidth, the SNR for each subchannel has been calculated as follows:

$$SNR(i) = \frac{PSD_{MASK}(i) \cdot |H(i)|^2}{PSD_{noise}(i)}$$

where: $PSD_{MASK}(i)$ is the FDD-ADSL PSD mask value at subchannel *i*.

$PSD_{noise}(i)$ is the aggregate power spectral density of all the channel impairments such as FEXT, NEXT, white Gaussian noise etc. for subchannel *i*.

$|H(i)|^2$ is the magnitude squared of the differential channel transfer function. at frequency corresponding to subchannel *i*.

The capacity is represented by the maximum number of bits, $C_{max}(i)$, per subchannel. The maximum number of bits that can be placed in the subchannel *i* is represented by $C_{max}(i)$. The capacity of bits per subchannel, $C_{max}(i)$, can then be calculated, which includes the SNR gap:

$$C_{\max}(i) = \left\lfloor \log_2\left(1 + \frac{SNR(i)}{\Gamma}\right) \right\rfloor$$

where: $\Gamma = 9.8$ dB $+ \gamma_m$ dB $- \gamma_c$ dB

the brackets $\lfloor \ \rfloor$ indicate the integer part

Since only Reed-Solomon coding (refer to Chapter 3) has been used, then the coding gain is about $\gamma_c = 3.6$ dB and the margin, γ_m, taken is 6 dB since DSLs are designed with a 6 dB SNR margin [UDSL].

Having a selected bitrate *R*, the total number of bits *K* to be assigned to the subchannels, is then $K = \frac{R \cdot 544}{f_s}$ since $\tilde{N} + v = 544$ samples are transmitted at $f_s = 2.208\,MHz$.

5.3.2 Bitloading Algorithm

The algorithm calculates the incremental power spectral density, $PSD_{inc}(i)$, required to transmit an additional bit on each subchannel. The subchannel with the minimum incremental power is assigned the additional bit by increasing its current bit load, $b(i) = b(i) + 1$, as long as $b(i)$ is less than the total capacity $C_{\max}(i)$ for the corresponding subchannel. The algorithm repeats until there are no more bits to place. The maximum number of bits to be assigned is restricted by the minimum between K and $\sum_{i=0}^{N-1} C_{\max}(i)$.

The incremental PSD, $PSD_{inc}(i)$, essentially scales the inverse of the subchannel $SNR(i)$ and is defined as:

$$PSD_{inc}(i) = \frac{PSD_{mask}(i) \cdot \Gamma}{SNR(i)} (2^{b_i+1} - 1) = \frac{PSD_{noise}(i) \cdot \Gamma}{|H(i)|^2} (2^{b_i+1} - 1)$$

Thus, the higher $SNR(i)$, the lower is $PSD_{inc}(i)$. Subchannels with high $SNR(i)$ have more bits allocated to them as long as their capacity is not exceeded. Figure 5-6 illustrates the bitloading algorithm flow chart.

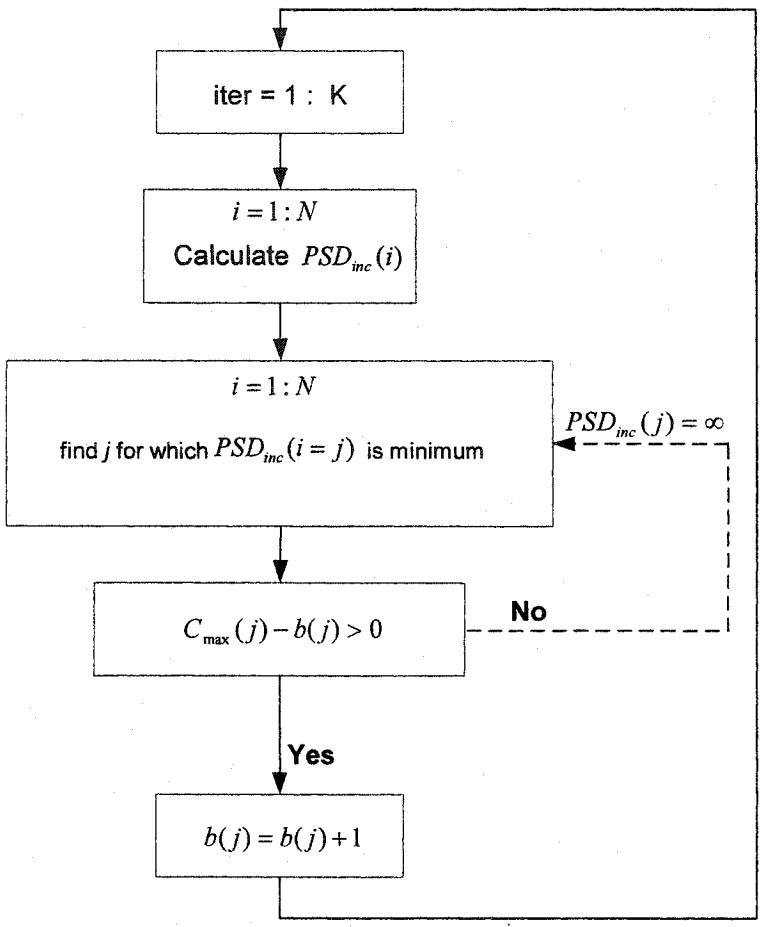

Figure 5-6: Bit allocation algorithm flow chart

It should be noted that the ADSL standard [STA99] specifies that the number of bits per subchannel cannot exceed 15 and the subchannels cannot carry a single bit. Consequently, if $C_{max}(i) > 15$ then $C_{max}(i) = 15$ and if $C_{max}(i) < 2$ then $C_{max}(i) = 0$.

In addition, depending on the DSL transmission technology, some subchannels are not used. For example, for FDD-ADSL, the downstream transmission from the central office to the customer premises does not use the first 32 subchannels, the algorithm is quite flexible by just imposing $C_{max}(i)_{i=0}^{31} = 0$ as an initial constraint.

Once the bit allocation is completed for the first time, some subchannels may only have a single bit assigned to them i.e. $b(i) = 1$. However, as mentioned above, the standard does not allow a single bit constellation. To resolve that, each bit from each single-bit subchannel is reallocated to another subchannel one at the time. For instance, the first subchannel i carrying a single bit will not be used by setting $C_{\max}(i) = 0$ and the bitloading algorithm is executed again in order to reallocate the bit to another subchannel. The same steps are undertaken for the next subchannel carrying a single bit. The algorithm is repeated until all the single-bit subchannels have been reallocated.

As an example, Figure 5-7 shows the $SNR(i)$ obtained using a downstream FDD-ADSL PSD mask over a 15kft 24-gauge transmission channel with some crosstalk noise. Figure 5-8 illustrates the bitloading allocation obtained for the subchannels corresponding to the downstream FDD-ADSL transmission at 1.5Mb/s. It can be noticed that only the subchannels from 45 to 126 have been used and the tone number 64 is not used since ADSL uses it as a pilot tone [ITU99]. The bit allocation is consistent with the $SNR(i)$ since higher number of bits has been allocated to subchannels with high SNRs.

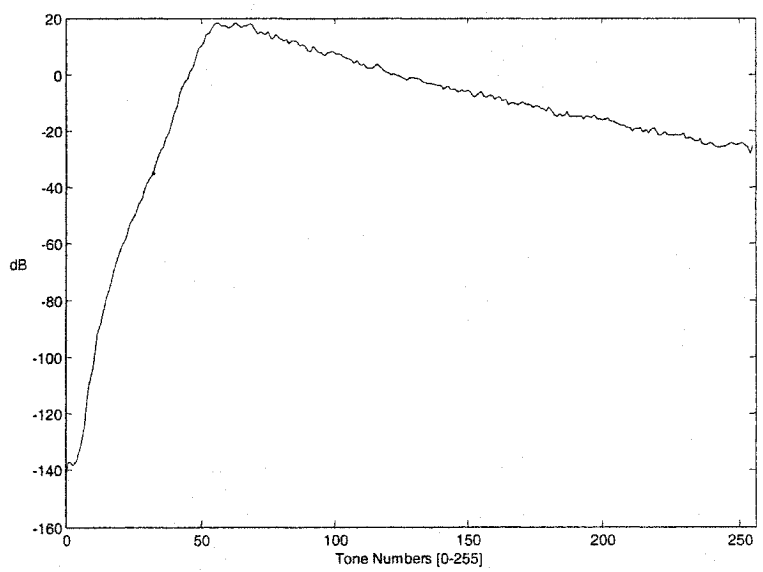

Figure 5-7: SNR per subchannel (*SNR(i)*)

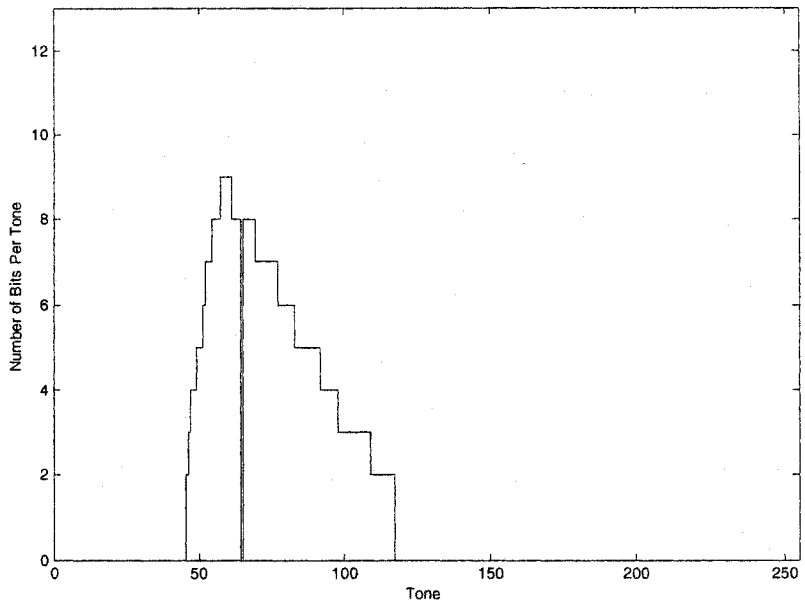

Figure 5-8: Bitloading allocation example for an FDD-ADSL transmission at 1.5Mb/s

5.3.3 Bitloading Gain Factor

Once all the bits have be allocated to the corresponding subchannels, the minimum required PSD signal to transmit the allocated bits for each subchannel i, $PSD_{subchannel}(i)$, is evaluated as follows:

$$PSD_{subchannel}(i) = \frac{PSD_{noise}(i) \cdot \Gamma}{|H(i)|^2} \cdot (2^{b_i} - 1)$$

As mentioned previously, during initialization, the power of the transmitted signal training sequence is set to – 40 dBm/Hz by the gain factor $G_{PSDlevel,i}$ for each subchannel. The initial - 40dBm/Hz PSD level for each subchannel can be increased, decreased or maintained depending on $PSD_{subchannel}(i)$ and is adjusted by the 3rd and last gain factor implemented, that is the bitloading gain factor $G_{bitloading,i}$.

From the bitloading algorithm, if the PSD of the i^{th} subchannel, $PSD_{subchannel}(i)$, is lower than - 40 dBm/Hz then, $G_{bitloading,i} = 1$, thus, the PSD of the i^{th} subchannel remains the same at – 40 dBm/Hz, according to static spectrum management [SML01].

If $PSD_{subchannel}(i)$ is higher than –40dBm/Hz, the subchannel PSD signal should be increased by 2.5dB [ITU99], thus $G_{bitloading,i} = \sqrt{10^{2.5/10}}$.

If – 40dBm/Hz is higher than $PSD_{MASK}(i)$, then the subchannel PSD signal is decreased to the $PSD_{MASK}(i)$, thus $G_{bitloading,i} = \sqrt{\frac{PSD_{MASK}(i)}{10^{\frac{-40}{10}}}}$.

Chapter 6

Twisted Pair Transmission Line Modeling

DSL systems use the existing telephone lines to transmit the data signal over the copper twisted-pair line. The two copper wires of a telephone lines are named Tip and Ring and the useful DSL signal is transmitted in differential mode. Differential mode signal transmission is when the Tip and Ring have equal but inverted voltage amplitudes, where both the Tip and Ring voltages are measured to ground. To get a better understanding of the different propagation modes on the twisted-pair line, this chapter starts by giving a brief explanation of the two modes of propagation, the differential and common modes, and their interaction. It then details the model for the differential mode propagation using two-port theory, and follows by elaborating a common-mode model derived from the differential mode model.

6.1 Propagation Mode Introduction

To produce a differential mode signal in the telephone line i.e. over the twisted-pair wires, the telephone system contains a hybrid circuit. A hybrid circuit is used to remove the voice signal echo from the duplex signal transmission. However, in order to transmit the desired signal in differential mode, each hybrid circuit contains a transformer on both ends, at the transmitter side and at the receiver side at the end of the transmission line. A simplified transmission system as in Figure 6-1 is shown to illustrate the differential current flow.

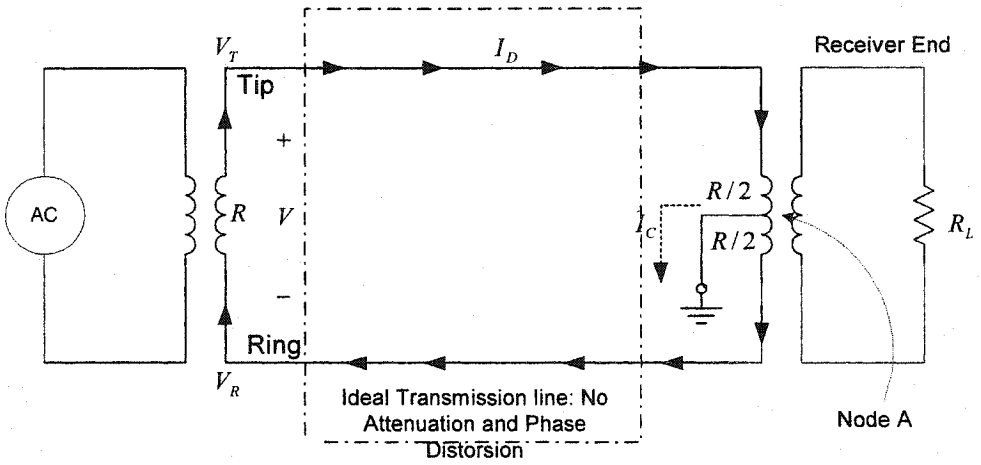

Figure 6-1: Simplified transmission system.

V_T is the voltage between Tip and ground and is the equal to $\frac{+V}{2}$, V_R is the voltage between Ring and ground and is equal to $\frac{-V}{2}$, resulting in a differential voltage V. The differential current is: $I_D = \frac{V_T - (V_R)}{R} = \frac{V}{R}$ where R is the reflected impedance R_L.

Without any source of noise, the common mode signal that is defined as being the average of the Tip and Ring wires would yield a null voltage. Therefore, the common mode current I_C is zero, which is easily verified by Kirchoff's current law at node A, the centre tap:

$$I_C = \frac{V_T - 0}{R/2} + \frac{V_R - 0}{R/2} = \frac{2}{R}[V + (-V)] = 0$$

In a telephone bundle, there are a certain number of telephone lines (twisted-pair wires) grouped together and each line is dedicated to a specific subscriber. Each line in use generates an electromagnetic field causing interference on other adjacent lines. This form of interference is called Crosstalk (Chapter 7). An additional current due to the electromagnetic field is induced on each wire of the pair of the subscriber's line creating

an undesired crosstalk signal. Each wire of the line, Tip and Ring, are tightly twisted together to allow any external noise such as crosstalk coming from adjacent twisted-pair lines located in the same bundle to couple with the line equally on both Tip and Ring wires. The coupling can be over a small portion of the line or the entire line.

As a simplified example shown in Figure 6-2, I_N is the crosstalk current signal induced on each wire of the pair since the pair is tightly twisted together. In an ideal case, a perfectly balanced line, results in an unchanged desired differential signal passed to the receiver and the differential current I_D would remain the same as in Figure 6-1.

$$V_N = I_N \cdot \frac{R}{2}$$

$$I_D = \frac{[V_T + V_N] - [V_R + V_N]}{R} = \frac{[\frac{V}{2} + V_N] - [-\frac{V}{2} + V_N]}{R} = \frac{V}{R}$$

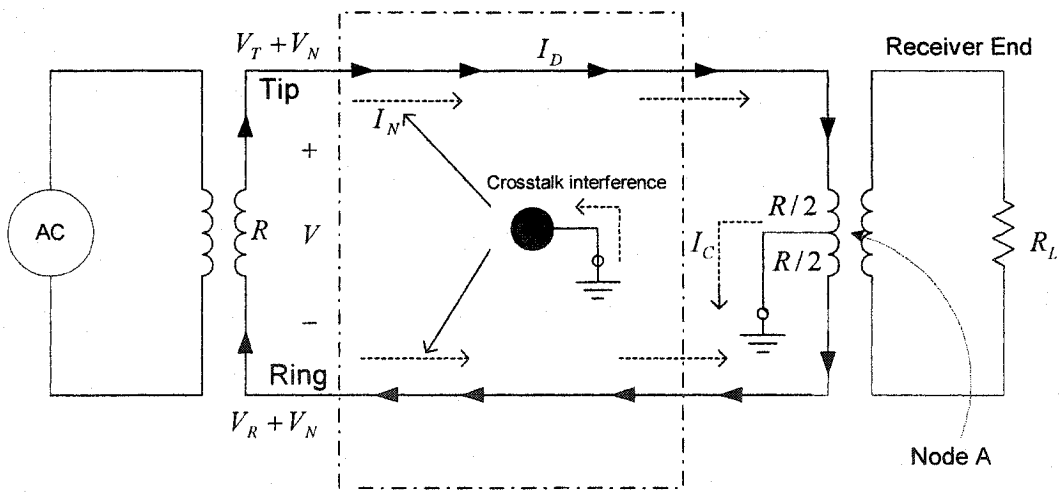

Figure 6-2: simplified circuit with crosstalk interference

However, with the presence of noise, the common mode signal will not be null anymore. The common mode current would be then:

$$I_C = \frac{[V_T + V_N] - 0}{R/2} + \frac{[V_R + V_N] - 0}{R/2} = \frac{4 \cdot V_N}{R}$$

Unfortunately, in practice, the lines are not perfectly balanced, causing the common mode signal to leak into the differential mode and therefore corrupting the desired differential signal intended to/from the customer, as explained in the next section.

It should noted that from Figure 6-2, the conceptual way to extract the common mode signal from the twisted pair transmission line would be the average of Tip and Ring signals [SHE03] as shown in Figure 6-3.

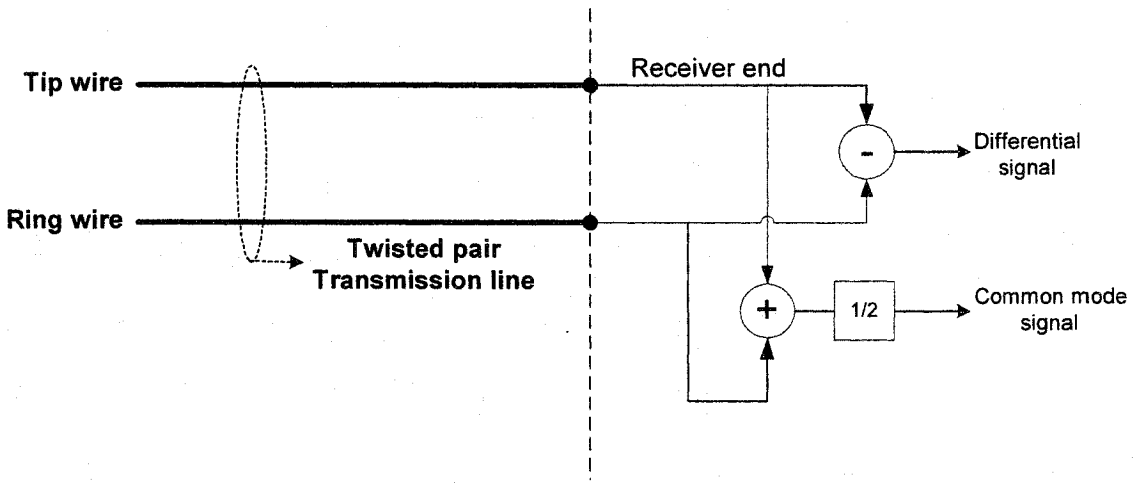

Figure 6-3: Differential and common mode signal extractions

However, the twisted pair cannot be considered ideal and therefore conforms to transmission line theory, having attenuation loss, phase distortions and reflections. In this case, the transmission line requires proper termination in differential mode and common mode to be able to efficiently extract both these signals from the twisted pair transmission line at the receiver end. This chapter is dedicated to modeling a twisted pair in both differential and common mode taking the above limitations into account. An example circuit to terminate the line and extract both signals is shown in [COO93].

6.2 Transmission Line Balance

As mentioned above, if the line (copper twisted-pair) was perfectly balanced and tightly twisted, then the desired differential signal intended for the subscriber would be barely affected with the presence of crosstalk noise. The term "balance" for a transmission line refers to the capacity to prevent differential signals from coupling (leaking) into the common mode and also the corresponding common mode signals from leaking into the differential mode [STA99].

Various factors can affect the transmission line balance such as the impedance imbalances to ground along the two wires of the pair, the number of twists per unit length, and the transmitter and the receiver hybrid circuits design [LAO02][COM98].

Therefore, along the transmission line, the signal traveling towards the receiver could encounter one or more major imbalance points and then could leak into the common mode and also a signal traveling in common mode could leak into the differential mode.

In the presence of noise, since the noise mostly couples in common mode [COM98], then a common mode current is induced on each wire of the pair, which corresponds to the crosstalk signal (i.e. common mode signal) that could leak into the differential mode if one or more imbalance points are encountered. Consequently, the original differential signal transmitted is corrupted by this unwanted crosstalk signal.

It is difficult to find mathematical models for a transmission line balance. [STA99] proposed a model for Category 3 twisted-pair lines. The magnitude of the balance is a function of the frequency and is defined as follows:

$$B(f) = \begin{cases} \sqrt{10^5} & 0 \le f < 150\,kHz \\ \sqrt{10^5 \cdot \left(\dfrac{150\,kHz}{f}\right)^{1.5}} & 150kHz \le f \le 30\,MHz \end{cases} \tag{6.1}$$

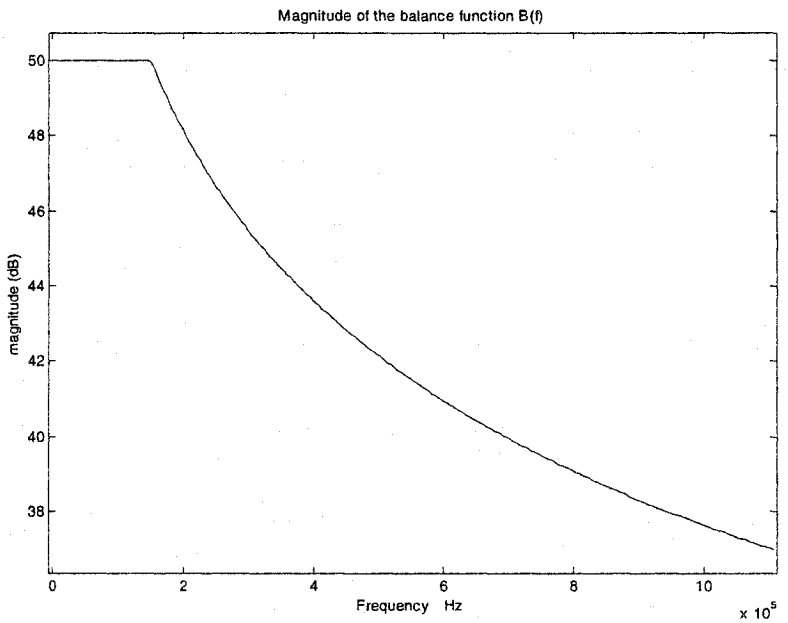

Figure 6-4: Magnitude of the balance function *B(f)*

The magnitude of the balance function has been used to represent the degree of attenuation when a signal traveling in one mode is coupled (leaked) to the other mode. Thus, a signal traveling in differential mode is attenuated by *B(f)* when coupled to common mode or a signal traveling in common mode such as an induced crosstalk signal is attenuated by *B(f)* when leaking into the differential mode. As mentioned previously, the signal can encounter one or more imbalance points along the transmission line. In this model, *B(f)* is assumed to be the resulting magnitude of the transfer from one mode to the other This means that *B(f)* will be applied at the receiver end on the received signal in one mode to get the corresponding signal that coupled (leaked) into the other mode.

It can be seen from the plot of $B(f)$ as in Figure 6-4, that as the frequency increases, the magnitude of the signal leaking from one mode to another is higher, implying that at high frequencies, the line balance gets poorer .

6.3 Differential Mode Channel Model

Major problems in data transmission such as DSL are the physical line impairments. It is essential to define the characteristic of a twisted-pair line in order to find a realistic channel transfer function to model the attenuations and phase distortions degrading the transmitted data signal.

6.3.1 Twisted-Pair Equivalent Circuit

A copper twisted-pair line is considered as a two-conductor transmission line that can be described with the following equivalent circuit [CHE92] as in Figure 6-5.

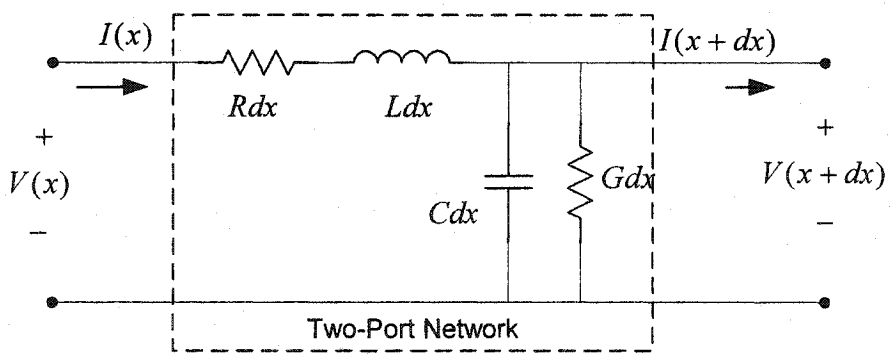

Figure 6-5: Equivalent twisted-pair transmission line

The circuit corresponds to a per-unit incremental section of a twisted-pair transmission line characterized by four parameters:

R: the resistance per unit length in Ω/m
L: the inductance per unit length in H/m
G: the conductance per unit length in S/m
C: the capacitance per unit length, in F/m

R and L are series elements and G and C are shunt elements. The quantities $V(x)$ and $V(x+dx)$ are the voltages at distance x and $x + dx$, $I(x)$ and $I(x+dx)$ denote the currents at distance x and $x + dx$ where dx corresponds to the differential incremental section of the transmission line. All the parameters: R, L, G and C are frequency-dependent as: $R(f)$, $L(f)$, $G(f)$ and $C(f)$ and consequently all the derived quantities from these parameters are frequency-dependent.

Applying Kirchhoff's voltage law and current law to the incremental section of Figure 6-5, fundamental results and equations can be derived [CHE92].
The impedance per unit length is:

$$Z = R + j\omega L \qquad \text{where } \omega = 2\pi f$$

The admittance per unit length is:

$$Y = G + j\omega C$$

At any given frequency, the propagation constant γ can be derived. It characterizes the segment of the transmission line.

$$\gamma = \alpha + j\beta = \sqrt{(R + j\omega L)\cdot(G + j\omega C)} = \sqrt{Z \cdot Y} \qquad (\text{m}^{-1})$$

The real part of the propagation constant γ is called the attenuation constant α in Np/m and the imaginary part β is called the phase constant in rad/m of the transmission line. The ratio of voltage and current at any distance d is called the characteristic impedance of the line:

$$Z_0 = \sqrt{\frac{R + j\omega L}{G + j\omega C}} = \sqrt{\frac{Z}{Y}} \qquad (\Omega)$$

The characteristic impedance depends only on R, L, G, C and the frequency ω but it is not a function of the length of line.

6.3.2 Two-Port Model

Having those fundamental results, the electrical properties of a transmission line at a given frequency can be fully characterized by a two-port model [STA99] as in Figure 6-6:

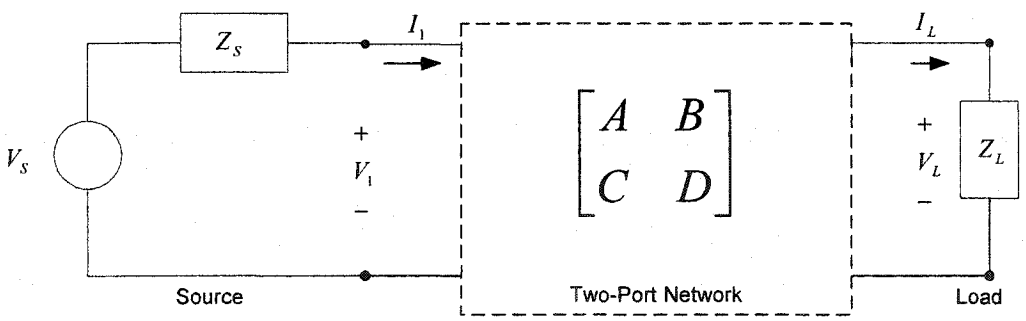

Figure 6-6: Two-Port Model

where $$\begin{bmatrix} A & B \\ C & D \end{bmatrix} = \begin{bmatrix} \cosh(\gamma d) & Z_0 \sinh(\gamma d) \\ \frac{1}{Z_0}\sinh(\gamma d) & \cosh(\gamma d) \end{bmatrix}$$

The two-port model representation is defined as:

$$\begin{bmatrix} V_1 \\ I_1 \end{bmatrix} = \begin{bmatrix} A & B \\ C & D \end{bmatrix} \begin{bmatrix} V_L \\ I_L \end{bmatrix} = \Phi \cdot \begin{bmatrix} V_L \\ I_L \end{bmatrix} \tag{6.2}$$

or in another form: $V_1 = AV_L + BI_L$

$$I_1 = CV_L + DI_L$$

where V_1, I_1 are the voltage and current at the transmitter end of the transmission line and V_L, I_L are the voltage and current at the receiver end for a given frequency f and a loop length d i.e. from $x = 0$ to $x = d$. Therefore, V_1, I_1, V_L and I_L are the short forms for: $V_1(f,d), I_1(f,d)$ $V_L(f,d)$ and $I_L(f,d)$ respectively.

Note that the four frequency-dependent parameters A, B, C and D depend only on the network and not on external connections. The voltage and currents are dependent on the voltage source V_s and the load impedance R_L but the matrix relationship shown in (6.2) always remains valid.

Using the matrix relationship in (6.2), the following transfer function can be found for a given frequency f and a loop length d:

$$H(f) = \frac{V_L}{V_1} = \frac{V_L}{AV_L + BI_L} = \frac{1}{A + B\dfrac{I_L}{V_L}}$$

since $Z_L = \dfrac{V_L}{I_L}$ then:

$$H(f) = \frac{Z_L}{AZ_L + B} \tag{6.3}$$

The magnitude of $H(f)$ represents the attenuation of the transmission line versus the frequency, also called the insertion loss.

In a transmission line, the optimum value for load impedance Z_L (meaning that half the power is transferred to the load) is found to be the conjugate of the characteristic impedance Z_0 of the transmission line as [CHE02]:

$$Z_L = Z_0^* \tag{6.4}$$

An overall transfer function $T(f)$ as shown in equation 6.5 can be found between the voltage supply $V_s(f)$ (with corresponding internal impedance Z_s) and the output voltage V_L.

$$T(f) = \frac{V_L}{V_s} = \frac{V_L}{V_1} \cdot \frac{V_1}{V_s} = \frac{Z_1}{Z_1 + Z_s} H(f) \tag{6.5}$$

with $Z_1 = \frac{V_1}{I_1}$ the input impedance of the terminated two-port

However, in practice, equation (6.3) is mostly used since it uses the voltage at the transmitter output and not the voltage at the source. The requirements of a communication system are often towards the voltage level or power level restriction at the transmitter end, on V_1 regardless of the voltage source V_s.

Furthermore, more complicated network models can be determined. If a two-port model is found for each subsection and each subsection is in a cascade form then a global two-port system can be derived. The cascade of several two-port systems is the matrix product of everyone of them in following manner:

$$\begin{bmatrix} V_1 \\ I_1 \end{bmatrix} = \Phi_1 \cdot \Phi_2 \cdot \Phi_3 \cdots \Phi_{M-1} \begin{bmatrix} V_M \\ I_M \end{bmatrix} = \Phi \cdot \begin{bmatrix} V_M \\ I_M \end{bmatrix}$$

where M is the last two-port subsection of the transmission line and Φ is the resulting two-port model.

6.3.3 *R, L, C, G* Parameters

As mentioned previously, a twisted-pair transmission is characterized by the set of parameters: *R*, *L*, *C*, *G*. All the parameters are a function of frequency. The *R, L, C, G* parameters used have been taken from VDSL system requirements contributions of ANSI [VAL97].

Resistance equation:

-For a 26-gauge twisted-pair:

$$R(f) = \sqrt[4]{286.17578^4 + 0.1476920 \cdot f^2} \qquad \Omega/\text{km}$$

-For a 24-gauge twisted-pair:

$$R(f) = \sqrt[4]{174.55888^4 + 0.053073481 \cdot f^2} \qquad \Omega/\text{km}$$

Figure 6-7 illustrates the resistance versus the frequency in differential mode for the 26-gauge wire.

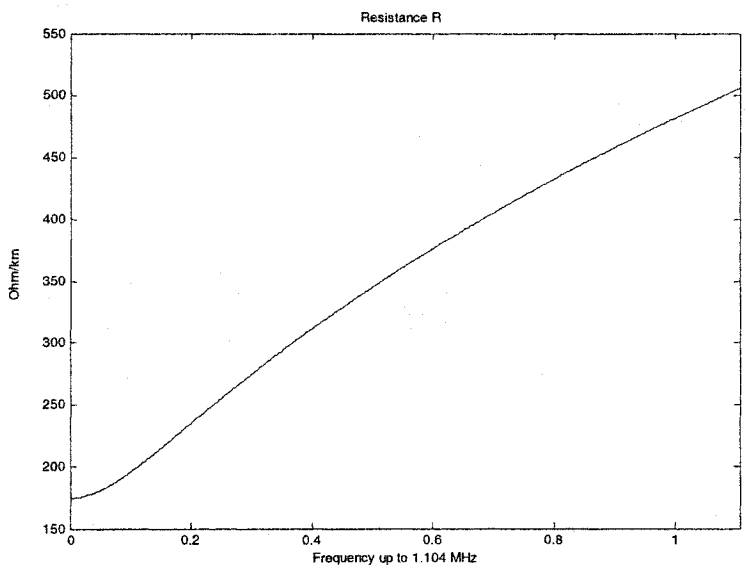

Figure 6-7: *R* vs frequency with 26-gauge wire

The high frequency content of the signal propagating through the copper wire, the skin effect makes the signal current flow mostly near the outer surface of the copper wire. So the resistance increases significantly as the frequency increases leading to stronger loop attenuations at high frequencies [COM98]. Also, a smaller wire diameter (higher wire gauge) implies an increase of the resistance *R*.

Inductance equation:

-For a 26-gauge twisted-pair:

$$L(f) = \frac{675.36888 + 488.95186 \cdot \left(\frac{f}{806.33863}\right)^{0.92930728}}{1 + \left(\frac{f}{806.33863}\right)^{0.92930728}} \quad \mu H/km$$

-For a 24-gauge twisted-pair:

$$L(f) = \frac{617.29539 + 478.97099 \cdot \left(\frac{f}{553.760}\right)^{1.1529766}}{1 + \frac{f}{553.760}\right)^{1.1529766}} \quad \mu H/km$$

Figure 6-8 illustrates the inductance versus the frequency in differential mode for the 26-gauge.

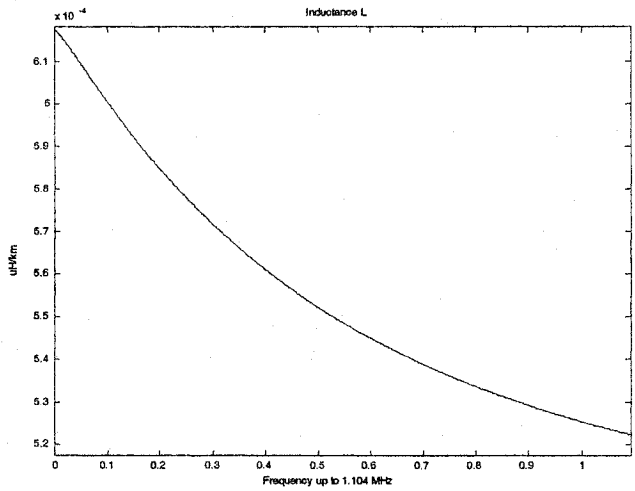

Figure 6-8: *L* vs frequency with a 26-gauge wire

The inductance is mostly a function of the distance between the wires, the diameter of the wire and the frequency. As the frequency increases, the inductance diminishes because of the skin effect.

The capacitance for the 26-gauge and 24-gauge AWG twisted-pairs are constant over all the frequencies: C = 49nF/km and C = 50nF/km respectively since the capacitance is mostly a function of the dielectric medium and the distance between the two wires.

Conductance equation:

-For a 26-gauge AWG twisted-pair:

$$G(f) = 43 \cdot f^{0.7} \qquad \text{nS/km}$$

-For a 24-gauge AWG twisted-pair:

$$G(f) = 234.87476 \cdot f^{0.7} \qquad \text{nS/km}$$

The effect of the conductance on the attenuation is much less pronounced than the effect of the resistance R [COM98].

6.3.4 Channel Transfer Function

Having the *RLCG* parameters defined in section 4.4.3 for the 24-gauge and 26-gauge twisted-pair transmission lines, the *ABCD* parameters for each two-port model for any frequency and loop length can then be determined. However, to get the impulse response of each channel, the load impedance, Z_L, has to be determined.

As mentioned in section 4.4.2, the characteristic impedance Z_0 is independent of the loop length. Figure 6-9 shows the magnitude of the characteristic impedance Z_0 for the 26-gauge and 24-gauge.

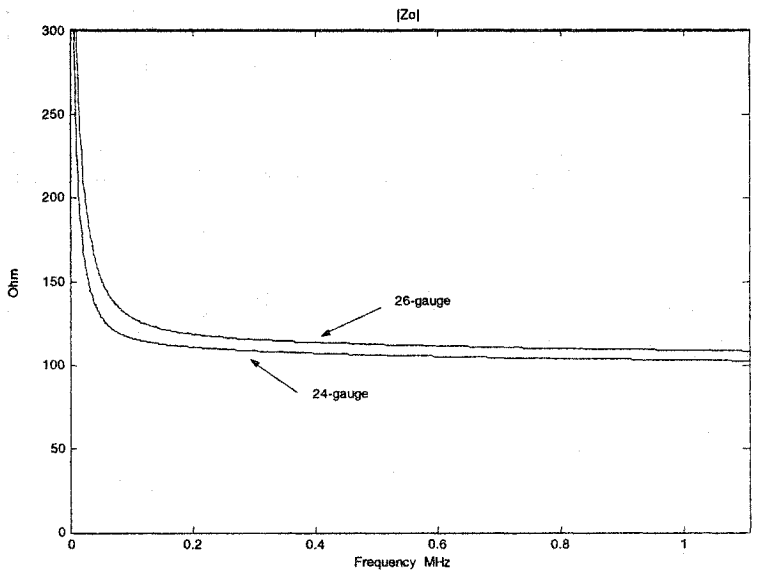

Figure 6-9: Magnitude of the characteristic impedance Z_0 for 26 and 24 gauges

Also, as the frequency increases(>250 kHz), the *R* and *G* parameters become negligible, the characteristic impedance Z_0 as in section 6.3.1 is then dominated by the reactive parameters, therefore, Z_0 can be approximated by [STA99]:

$$Z_0 \cong \sqrt{\frac{L}{C}} \tag{6.6}$$

The plot of $Z_0 \cong \sqrt{\frac{L}{C}}$ and the magnitude plot of Z_0 as in Figure 6-9 become very comparable for frequencies higher that 250 kHz. Z_0 becomes then resistive, so as for the simulation, looking at Figure 6-9, Z_0 varies between 100 Ω and 110 Ω, the load impedance, Z_L, chosen is 100 Ω. The simulation was set purposely not to adapt to a specific optimum load impedance for a specific transmission line as explained in section 4.3.2 since realistically, ADSL transceivers (modems) do not have a load impedance matching the characteristics for every particular transmission lines that they are connected to. Therefore, the value of 100 Ω has been chosen to be a compromise between the 26-gauge and 24-gauge. Also, this value has been chosen because most US cables have an impedance of 100 Ω [STA99].

Finally, having Z_L and the two-port models defined, the respective channel transfer functions $H(f)$ using equation 6.3 can be then calculated. The magnitude of a transfer function gives the attenuation (insertion loss) versus frequency of the transmission line as in Figure 6-10 for a 5 kft AWG 26-gauge loop and for a 15 kft AWG 24-gauge loop respectively.

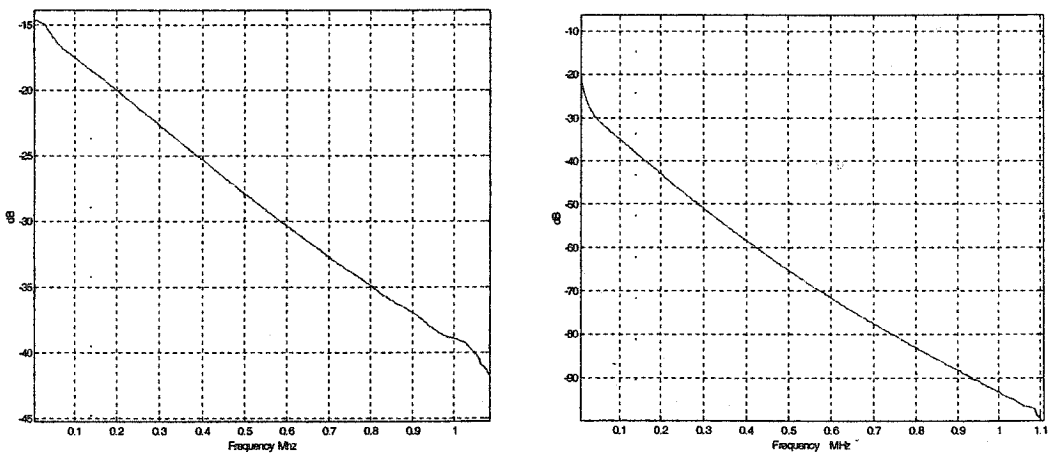

Figure 6-10: Insertion Losses for 26-gauge 5kft (left) and 24-gauge 15kft (right) differential channels

It can be seen that the longer the loop length, the higher the attenuation, and also high frequencies are much more attenuated than the low frequencies. The bitloading will most likely not assign any bits to tones located at frequencies higher than 700kHz for the 15kft loop because the transmitted signal on those tones would be attenuated by over 80 dB.

In order to find the impulse response of each channel, the complex conjugate values of $H(f)$ defined up to half of the sampling frequency (f_s = 2.208Mhz), have been appended to get Hermitian symmetry and by taking the IDFT yields a real impulse response as shown in Figure 6-11.

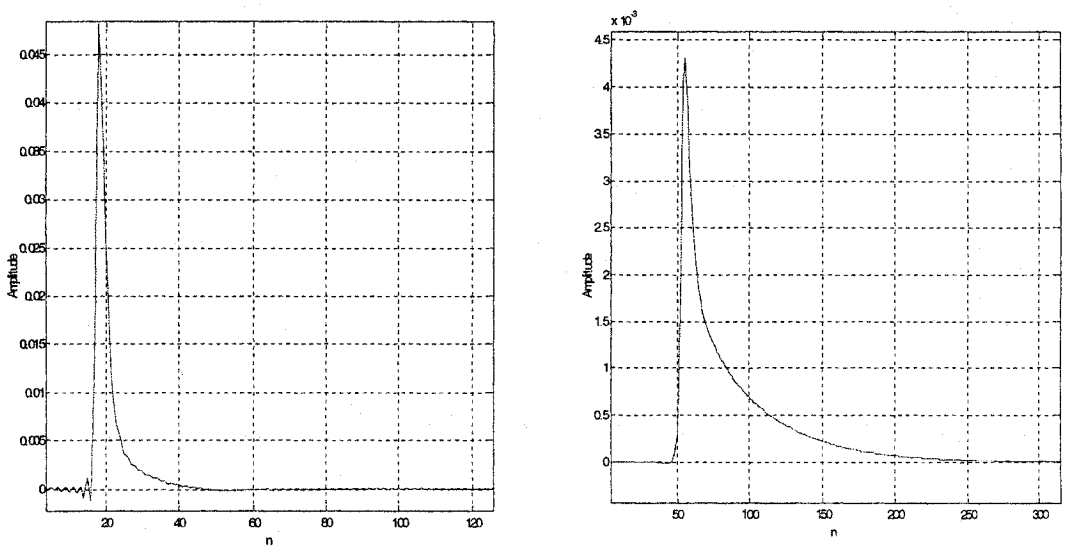

Figure 6-11: Differential Channel Impulse Responses for 26-gauge 5kft (left) and for 24-gauge 15kft (right)

Looking at Figure 6-12, the plot of the impulse response is not a single Dirac function (ie. a single spike), causing some phase distortions on the transmitted signal. Both channels will exhibit ISI. The sampling frequency being 2.208Mhz, the two plots help to see the propagation delays caused by the two transmission lines. For the 5kft loop, the main spike is at 18 time-samples, meaning a principal propagation delay of about 8.2 μsec and about 25 μsec for the 15kft loop. Also, the length of the channels exceeds (mostly the

15kft line) the cyclic prefix length, the guard period, consequently a time-domain equalizer is needed at the receiver end as explained in Chapter 4.

6.4 Common Mode Channel Model

In section 6.3, the differential mode channel attenuation and phase distortion have been modeled. It is also possible to find a two-port model for the common mode channel. The purpose of finding a common mode channel will become evident in section 6.5 when it will be used to calculate the propagation delay difference between the common mode and differential mode.

However, since an accurate two-port model for the common mode propagation is not readily available, an approximate model has been generated by adapting the differential model parameters found previously. The exact value of each derived parameter is not critical since the common mode channel will not be used to determine common mode signal attenuation but only the phase information is necessary.

The criteria used to adapt the differential R, L, G, C parameters to obtain the corresponding common mode parameters named: R_{comm}, L_{comm}, G_{comm}, C_{comm} are described as follows:

- For R_{comm}:

In contrast with the differential signal, in which the differential currents travel in opposite directions, the common currents travel down both wires (Tip and Ring) simultaneously in the same direction as in Figure 6-2. The return path is considered to be through the cable shield (bundle shielding). Therefore, the common mode signal sees the twisted-pair as a single wire [COM98]. Thus, it is reasonable to say that the common mode resistance,

R_{comm}, is approximately half the resistance of the differential mode, R, since the common mode signal propagation travels half the distance of the loop. The current return path is through the cable shield, which has much less resistance than the wire [COM98]. Therefore, the overall estimate of the common mode resistance could be about 0.55 times the differential resistance R [FEN99].

- For C_{comm} and G_{comm}:

It is also mentioned in [COM98], that the unit length capacitance is slightly less than differential one and the conductance is usually negligible. So the capacitance, C_{comm}, has been chosen to be 0.9 times the differential capacitance C and the conductance, G_{comm}, is taken to 0.1 times the differential conductance G (adapted from [FEN99]).

- For L_{comm}:

Similar to the differential case, at high frequencies, the common mode characteristic impedance Z_{0_comm} was approximated by:

$$Z_{0\_comm} \cong \sqrt{\frac{L_{comm}}{C_{comm}}}$$

From [COM98], at 1 Mhz, for a 26 gauge, the twisted-pair characteristic impedance for the differential mode, Z_0, and common mode, Z_{0_comm}, were approximately 100 Ω and 215 Ω respectively. Knowing those values, it is possible to find the ratio between the differential inductance and the common mode inductance.

$$Z_{0\_comm} \cong \sqrt{\frac{L_{comm}}{C_{comm}}} = \sqrt{\frac{x \cdot L}{0.9 \cdot C}} = 215 \quad \text{since} \quad Z_0 = \sqrt{\frac{L}{C}} = 100$$

$$\text{then} \quad L_{comm} \cong 4.16 \cdot L \tag{6.7}$$

Although this approximation is for a 26-gauge wire, for the 24-gauge, the same ratio has been used. The resulting common mode magnitude characteristic impedance is shown in Figure 6-12:

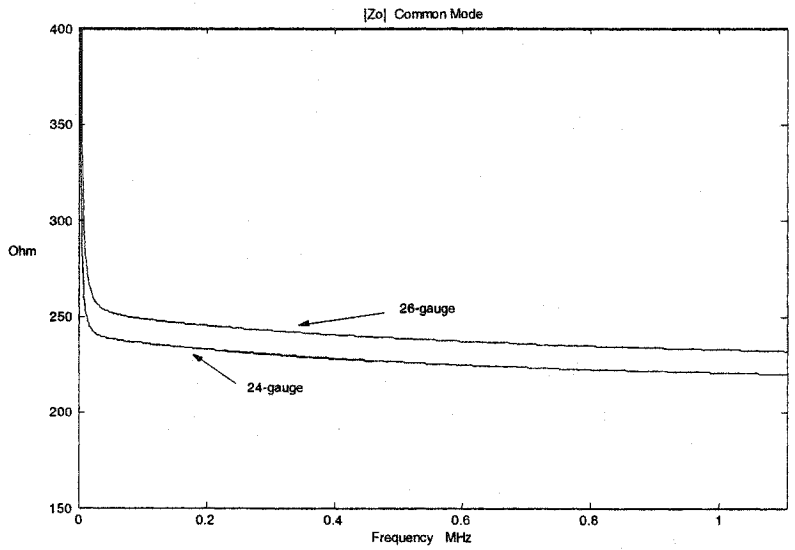

Figure 6-12: Magnitude of the common mode characteristic impedance Z_{0_comm} for 26 and 24 gauges

-For the common mode load impedance, Z_{L_comm}:

By the same reasoning as for the differential case, from Figure 6-12, the magnitude of Z_{0_comm} varies between 240 Ω and 220 Ω for the 24-gauge and 240 Ω and 230 Ω for 26-gauge, the common mode load impedance, Z_{L_comm}, chosen for the simulation is then 230 Ω.

6.5 Velocity Difference between Differential and Common Mode Signals

The characteristic impedance of the common mode is higher that the characteristic impedance of the differential mode. Also the common mode signals are attenuated less

than the differential since the common mode resistance, R_{comm}, is much lower than the differential mode R.

An important aspect is that the common mode signal travels much slower than the differential signal along the transmission line (at about half the speed)[COM98].
The phase velocity is given by [CHE92]:

$$v_p = \frac{\omega}{\beta}$$

where $\omega = 2\pi f$ and β is the phase constant i.e. the imaginary part of the propagation constant.

At high frequencies, the phase velocity can be approximated by:

$$v_p \cong \frac{1}{\sqrt{L \cdot C}} = \frac{1}{Z_o \cdot C} \tag{6.8}$$

since $Z_0 \cong \sqrt{\frac{L}{C}}$ at high frequencies

The capacitance C of the common mode transmission line is similar to the differential mode and the inductance L of the common mode is dominant [COM98] (about 4 times) compared to the differential mode as shown in equation 6.7. Clearly, the propagation speed of the common mode would then be much less.

Using equation 6.8, at high frequencies, the velocity of the differential signal is then about:

$$v_p = \frac{1}{Z_o \cdot C} = \frac{1}{100 \cdot 49 \cdot 10^{-9} \frac{F/km}{1000}} = 2.04 \cdot 10^8 m/s = 0.68c$$

where C = 49 nF/km (for a 26-gauge cable, section 6.3.3) and $c = 3 \cdot 10^8$ m/s.

From the differential impulse response found for a 5kft 26-gauge transmission line (Figure 6-11), the propagation delay was about 8.2μsec giving a differential signal velocity of:

$$\frac{5kft \cdot 0.3048\,km/kft \cdot 1000}{8.2 \cdot 10^{-6}} \cong 0.63c$$

This result is consistent with the value obtained in [COM98] at 1Mhz with a 26-gauge cable where the differential signal velocity was found to be $0.65c$.

To verify the common mode model designed by adapting the differential mode parameters, the common mode impulse response of a 5 kft 26-gauge channel is plotted as shown in Figure 6-13.

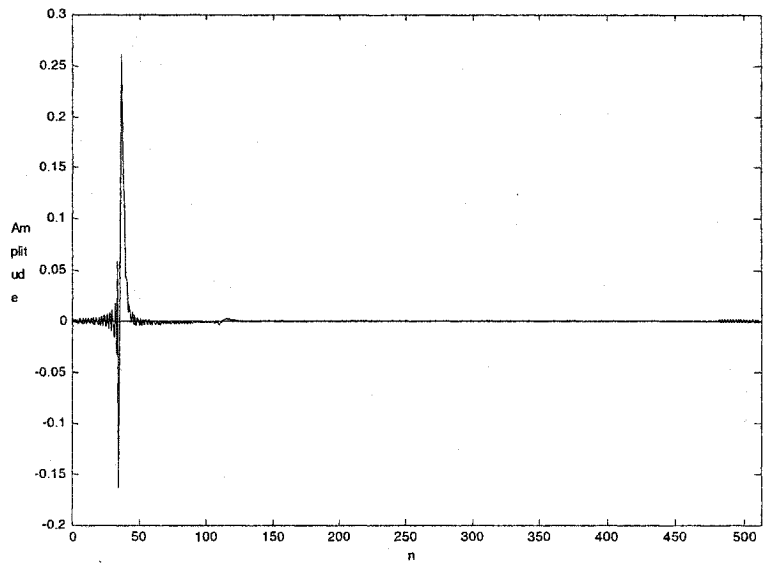

Figure 6-13: Common mode Impulse response for a 5kft 26-gauge transmission line

The main spike is at time-samples $n = 36$ giving a principal propagation delay of about 16μsec at a sampling frequency of 2.208Mhz. The common mode signal velocity is then

about 0.32*c*, which is consistent with the velocity of 0.34*c* found in [COM98] for a 26-gauge cable.

Superposing the plots as in Figure 6-14 shows clearly the delay difference between the common mode channel and the differential channel. The delay difference is about 18 samples corresponding to 8.2μs (half of the delay of the common mode channel being at 16 μsec), therefore, the common mode signal travels about half the speed of the differential signal as expected and consistent with [COM98].

From [COM98], the common mode insertion loss for a 26-gauge is 6.4dB/km at 1 MHz. Figure 6-15 shows that the insertion loss for the same loop is 7.6 dB. The order of magnitude appears to be consistent. Furthermore, as anticipated, the differential attenuation is much greater than the common mode attenuation as shown in Figure 6-15 since one major factor is that common mode resistance, R_{comm}, is only half lower than the differential resistance R as mentioned previously.

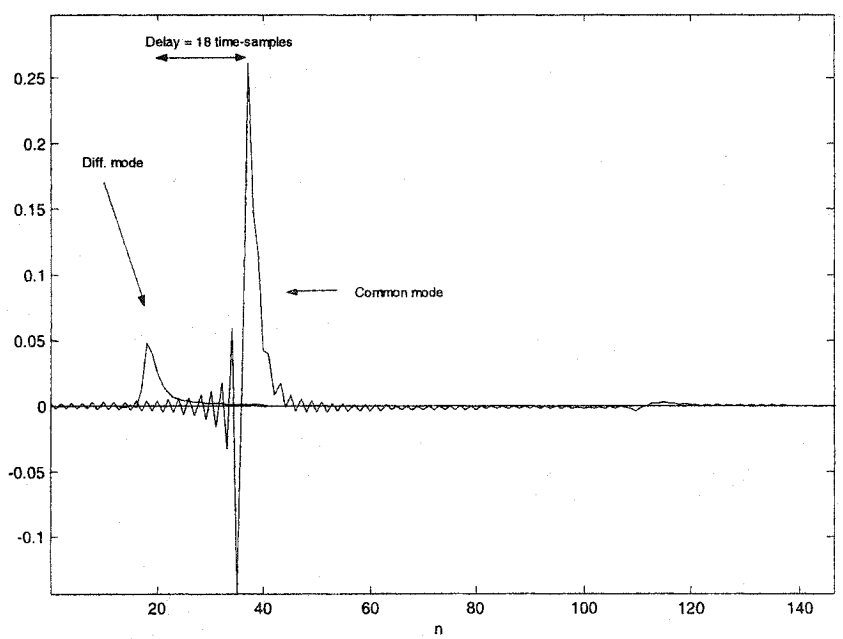

Figure 6-14: 5kft 26-gauge Differential mode and Common mode channel impulse response

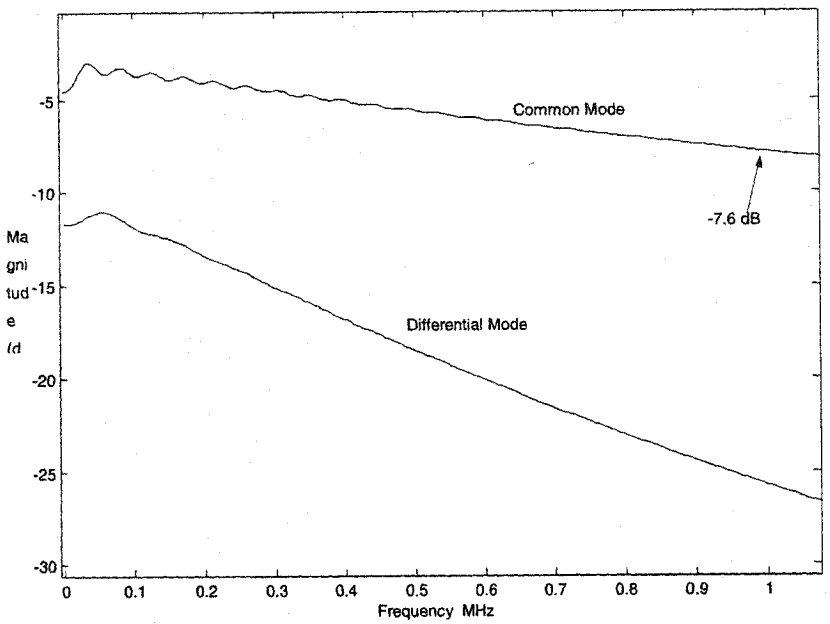

Figure 6-15: 1km 26-gauge Differential mode and Common mode channel Insertion loss

Chapter 7

Crosstalk Model

A major limiting impairment in DSL is crosstalk. A telephone bundle contains a number of twisted wire pairs. Crosstalk noise arises because individual wires in a telephone bundle radiate electromagnetically. Since the twisted pairs in the bundle are not shielded from one another (UTP), the electric and magnetic fields created induce currents in other neighbouring twisted pairs, leading to an undesired signal (called crosstalk signal) on other pairs. A number of individual twisted pairs are wrapped together in a shielded bundle and a number of bundles make up a telephone cable. There are typically 12, 13, 25, 50 or 100 pairs in a bundle. Crosstalk between pairs in the same bundle is much higher than it is between pairs in different bundles [GAL01].

Two types of crosstalk can be distinguished: Near-End Crosstalk (NEXT) and Far-End Crosstalk (FEXT).

In sections 7.1 and 7.2, NEXT and FEXT power spectral densities at the receiver will be defined. However, to simulate the interaction of a DSL transmission line in the presence of crosstalk impairments, the corresponding time-domain signals are required. In the up-coming sections, the modeling of crosstalk signals in differential and common mode will be described as well as the approach taken to model them for a considered DSL architecture. The crosstalk canceller will be briefly introduced since it uses the common mode crosstalk signal as an input reference to mitigate crosstalk. The crosstalk canceller will be explained in greater detail in the following chapter.

7.1 Near-End Crosstalk

Near-end crosstalk (NEXT) as shown in Figure 7-1 occurs when a receiver detects other signals in the same bundle from transmitters that are located in proximity (i.e. from a transmitter into a "near-end receiver"). In other words, the interfering signals coupling into the line are traveling in the direction opposite to the received signal but in an overlapping frequency band depending on the DSL technology.

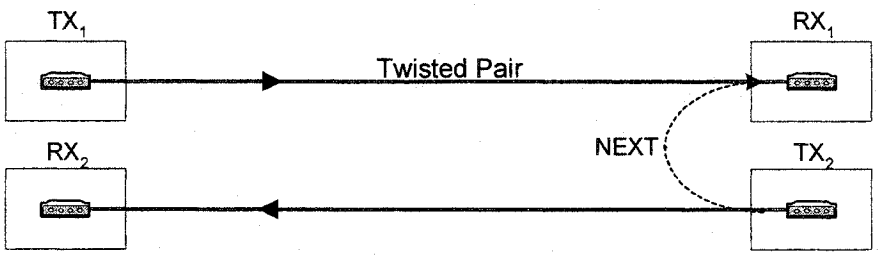

Figure 7-1: Illustration of NEXT

The level of NEXT detected at a receiver is dependent primarily on the number of disturbers (crosstalkers), their proximity to the considered line and the relative powers of the interfering signals and the frequency band over which NEXT occurs. For instance, as in Figure 7-2, Transmitter 2 (TX_2) is further from Receiver 1 (RX_1), and so the NEXT interference power level received by Receiver 1 is weaker than the NEXT power level received as in the configuration shown in Figure 7-1where both RX_2 and TX_2 are in proximity (co-located). The NEXT level as shown Figure 7-2 is attenuated by the difference in length separating RX_1 and TX_2.

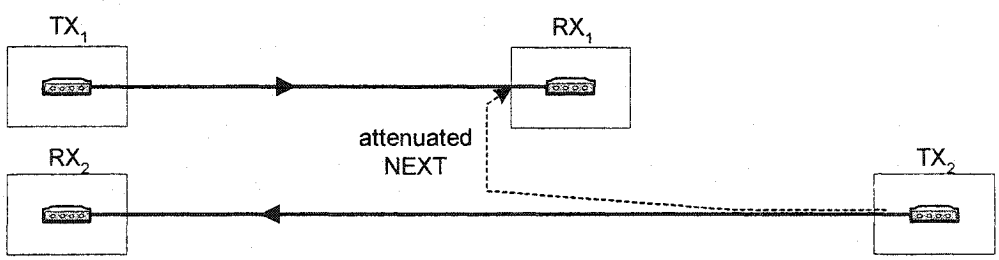

Figure 7-2: Illustration of attenuated NEXT

If the same technology is used for all the lines sharing the same bundle, and also the DSL technology uses frequency division duplexing such as FDD-ADSL, then NEXT (i.e. self-NEXT) should not be a problem. The transmitted signal from TX_2 (causing NEXT) should not overlap the frequency band of the useful signal received by RX_1 from TX_1.

DSL standards and theoretical studies with measurements have modeled NEXT crosstalk in a 50-twisted pair bundle with a coupling function [STA02] referred also as the NEXT Power Spectral Density model as shown in equation 7.1. It should be noted that the PSD model is the resulting PSD of the NEXT signal at the receiver end.

$$PSD_{NEXT}(f) = PSD_{Disturber}(f) \cdot (\tfrac{N}{49})^{0.6} \cdot 10^{-13} \cdot f^{1.5} \qquad (7.1)$$

where $PSD_{disturber}$ is the power spectral density of the adjacent transmitter (disturber) and N is the number of disturbers in the bundle carrying similar DSL service.

Referring to Figure 7-1, Receiver 1 (RX_1) will detect a NEXT signal having a power spectral density (PSD_{NEXT}) defined by 7.1. The power spectral density of the transmitted signal at Transmitter 2 (TX_2) is considered as $PSD_{Disturber}$ and N=1 since there is only one disturber in this case.

7.2 Far-End Crosstalk

Far-end crosstalk (FEXT) as shown in Figure 7-3 occurs when a receiver detects other signals in the same bundle from remote transmitters, which can be located at a Remote Terminal (cabinet) or Central Office (i.e. from a transmitter into a "far-end receiver"). In this case, the interfering signals coupling into the line are traveling in the same direction as the received signal in an overlapping frequency band.

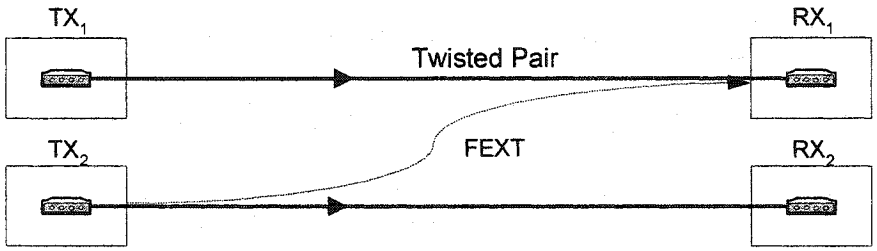

Figure 7-3: Illustration of FEXT

Similar to NEXT, the level of FEXT detected is dependent on the number of disturbers and their proximity to the considered line, the relative powers and the frequency band over which FEXT occurs. However, in contrast to NEXT, FEXT levels depend on the length of the line over which the coupling of interference signals occurs. FEXT decreases with increasing line length because the interference signals are attenuated since they have to travel through the transmission line.

Another scenario is represented in Figure 7-4 when for example the transmitter TX_2 is located in a Remote Terminal, which is at a distance closer to the receiver RX_2. In contrast to Figure 7-3, RX_1 will experience a much stronger FEXT signal originating from TX_2 (amplified FEXT) since the distance *d* separating TX_2 and RX_1 is much shorter than the distance in Figure 7-3. This scenario is encountered when for example ADSL signals from a Central Office share a distribution cable with VDSL signals from a Remote Terminal. The FEXT signal from a downstream transmitter (TX_2) into a ADSL receiver (RX_1) may be severe [BIN00] since the transmitted signal from the central office (TX_1) gets more attenuated because the distance (loop length) to reach the receiver RX_1 is greater. Therefore, the higher level FEXT crosstalk signal from the remote terminal causes signal interference with the lower level (attenuated) desired signal (from the CO) at the receiver.

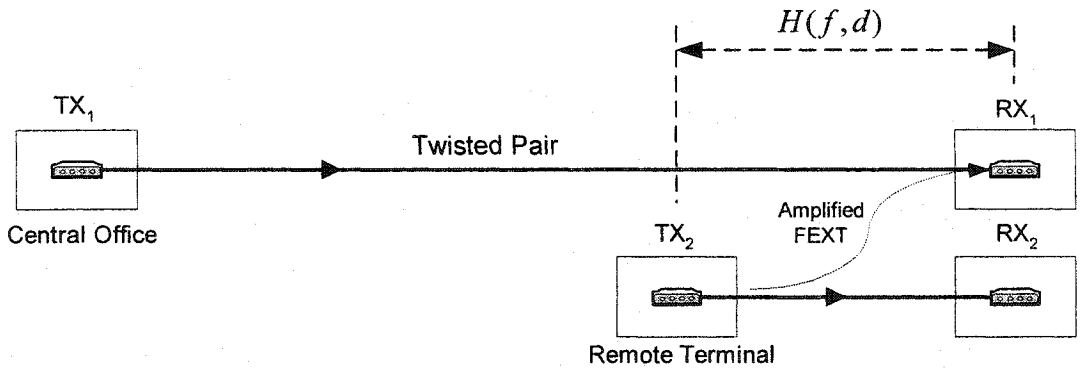

Figure 7-4: Illustration of amplified FEXT due to shorter distance

FEXT modeling parallels NEXT modeling with the FEXT Power Spectral Density model defined as:

$$PSD_{FEXT} = PSD_{Disturber}\left|H(f,d)\right|^2 (\tfrac{N}{49})^{0.6} \cdot 9 \cdot 10^{-20} \cdot d \cdot f^2 \qquad (7.2)$$

where $PSD_{disturber}$ is the power spectral density of the far-end transmitter (disturber), N is the number of disturbers in the 50-pair bundle carrying similar DSL service, f is the frequency, d is the distance between the far-end transmitter and the considered receiver and $H(f, d)$ is the differential channel transfer function for the considered line where the coupling is occurring. It should be noted that the PSD model is the resulting PSD of the FEXT signal at the receiver end.

7.3 DSL Architecture Considered

The performance of DSL systems is severely constrained by crosstalk. With DSL architecture using a central office (CO) and a remote-terminal (RT) (referred to as "CO-RT architecture), crosstalk impairments are even more critical. Figure 7-5 illustrates the DSL architecture considered with RT-served customers located within proximity to a CO-served customer, and where all the transmission lines are sharing the same bundle.

This scenario has been chosen because it represents the worst-case crosstalk for the customer attached to the line deployed from the CO, during downstream transmission. As explained in section 7.2 and briefly introduced in Chapter 2, having this configuration, the customer serviced by the CO will be prone to NEXT impairments from the RT-served customers, but will also experience strong FEXT impairments from the Remote-Terminal transmitters.

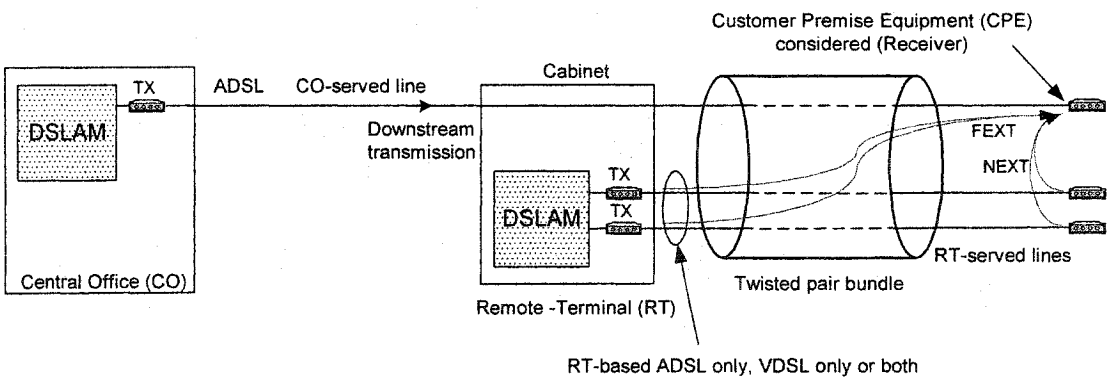

Figure 7-5: DSL architecture with a Central Office and a Remote Terminal (referred to as "CO-RT architecture"), with a shared bundle consisting of several ADSL and/or VDSL lines

7.4 CO-RT Crosstalk Modeling

In the CO-RT architecture, the crosstalk signals, NEXT and FEXT, originated from the transmission lines deployed from the Remote Terminal to the customer premise equipments (CPE) i.e. the RT-served lines. The crosstalk signals as shown in Figure 7-5 are corrupting the desired received signal by the CPE connected to the line deployed from the Central Office i.e. the CO-served customer during downstream transmission.

The following subsections will first elaborate the model for the NEXT time-domain signals in differential mode and common mode that originated from the RT-served lines, followed by the model for the FEXT. Finally, the modeling will consider the cases when the disturbers (i.e. the crosstalkers) are from a single technology or mixed technologies such as ADSL and VDSL sharing the same bundle.

7.4.1 NEXT Time-Domain Signal in Differential Mode

The text below will describe how to generate the NEXT time-domain signal in differential mode. It is necessary to find a time-domain signal that would yield the NEXT power spectral density as given by equation 7.1. Note that the given crosstalk PSD equations of section 7.3 represent the PSDs of crosstalk signals at the receiver.

For the parameters of the NEXT PSD equation 7.1, $PSD_{Disturber}$ is replaced by the upstream PSD mask of the technology serviced by the Remote Terminal such as ADSL or VDSL (refer to Chapter 2). The number of disturbers, N, is the number of RT-served lines in the bundle.

In order to achieve this, a noise source has been filtered to produce an output signal, $NEXT_{Diff.\ Signal}$, that would give the NEXT PSD. The shaping filter $H_{NEXT\_Diff\_shaping}(f)$ is represented by *NEXT Differential PSD shaping* as in Figure 7-6.

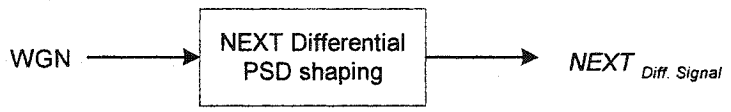

Figure 7-6: NEXT differential time-domain model

The appropriate shaping filter, $H_{NEXT\_Diff\_shaping}(f)$, is determined as the following:

In [KER93], the probability density of NEXT and FEXT have been studied and it turns out that both NEXT and FEXT time-domain noise signals follow a Gaussian distribution. Also, it is known that a Gaussian input to a linear system produces an output, which is still Gaussian [HAY94.]. Thus, a White Gaussian Noise source (WGN) has been selected as the source noise, with zero mean and variance, $\sigma^2 = 1$.

The relation between input-output PSDs in the system is defined as:

$$PSD_{NEXT}(f) = |H_{NEXT\_Diff\_shaping}(f)|^2 \cdot PSD_{WGN}(f)$$

Since a white Gaussian distribution random process has the property that the PSD is constant over the frequency and equals its variance [LEO94], then $PSD_{WGN}(f) = \sigma^2 = 1$. Therefore, the magnitude of the shaping filter is found to be:

$$|H_{NEXT\_Diff\_shaping}(f)| = \sqrt{PSD_{NEXT}(f)}$$

The Yule-walker design has been used to find $H_{NEXT\_Diff\_shaping}(f)$. Yule-walker designs IIR digital filters using a least-squares fit to a specified frequency magnitude response. The function takes as a parameter the magnitude response over specific frequencies. In this case, it would be: $\sqrt{PSD_{NEXT}(f)}$ and it finds the resulting filter coefficients, which will be used for $H_{NEXT\_Diff\_shaping}(f)$. The resulting filter has an arbitrary phase response, but matches the specified desired magnitude response. Having $H_{NEXT\_Diff\_shaping}(f)$ defined, the NEXT time-domain differential signal $NEXT_{Diff.\ Signal}$ can be then generated.

7.4.2 NEXT Time-Domain Signal in Common Mode

The steps taken to model the NEXT time-domain signal $NEXT_{Diff.\ Signal}$ in common mode are described as follows:

In DSL literature, the differential crosstalk PSD as in equation 7.1 or 7.2 is well defined but the PSD characteristic of the common mode crosstalk signal is not readily available. However, as mentioned in Chapter 6, crosstalk interference due to adjacent lines in a telephone couples initially in common mode. The desired differential received signal is corrupted by the process of the common mode crosstalk signal partially leaking to the differential mode because of an imperfect transmission line balance. Using the overall magnitude balance function of the line $B(f)$ as a scaling function (refer to equation 6.1), it is possible to model the reverse of the process by scaling the differential crosstalk model designed previously to find the corresponding original common mode crosstalk signal that has leaked. The scaling function, $B(f)$, is represented by *Scaling function from Differential to Common mode* in Figure 7-7.

Figure 7-7 illustrates the model to generate the NEXT common mode time-domain signal.

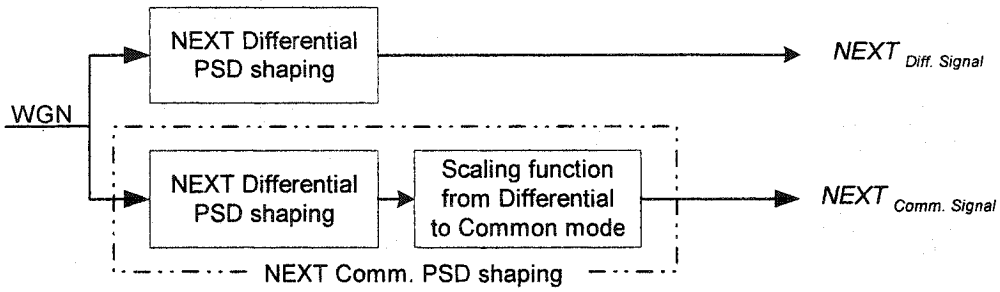

Figure 7-7: NEXT common mode time-domain model

The NEXT differential time-domain signal, $NEXT_{Diff.\ Signal}$, and NEXT common mode time-domain signal, $NEXT_{Comm.\ Signal}$, have the same phase information since NEXT, as opposed to FEXT, does not propagate through the transmission line. Consequently, the $B(f)$ scaling function applied to the differential NEXT signal should not introduce a change in the phase information.

Scaling the magnitude frequency response of the previously found differential shaping filter, $H_{NEXT\_Diff\_shaping}(f)$, by $B(f)$ will yield the magnitude response of the common mode shaping filter, $H_{NEXT\_Comm\_shaping}(f)$ shown in equation 7.3.

$$|H_{NEXT\_Comm\_shaping}(f)| = |H_{NEXT\_Diff\_shaping}| \cdot B(f) \tag{7.3}$$

The phase information of $H_{NEXT\_Comm\_shaping}(f)$, should be kept the same as $H_{NEXT\_Diff\_shaping}(f)$ as previously mentioned, consequently $H_{NEXT\_Comm\_shaping}(f)$ is found to be:

$$H_{NEXT\_Comm\_shaping}(f) = |H_{NEXT\_Comm\_shaping}(f)| e^{j\angle H_{NEXT\_Diff\_shaping}(f)}$$

Having $H_{NEXT\_Comm\_shaping}(f)$ defined, the NEXT common mode time-domain signal $NEXT_{Comm.\ Signal}$ can be then generated as in Figure 7-7.

7.4.3 FEXT Differential Mode Signal

The steps taken to model the FEXT time-domain signal in differential mode, $FEXT_{\ Diff.\ Signal}$, as in Figure 7-8, are identical to the ones used to find the NEXT differential time-domain signal. The difference is that the FEXT shaping filter, $H_{FEXT\_Diff\_shaping}(f)$, uses the FEXT PSD as in equation 7.2.

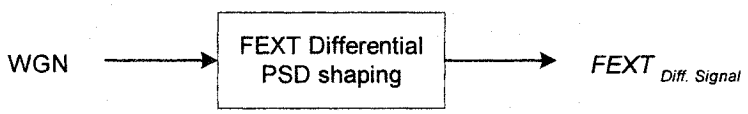

Figure 7-8: FEXT differential time-domain model

However, as mentioned in section 7.2, the PSD equation contains the magnitude transfer function of the differential channel as a parameter. As opposed to NEXT, the FEXT signal propagates through the differential channel i.e. the transfer function of the line deployed from the CO to the considered CPE. But the crosstalk is over a shorter distance from the cabinet to the CPE as illustrated in Figure 7-9. Therefore, the magnitude of the transfer function corresponding to the CO-served line channel, $H(f,d_2)$, should be designed for a propagation distance from the cabinet to the CPE, d_2.

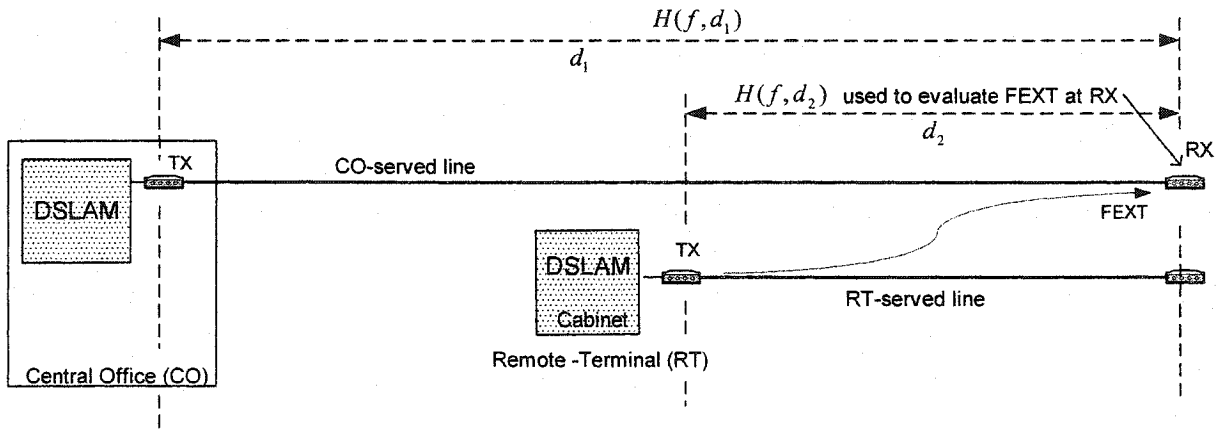

Figure 7-9: Channel transfer function definitions for the CO-RT architecture

Using equation 7.2, the FEXT PSD becomes then:

$$PSD_{FEXT.Cab} = PSD_{Disturber} \left|H(f,d_2)\right|^2 (\tfrac{N}{49})^{0.6} \cdot 9 \cdot 10^{-20} \cdot d_2 \cdot f^2 \qquad (7.2)$$

where N is the number of disturbers, i.e. number of RT-served lines in the bundle, and $PSD_{Disturber}$ is replaced by the downstream PSD mask of the corresponding technology.

Therefore the magnitude transfer function of the FEXT shaping filter, $H_{FEXT\_Diff\_shaping}(f)$, is calculated as:

$$|H_{FEXT\_Diff\_shaping}(f)| = \sqrt{PSD_{FEXT.Cab}(f)}$$

As in the NEXT case, the Yule-walker design has been used to find the coefficients for $H_{FEXT\_Diff\_shaping}(f)$ taking as a parameter: $\sqrt{PSD_{FEXT.Cab}(f)}$. The resulting filter has then again an arbitrary phase response but approximates the specified desired magnitude response. Having $H_{FEXT\_Diff\_shaping}(f)$ defined, the FEXT time-domain differential signal $FEXT_{Diff.Signal}$ can be then generated.

7.4.4 FEXT Common Mode Signal

To model the FEXT time-domain signal in common mode, $FEXT_{Comm.\ Signal}$, is slightly more complex than the NEXT time-domain signal common mode model. The modeling is separated into two steps as in Figure 7-10.

The first step of the design is similar to the NEXT common-mode model and produces an intermediate FEXT common mode signal, $inter\text{-}FEXT_{Comm.\ Signal}$, with the same phase information as the differential FEXT signal $FEXT_{Diff.\ Signal}$.

The second step adds an additional phase element to $inter\text{-}FEXT_{Comm.\ Signal}$ that yields $FEXT_{Comm.\ Signal}$. The added Phase element represents the delay incurred by the actual common mode FEXT signal, with respect to the differential FEXT signal, since both signals travel at different velocities as mentioned in Chapter 6.

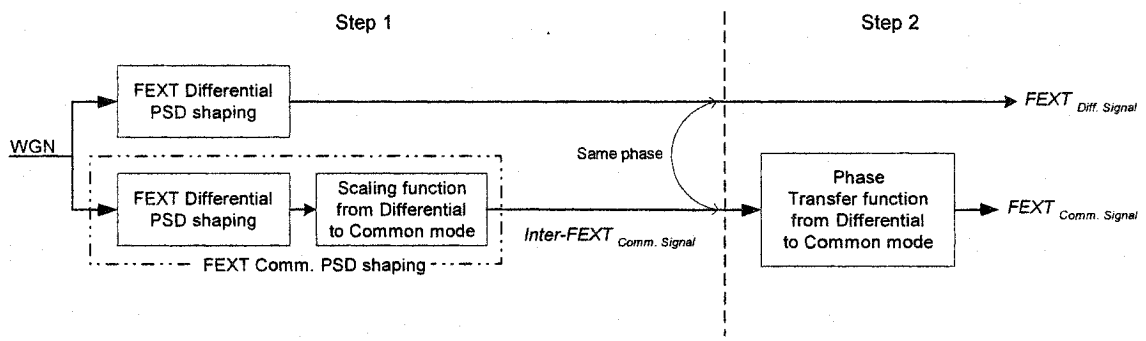

Figure 7-10: FEXT common mode time-domain model

Step 1:

To produce $inter\text{-}FEXT_{Comm.\ Signal}$, the same assumption is used, being that the coupling of crosstalk is being induced initially in common mode as previously explained with the NEXT common mode signal case. Therefore, scaling the magnitude frequency response

of the previously found differential shaping filter $H_{FEXT\_Diff\_shaping}(f)$ by $B(f)$ will give the magnitude frequency response of the common mode shaping filter, $H_{FEXT\_Comm\_shaping}(f)$ shown in equation 7.4.

$$|H_{FEXT\_Comm\_shaping}(f)| = |H_{FEXT\_Diff\_shaping}| \cdot B(f) \tag{7.4}$$

For the first step, the phase of $H_{FEXT\_Comm\_shaping}(f)$ is kept the same as $H_{FEXT\_Diff\_shaping}(f)$. Consequently, $H_{FEXT\_Comm\_shaping}(f)$ is found to be:

$$\begin{aligned} H_{FEXT\_Comm\_shaping}(f) &= |H_{FEXT\_Diff\_shaping} \cdot B(f)| e^{j\angle H_{FEXT\_Diff\_shaping}(f)} \\ &= |H_{FEXT\_Comm\_shaping}(f)| e^{j\angle H_{FEXT\_Diff\_shaping}(f)} \end{aligned}$$

Having $H_{FEXT\_Comm\_shaping}(f)$ defined, *inter-FEXT* $_{Comm.\ Signal}$ can then be generated.

Step 2:

In sections 7.4.1 and 7.4.2, NEXT differential signals and common mode signals have been modeled with the same phase information since NEXT signals do not propagate through the transmission line. In contrast, FEXT propagates through the line. Thus FEXT differential signals and FEXT common mode signals cannot have the same phase at the customer receiver because as mentioned in Chapter 6, it was found that the velocity of the differential signal is about $0.63c$ and the common mode signal is about $0.34c$. The common mode signal travels then at about half the velocity of the differential signal. Consequently, at the customer receiver, the common signal arrives with a delay with respect to the differential signal. In step 1, the intermediate FEXT common mode signal has been modeled with the same phase as the differential FEXT signal. In step 2, the delay is now considered and will be used to modify the phase content of the intermediate FEXT signal found.

In the CO-RT architecture presented, in theory, FEXT interference couples into the common mode line along the entire CO-served transmission line, giving a resulting common mode FEXT signal at the customer receiver. The resulting common mode FEXT signal can be represented as the sum of signal components coupled at different locations along the line towards the receiver as shown in Figure 7-11. The strongest signal component of the resulting common mode FEXT signal is the one that has been coupled in proximity to the Remote Terminal transmitter. If considering that the other signal components are respectively negligible, then the resulting common mode FEXT signal is represented by the strongest signal component. Consequently, it has to travel a distance of d_2 to reach the customer receiver or in other words there is a certain delay at a speed of $0.34c$.

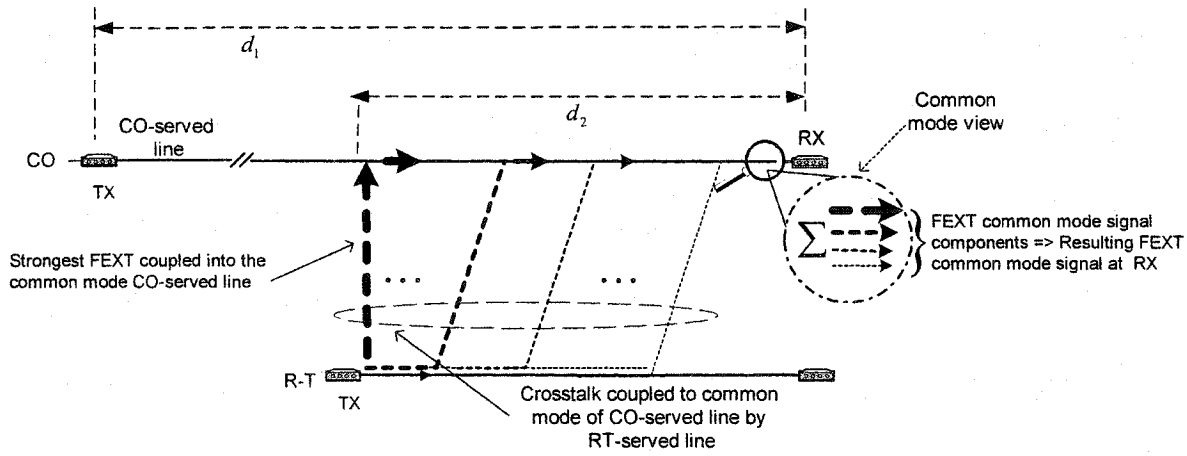

Figure 7-11: Resulting common mode signal in CO-served line at RX due to RT-served line causing crosstalk interference

As mentioned previously, since the transmission line is not perfectly balanced, the FEXT common mode signal leaks into the differential mode, giving the differential FEXT signal. The leakage occurs along the entire transmission line towards the receiver as shown in Figure 7-12. Therefore, the resulting differential FEXT signal is composed of multiple signals leaked along the transmission line and each differential FEXT signal component travels a different distance towards the receiver.

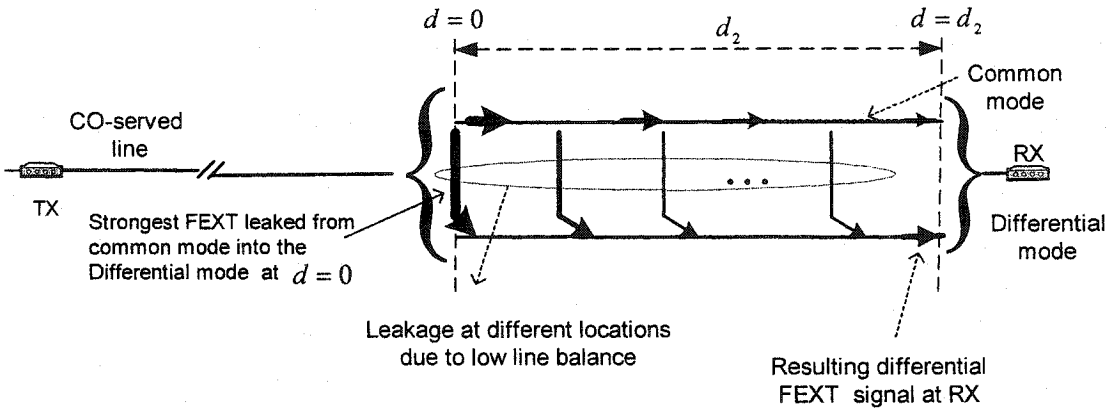

Figure 7-12: Leakage from the FEXT common mode signal to the differential mode of the CO-served line

For simplicity, to model the delay of the resulting FEXT common mode signal with respect to the resulting FEXT differential signal at the receiver, the strongest FEXT common mode signal component has been compared with its corresponding differential signal. It was assumed that the corresponding differential signal is the result of the strongest FEXT common mode signal that has leaked within the proximity of the RT-transmitter at $d = 0$. Thus, as shown in Figure 7-13, both signals in differential or common mode have to travel the same distance, d_2, towards the receiver, at respective velocities of $v_{Diff} = 0.63$ and $v_{Comm} = 0.34$.

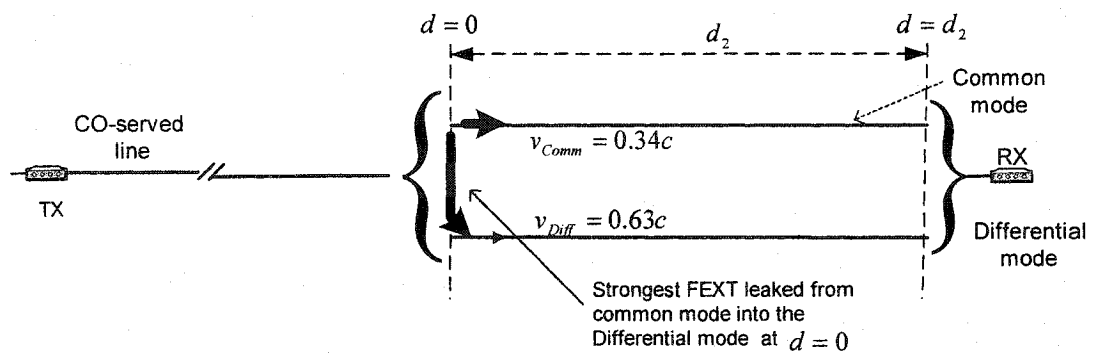

Figure 7-13: FEXT common mode signal and respective FEXT Differential signal traveling a distance of d_2 towards the receiver at different velocities

From above, it is then possible to find the delay difference between the differential mode and the common mode signals at the receiver. However, in DSLs, the transmission line is dispersive, so different frequencies travel with different velocities [STA99]. The previously given velocities represented an approximation of the velocities of the signals at high frequencies. So, simply applying a delay to the common mode signal with respect to the differential signal is not quite accurate. A better implementation is to find the phase transfer function from the differential mode to the common mode. It has been designed as follows:

The given FEXT PSD of equation 7.2, is the crosstalk PSD at the customer receiver of the CO-served line. From the latter, the corresponding FEXT differential signal and the intermediate FEXT common signal have both been modeled with identical phase.
In Chapter 6, the differential channel transfer function, $H_{Diff}(f)$, and the common mode channel transfer function, $H_{Comm}(f)$, have been designed. The unity phase transfer function from the differential mode to the common mode, $\phi_{Diff\ To\ Comm}(f)$, can be determined by taking the difference between the common mode channel phase, $\angle H_{Comm}(f,d_2)$, and the differential channel phase, $\angle H_{Diff}(f,d_2)$, as in equation 7.5. It should be noted that the common mode channel and the differential channel have been designed for a distance of d_2, the FEXT common mode signal and FEXT differential signal travel the same distance, d_2, to reach the receiver.

Also, $\phi_{Diff\ To\ Comm}(f)$ should not change the magnitude of the intermediate FEXT common mode signal, *inter-FEXT* $_{Comm.\ Signal}$. Therefore, a unity gain has been applied for the design of $\phi_{Diff\ To\ Comm}(f)$.

$$\phi_{Diff\ To\ Comm}(f) = 1 \cdot e^{j(\angle H_{Comm}(f,d_2) - \angle H_{Diff}(f,d_2))} \qquad (7.5)$$

Having $\phi_{Diff\ To\ Comm}(f)$ defined, the phase of *inter-FEXT* $_{Comm.\ Signal}$ can be then modified with respect to the differential signal and $FEXT_{Comm.\ Signal}$ can then generated as in Figure 7-10.

Figure 7-14 shows the differential and common channel impulse responses for a d_2 = 5kft, 26-gauge twisted pair and their respective phase responses. It can be seen that the approximate delay difference between the differential channel and common mode channel is about 18 time-samples. Figure 7-15 shows the phase impulse response obtained from differential mode to common mode, $\phi_{Diff\ To\ Comm}(f)$. The main spike is at 18 time-delay samples as expected.

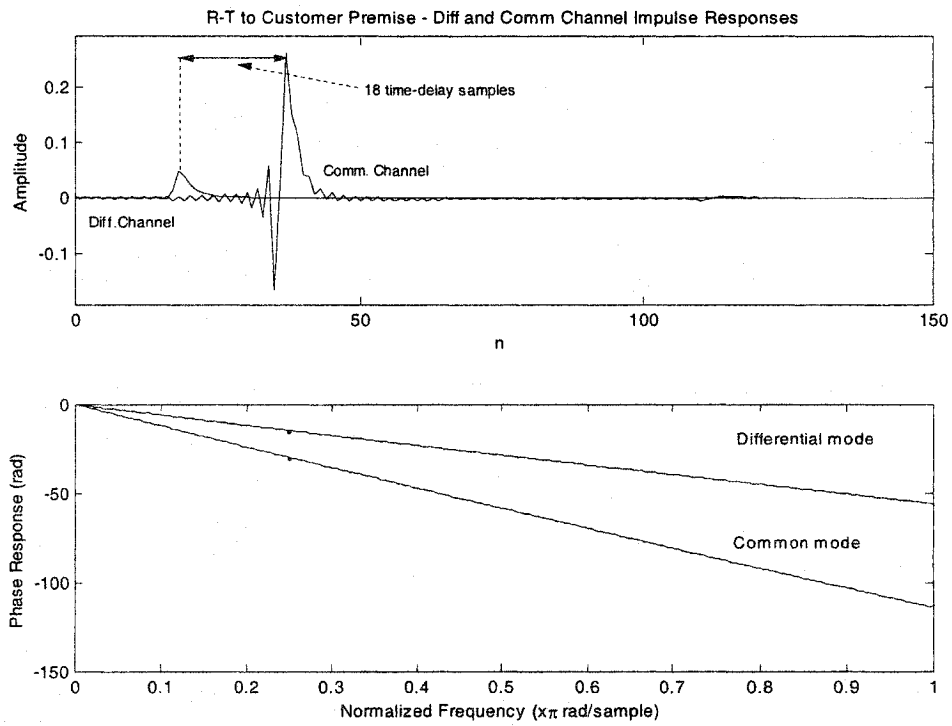

Figure 7-14: Differential and Common mode channel impulse responses and respective phase responses

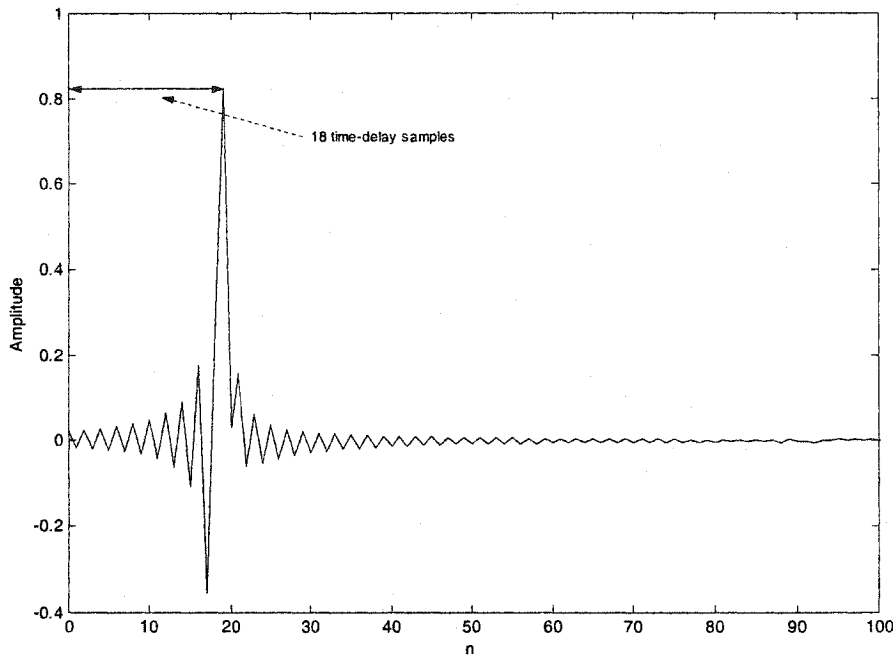

Figure 7-15: Corresponding impulse response of $\phi_{Diff\ To\ Comm}(f)$

7.5 Resulting Design Model with only ADSL Disturbers

In the previous sections, the common and differential crosstalk signals have been modeled for the considered DSL architecture, which has a central office and a remote terminal sharing the same bundle (CO-RT architecture). The overall system showing the various signals involved is represented as in Figure 7-16. The crosstalk signals (NEXT and FEXT) are caused by the lines deployed from the Remote terminal that provides DSL services. The differential crosstalk signals are corrupting the desired differential signal received by the Customer attached to the line deployed from the Central Office. However, in Figure 7-16, NEXT and FEXT signals refer to the scenario when only one type of disturber such as ADSL (originating from the remote terminal) is present in the bundle.

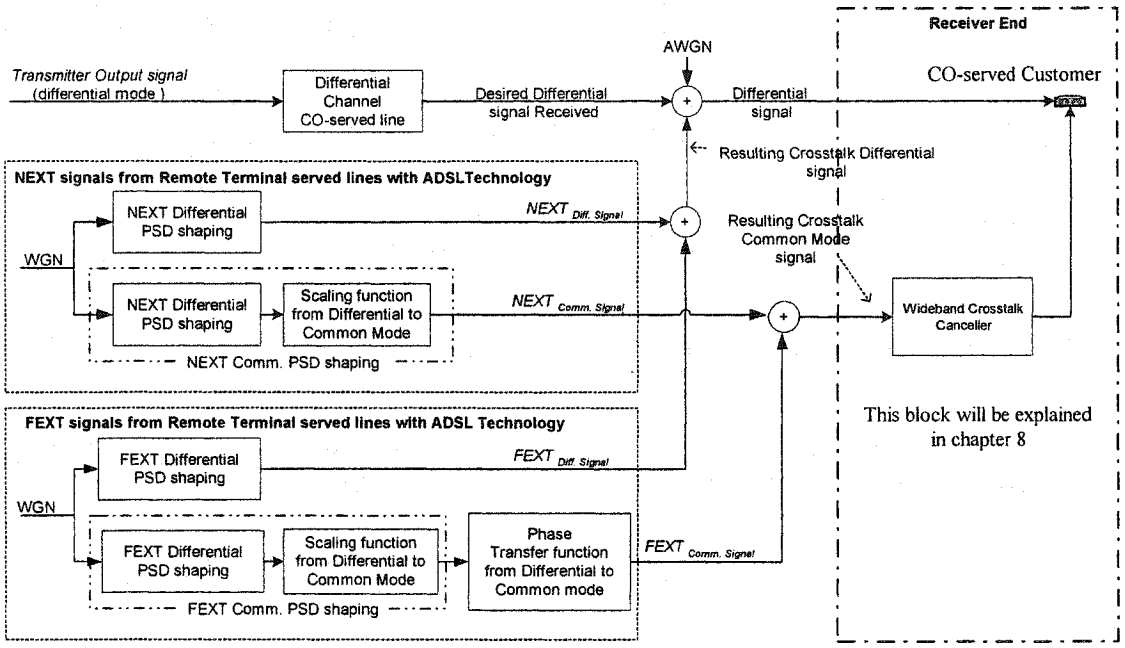

Figure 7-16: Overall system representing the CO-RT architecture with only one type of disturber i.e. ADSL present in the bundle.

In Figure 7-16, the *Transmitter Output signal* is the downstream desired differential signal transmitted from the CO to the customer (CO-served customer). The desired signal has been generated using the DMT ADSL protocol stack (transmitter side) shown in Chapter 2.

NEXT and FEXT common mode signals are summed to produce the *Resulting Crosstalk Common Mode signal* at the receiver end. The resulting common mode signal will be used for the wideband crosstalk canceller as an input reference to mitigate the differential crosstalk signal at the receiver. It will be explained in greater detail in Chapter 8.

7.6 Resulting Design with ADSL and VDSL Lines in the Bundle

When considering more than one type of disturber, i.e. ADSL and VDSL in the same bundle, the overall interference caused by each type of disturber must be combined. There are several techniques to combine mixed PSD crosstalkers from mixed sources [KER02a] [GAL02].

For each type of PSD crosstalkers (ADSL and VDSL) in the simulation, their respective time-domain crosstalk signals have been generated using the same modeling techniques as in previous sections and then summed in the time domain to obtain the overall interference signal as shown in Figure 7-17. It should be noted that the white Gaussian noise source (WGN) used to generate the crosstalk signals are independent to one another.

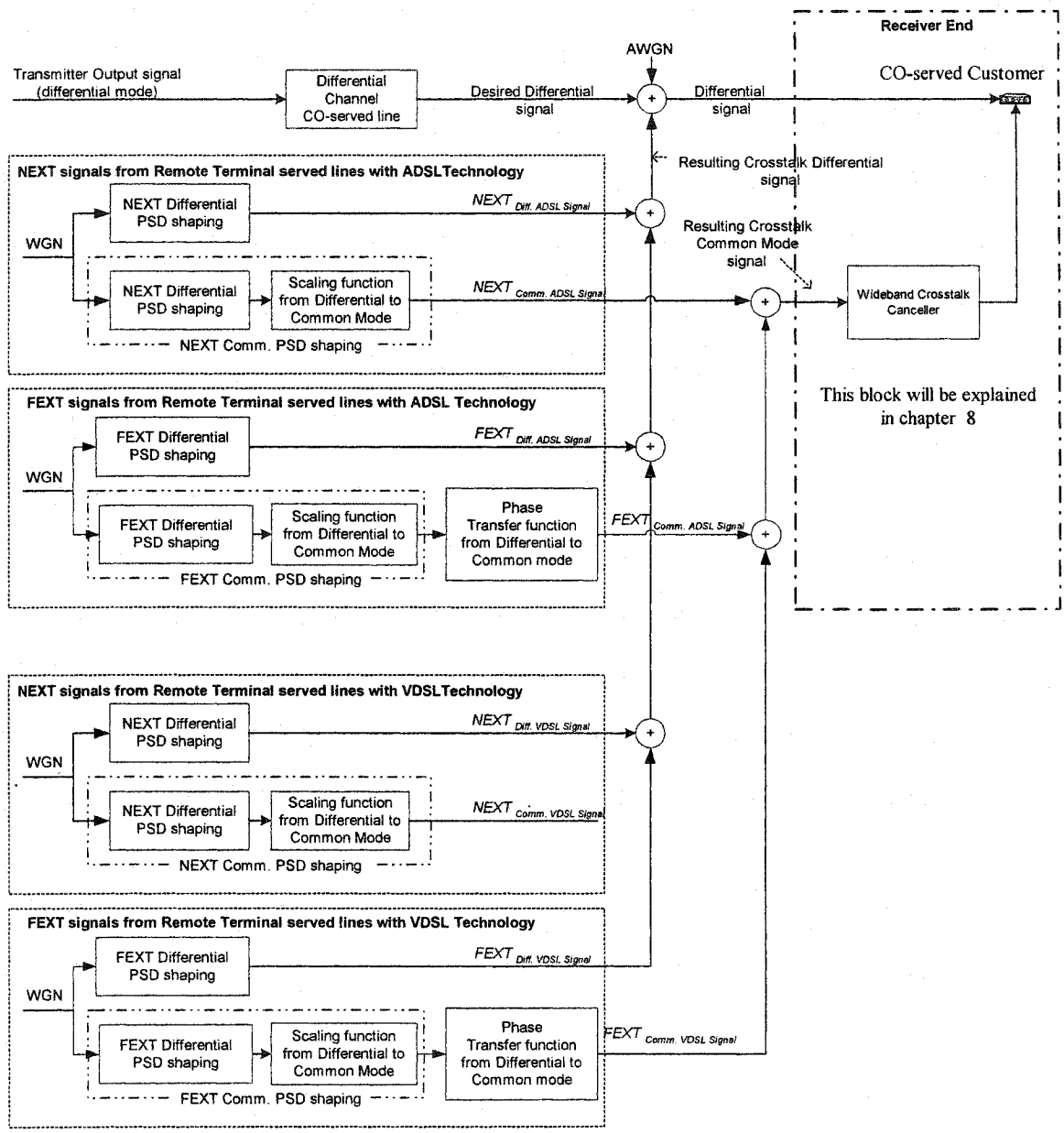

Figure 7-17: Overall system representing the CO-RT architecture with mixed technology disturbers i.e. ADSL and VDSL present in the bundle.

Chapter 8

Wideband Crosstalk Canceller

This chapter will present the wideband crosstalk canceller performed by adaptive filtering, the measure to evaluate the performance of the canceller (via convergence level), and briefly introduces and compares three adaptive algorithms.

As briefly introduced in the previous chapter, the adaptive wideband crosstalk canceller uses as input reference the resulting crosstalk common mode signal. The goal of the canceller is to produce an output y, which closely resembles the differential crosstalk signal that corrupted the desired differential signal. Figure 8-1 shows the implementation of the adaptive canceller in the CO-RT system to reduce the differential crosstalk at the receiver.

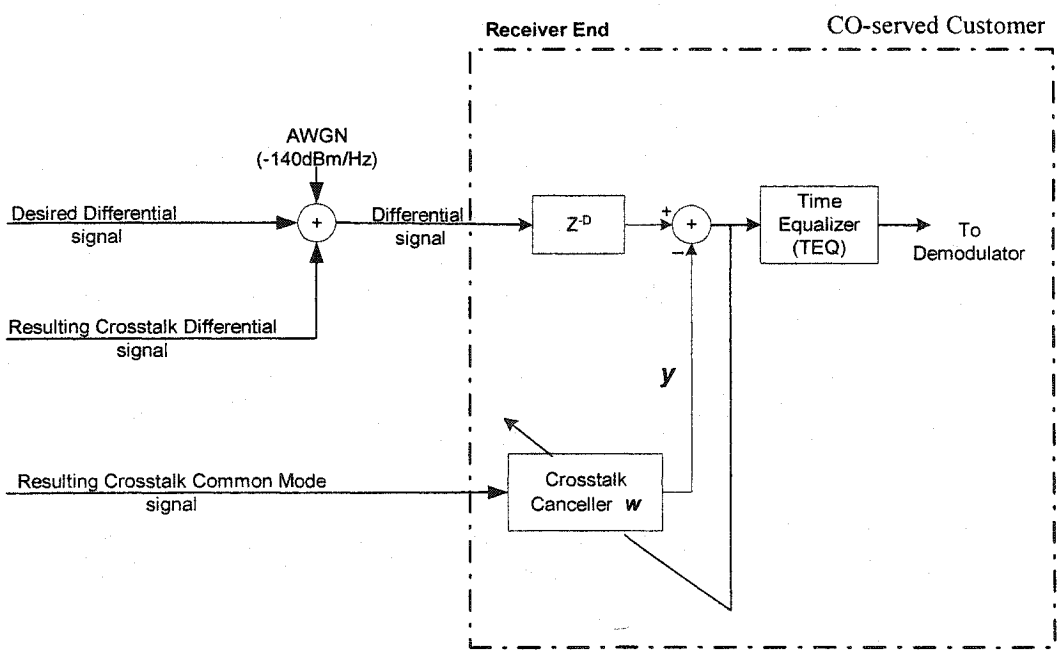

Figure 8-1: Crosstalk canceller implementation in the CO-RT system

The delay Z^{-D} is required to force the solution of the adaptive filter (canceller) to be causal. The delay is mostly required to compensate for the *phase Transfer Function from Differential to Common* filter since the FEXT common signal lags the FEXT differential signal. Also, Additive white Gaussian noise (AWGN) of –140 dBm/Hz (single-sided) is added at the receiver side in the simulation since background noise in DSL systems is often presumed to be –140dBm/Hz [STA02].

It should be noted that the CO-served line considered operates a Frequency Division Duplexing ADSL (FDD-ADSL) for upstream/downstream transmissions, therefore, an echo canceller would not be required. During downstream transmission (from to CO to Customer), only the desired downstream signal is present at the receiver end (customer) as shown in Figure 8-1. The assumption made is that the hybrid circuit is assumed to be fairly ideal; therefore, the upstream signal from the CO-served customer is mostly removed by the hybrid circuit. However, if any residual upstream signal remains in received signal due to line imperfections or echo, an echo canceller can be used to remove any remaining signal components.

8.1 Convergence Level

The adaptive crosstalk canceller was trained until it had reached a selected convergence level, where the convergence level is defined here as the power ratio of the initial FEXT/NEXT levels over the remaining FEXT/NEXT components not removed by the canceller. However, the achievable convergence depends on the power ratio between the NEXT signal and FEXT signal in the system. The following will further explain the concept.

From the interference (crosstalk) canceling system of Figure 8-2, the optimum solution is the Wiener solution defined as [HAY02]:

$$w = R_{xx}^{-1} \cdot P_{x \cdot d} \Rightarrow \quad w = R_{(x_1+x_2)\cdot(x_1+x_2)}^{-1} \cdot P_{(x_1+x_2)\cdot(d_1+d_2)}$$

For simplicity of presentation, the useful signal (downstream transmitted differential signal) and the AWGN have been purposely omitted (set to zero) in Figure 8-2.

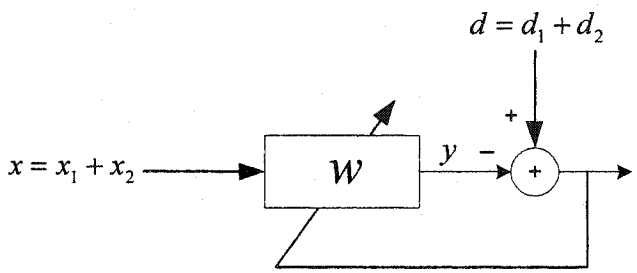

Figure 8-2: Interference canceling system

where: x = resulting crosstalk common mode signal as the input reference of w

x_1 = NEXT common mode signal component of x

x_2 = FEXT common mode signal component of x

d = resulting crosstalk differential mode signal as the desired signal

d_1 = NEXT differential signal component of d

d_2 = FEXT differential signal component of d

y = canceller output predicting $d_1 + d_2$

R_{xx} is the auto-correlation matrix of the input x and P_{xd} is the cross-correlation vector between d and x

By expanding the cross-correlation vector P,

$$P_{(x_1+x_2)\cdot(d_1+d_2)} = E[(x_1+x_2)\cdot(d_1+d_2)]$$

$$= E[(x_1+x_2)\cdot d_1] + E[(x_1+x_2)\cdot d_2]$$

$$= P_{(x_1+x_2)\cdot d_1} + P_{(x_1+x_2)\cdot d_2}$$

the optimum Wiener solution can be expanded as follows:

$$w = R^{-1}_{(x_1+x_2)\cdot(x_1+x_2)} \cdot (P_{(x_1+x_2)\cdot d_1} + P_{(x_1+x_2)\cdot d_2})$$

$$w = R^{-1}_{(x_1+x_2)\cdot(x_1+x_2)} \cdot P_{(x_1+x_2)\cdot d_1} + R^{-1}_{(x_1+x_2)\cdot(x_1+x_2)} \cdot P_{(x_1+x_2)\cdot d_2}$$

$$w = \underbrace{R^{-1}_{(x_1+x_2)\cdot(x_1+x_2)} \cdot P_{(x_1+x_2)\cdot d_1}}_{\text{system 1}} + \underbrace{R^{-1}_{(x_1+x_2)\cdot(x_1+x_2)} \cdot P_{(x_1+x_2)\cdot d_2}}_{\text{system 2}}$$

Thus, from the above expansion, the optimum solution is the sum of two systems:

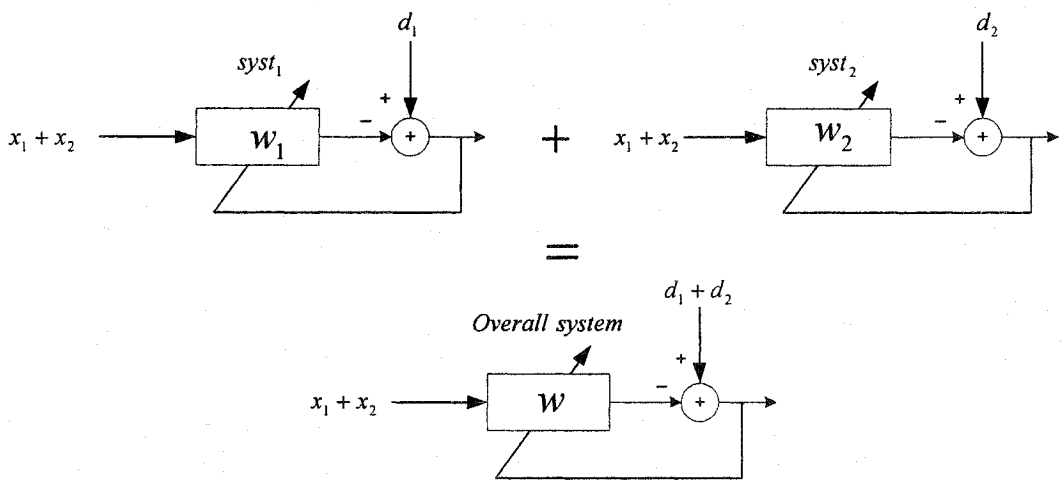

It can be seen that for the first system ($syst_1$), x_2 is some noise signal on the reference or input signal for the prediction of the desired signal d_1. For the second system ($syst_2$), x_1 is also some noise signal for the prediction of the desired signal d_2. As a result, for the overall system, the noisy/biased solution, w, will mostly predict (d_1 and d_2) depending on which reference (x_1 or x_2) is the most powerful.

For instance, if the common mode signal x_1 is X dB greater that the common mode signal x_2, then heuristically, d_1 can be predicted with X dB accuracy (achievable convergence), and d_2 is not predicted. The overall corrupting crosstalk differential signal, $d_1 + d_2$ in the

system, is then predicted to about X dB accuracy, again heuristically assuming d_1 is also greater than d_2 by at least X dB. Consequently, one of the main limitations of the crosstalk canceller convergence is then found in the case of different crosstalk signals that went through different paths (i.e. transmission lines) before reaching the receiver. FEXT crosstalk coming from the Remote Terminal transmitters ($syst_2$) and NEXT crosstalk coming from the transmitters in the neighbourhood of the customer receiver ($syst_1$) all travel through different paths, which means that the ideal solution of the adaptive filter canceller is different for each one of those cases. However, the only reference signal available for the crosstalk canceller is the sum of the crosstalk signals (x_1 + x_2) found in the common mode. This is different from having access to different reference signals (one for each crosstalk source i.e. d_1 and d_2) as shown in Figure 8-3, in which case the optimal canceller of each different crosstalk source could be computed and used separately to cancel individually each crosstalk source.

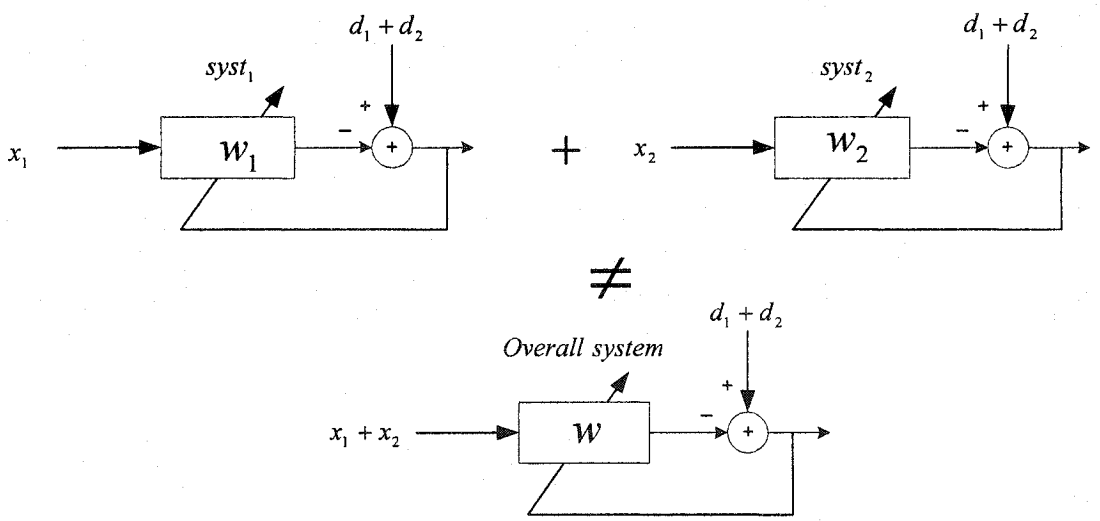

Figure 8-3: Having access to different reference signals x_1 and x_2 separately for each source d_1 and d_2 respectively

Instead, as previously indicated, in the case of having different crosstalk sources traveling through different paths and having different power levels at the receiver, the crosstalk canceller using the common mode signal can then in practice only converge to minimize

the most energetic crosstalk source down to the level of the second most powerful source (or down to the level of the sum of all other crosstalk sources if there are many sources).

As an example, two independent white Gaussian noise sequences were generated (x_1, x_2), with respective average power of $P_{x_1} = -39\ dBm$ and $P_{x_2} = -59\ dBm$. d_1 was obtained by filtering x_1 with a band pass filter (Figure 8-4), H_{BP}, with cutoff frequencies of 0.4π rad/samples and 0.8π rad/samples. d_2 was obtained by filtering x_2 with a low pass filter (Figure 8-5), H_{LP}, with a cutoff frequency of 0.1π rad/samples. The resulting average power for d_1 and d_2 were respectively $P_{d_1} = -43.9\ dBm$ and $P_{d_2} = -70.5\ dBm$.

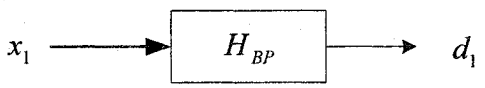

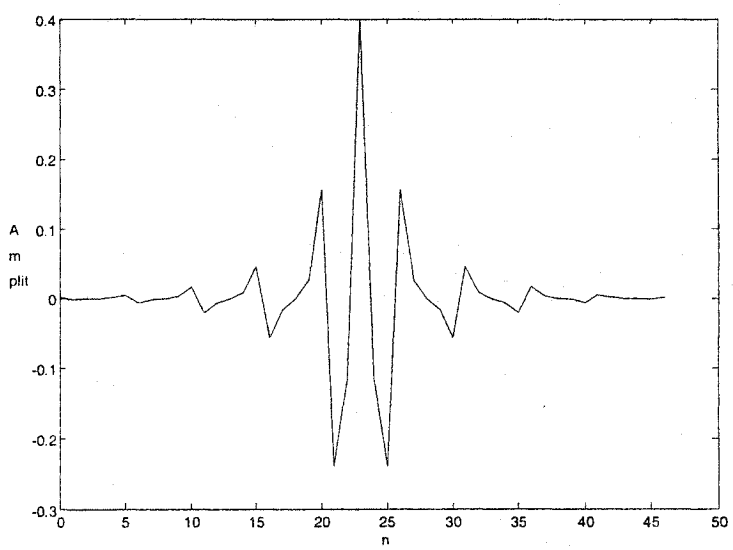

Figure 8-4: Impulse response of $H_{BP}(n)$

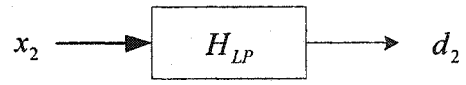

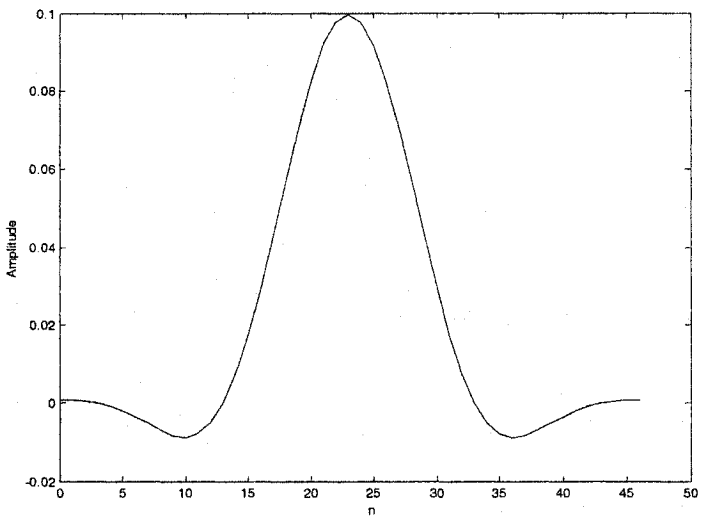

Figure 8-5: Impulse response of $H_{LP}(n)$

With the simulations of the interference canceling system using the above parameter settings and input signal powers, the convergence (Figure 8-6) reached was about 19.4 dB. This is approximately equal to the power ratio $X = | P_{x_1} - P_{x_2} |$ dB as expected.

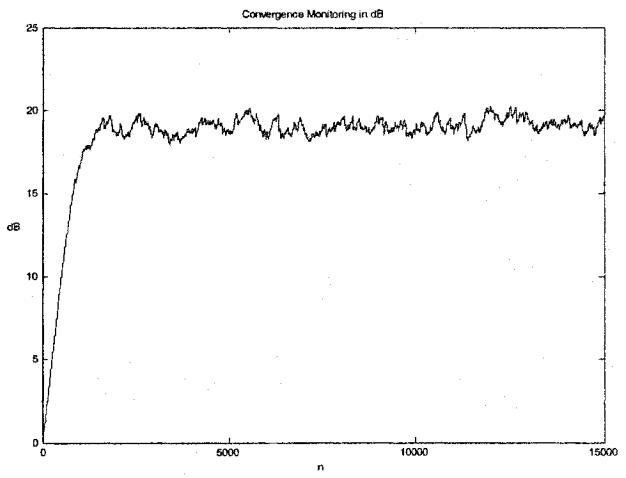

Figure 8-6: Convergence plot

Since x_1 is more powerful than x_2 the signal d_1 was predicted with about 19.4 dB accuracy, but not d_2. The resulting adaptive filter (Figure 8-7) impulse response has the shape of $h_{BP}(n)$ as anticipated.

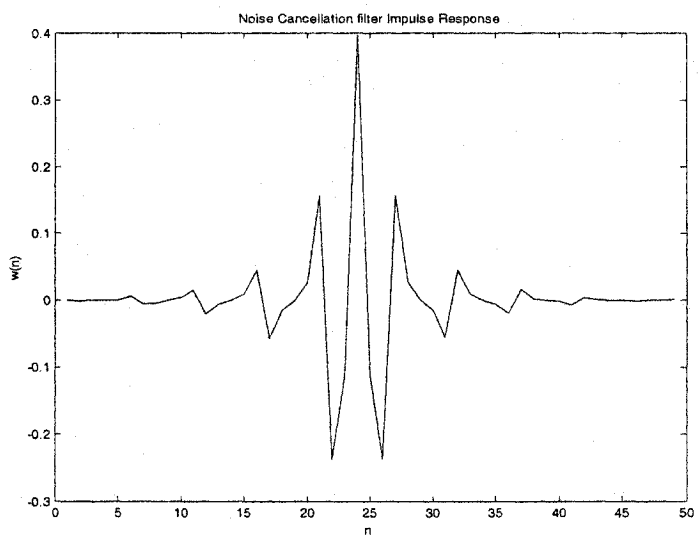

Figure 8-7: Adaptive noise cancellation filter obtained, $w(n)$

The value of the power ratio X as defined above (i.e. power difference in dB scale), which represents a measure of the achievable convergence, is only an heuristic approach at estimating the achievable convergence. In certain situations, the heuristic approach does not reflect adequately the achievable convergence. For these cases, the achievable convergence is calculated for individual frequencies by taking the ratio of the PSDs of x_1 and x_2. The following example illustrates a typical situation where the heuristic approach is not necessarily representative of the achievable convergence.

When x_1 and x_2 are in disjoint frequency bands such as typical frequency division multiplexed signals, it causes the NEXT and FEXT to be in a non-overlapping frequency bands.

As an example, two typical NEXT and FEXT common mode signals (with corresponding differential signals d_1 and d_2) have been generated and are represented by x_1 and x_2 respectively with common mode powers of $P_{x_1} = -1.5\ dBm$ and $P_{x_2} = -0.8\ dBm$. Their respective PSDs are shown in Figure 8-8.

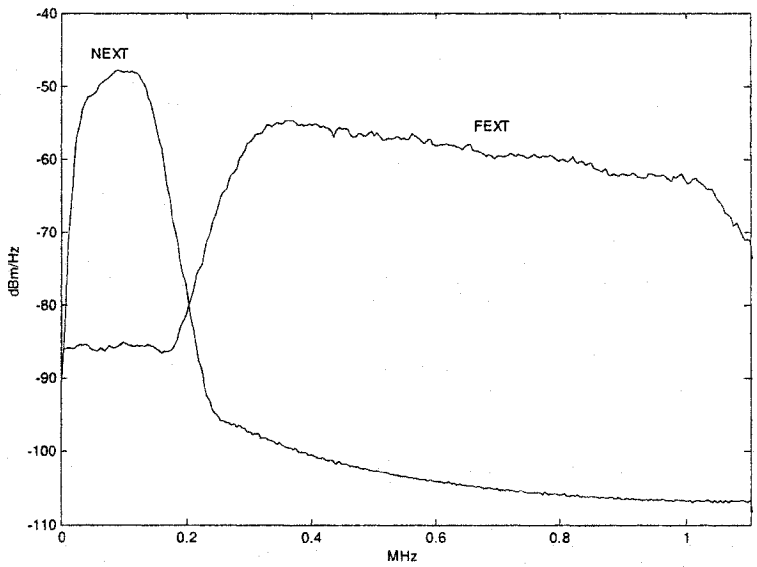

Figure 8-8: x_1 (NEXT) and x_2 (FEXT) common mode PSDs

Using the heuristic approach, the maximum achievable convergence of the canceller should be $X = |P_{x_1} - P_{x_2}| = 0.7$ dB. However, running the simulation, the actual convergence reached was 30.5 dB. The correct approach is to calculate the achievable convergence for individual frequencies by taking the ratio of the PSDs of x_1 and x_2 as shown in Figure 8-9.

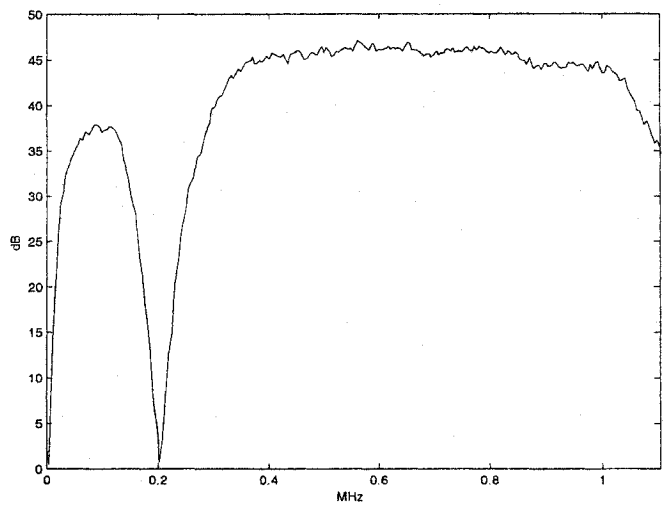

Figure 8-9: Frequency dependent achievable convergence

Furthermore, the frequency dependent convergence permits to evaluate the quality of the crosstalk canceller over different frequency bands. This information allows in determining the efficiency of the crosstalk canceller across the frequencies where the useful signal (i.e. desired differential signal as in Figure 8-1) has been transmitted and the frequencies outside this region of interest are not being crucial in this case.

8.2 Adaptive Noise Canceller Algorithm Comparisons

The adaptive noise canceller $w(n)$ was implemented using different adaptive filtering algorithms including the normalized least-mean-squares (NLMS) algorithm, a fast implementation of the recursive-least-squares algorithm (Fast-RLS), and the fast affine projection algorithm (FAP). The three algorithms will be briefly introduced, the order of complexity will be compared i.e. the computational load and a coarse estimation of the complexity with the number of adds and multiplies per iteration required will be also given for each algorithm. Finally, the relative convergence speed of the adaptive

algorithms will be also shown through the simulation of a selected scenario involving mixed technologies i.e. ADSL and VDSL.

The general structure of the adaptive crosstalk canceller for the transmission over the twisted pair wire is shown in Figure 8-10.

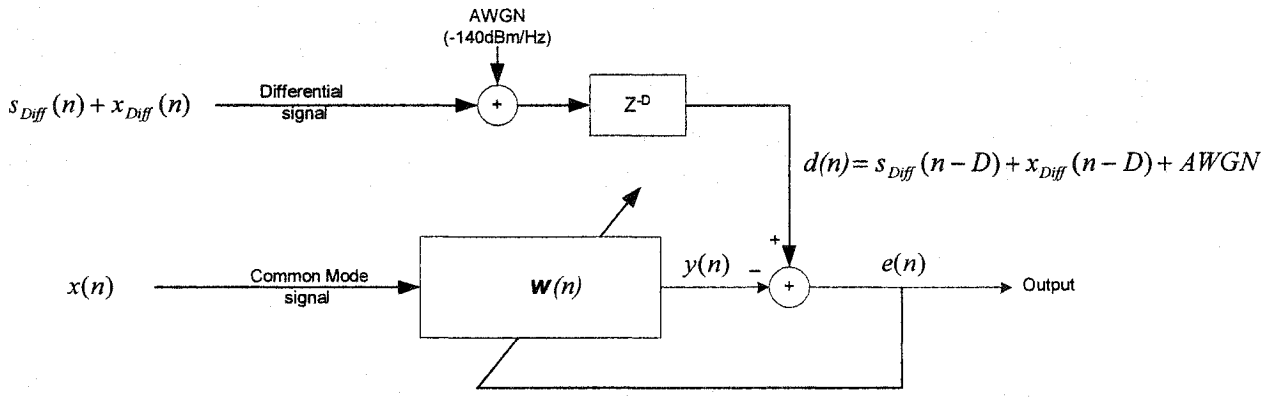

Figure 8-10: General structure of the adaptive crosstalk canceller

The common mode crosstalk signal $x(n)$ is the reference signal used by the canceller. It is assumed to be uncorrelated with the desired distorted differential signal (from the CO through the transmission channel), $s_{Diff}(n)$. $x_{Diff}(n)$ is the induced differential crosstalk signal correlated to $x(n)$. The coupling from the differential signal $s_{Diff}(n)$ to the common mode may exist but it is considered negligible with respect to the common mode crosstalk signal $x(n)$ level. $d(n)$ is the desired signal used by the canceller. It is a combination of $s_{Diff}(n)$ and $x_{Diff}(n)$ and AWGN, all delayed. The delay parameter Z^{D} as previously mentioned is to force the solution of the canceller (assumed to be FIR), $\boldsymbol{W}(n)$, to be causal. The filter coefficients may be adjusted such that the output of the filter $y(n)$ closely approximates $x_{Diff}(n-D)$.

In order to adjust the adaptive filter's coefficient weights, it is necessary to develop a performance function, which can be used to estimate the progress of the adjustments. Often, the performance function is taken to be the mean-squared error, $J(\boldsymbol{W})$, between the desired response $d(n)$ and the output of the filter $y(n)$ as represented by equation 8.1.

$$J(\boldsymbol{W}) = E\left\{|\, e(n)\,|^2\right\} = E\left\{|\, d(n) - y(n)\,|^2\right\} \tag{8.1}$$

where $y(n) = \boldsymbol{W}^T \cdot \boldsymbol{X}(n)$

$$\boldsymbol{W} = [w(0), w(1), \ldots, w(L-1)]^T$$

$$\boldsymbol{X}(n) = [x(n), x(n-1), \ldots, x(n-L+1)]^T$$

It is observed that the MSE is a quadratic function of the filter coefficients [PRO88]. Consequently, the minimization of $J(\boldsymbol{W})$ with respect to the coefficients leads to the set of L linear equations, which is known as the Wiener-Hopf equations [PRO88], with L being the number of coefficients of the filter. The equations may be expressed in matrix form as:

$$\boldsymbol{R}_{xx}\, \boldsymbol{W} = \boldsymbol{P}_{x \cdot d}$$

where $\boldsymbol{R}_{xx}$ is the L by L statistical auto-correlation matrix of the input $\boldsymbol{x}$ and $\boldsymbol{P}_{xd}$ is the L by 1 statistical cross-correlation vector between d and $\boldsymbol{x}$. The analytical solution of the optimum filter coefficients (the Wiener solution) is then given by:

$$\boldsymbol{W}_{wiener} = \boldsymbol{R}_{xx}^{-1}\, \boldsymbol{P}_{x \cdot d}\,.$$

However, in practice, the autocorrelation and cross-correlation are obtained from the data and represent estimates of the statistical ones. As a result, the filter coefficients obtained are estimates of the optimum coefficients and the quality depends on the data record that is available for the estimates. Also, L is often large, so the analytical approach could take a great amount of computational load. Furthermore, the statistical properties of $\boldsymbol{x}$ and $\boldsymbol{d}$ can slowly vary in time. Consequently, the statistical autocorrelation and cross-correlation and hence their estimates may vary in time. Therefore, it is necessary to find a

method which can track the variations in a non-stationary environment and also reduce the mathematical complexity required to solve the filter coefficients.

There are various numerical methods that can be used to solve the Wiener-Hopf equations for the optimum filter coefficients. The most popular are iterative methods that have been used to find the minimum of a function, such as $J(\boldsymbol{w})$ of several variables. The simplest iterative method is called the steepest-descent based on successive adjustments applied to the weight vector $\boldsymbol{W}(n)$ in the direction of the steepest descent, that is, in a direction opposite to the gradient vector $\boldsymbol{g}(n)$,of the performance function, $\boldsymbol{J}(n)$, at the n^{th} iteration. The update of the weight vector $\boldsymbol{W}(n)$ is illustrated as follows [HAY02]:

$$\boldsymbol{W}(n+1) = \boldsymbol{W}(n) - \frac{1}{2}\mu \cdot \boldsymbol{g}(n)$$

where μ is the step size parameter, which will be discussed shortly.

It should be noted that under stationary environments, the iterative solution converges (as $n \to \infty$) to the Wiener solution without having to invert the correlation matrix of the input vector [PRO88]. However, the steepest-descent method requires the knowledge of $\boldsymbol{R}_{xx}$ and $\boldsymbol{P}_{xd}$ because the equation for gradient vector is found to be [HAY02]:

$$\begin{aligned} \boldsymbol{g}(n) = \Delta \boldsymbol{J}(n) &= \frac{\partial \boldsymbol{J}(n)}{\partial \boldsymbol{W}} \\ &= -2P_{xd} + 2R_{xx}\boldsymbol{W}(n) \end{aligned}$$

Thus, the computations are still intensive and also in reality exact measurements of the gradient vector are not possible. The gradient vector must be estimated from the available data when operating in an unknown environment. In contrast, the least-mean square (LMS) algorithm does not require measurements of the pertinent correlation functions, nor does it require matrix inversion. The LMS algorithm takes the estimate of the gradient, $\hat{\boldsymbol{g}}(n)$, using the instantaneous squared error $|e(n)|^2$ instead of the mean-squared error, $J(n) = E\{|e(n)|^2\}$ [WID85].

$$\hat{\boldsymbol{g}}(n) = \frac{\partial |\, e(n)\,|^2}{\partial \boldsymbol{W}} = -2 \cdot e(n)\boldsymbol{X}(n)$$

The weight vector $\boldsymbol{W}(n)$ is then updated as the following:

$$\boldsymbol{W}(n+1) = \boldsymbol{W}(n) + \mu \cdot e(n) \cdot \boldsymbol{X}(n) \tag{8.2}$$

From its form as in equation 8.2, it can be seen that the LMS algorithm can be implemented in a practical system without squaring, averaging or differentiation, which reduces the system complexity. On the other hand, without averaging, the estimation of the gradient follows a noisy path that could occasionally steer in the wrong direction. However the LMS algorithm is recursive in nature (the presence of feedback), so the noise is attenuated with time by the adaptive process, which acts as a low-pass filter in this respect [WID85].

From the equation 8.2, one important parameter of the adaptive LMS algorithm is the step size parameter μ, which will be discussed by introducing one of the derivatives of the LMS algorithm that is the normalized LMS (NLMS).

8.2.1 NLMS

In the LMS algorithm, the adjustment applied to the tap-weight vector (filter coefficients) at iteration $n+1$ as shown in equation 8.2, is the product of three terms, the step size parameter, μ, which is under the designer's control, the input vector $\boldsymbol{X}(n)$ and the estimation error $e(n)$ at iteration n. However, to ensure convergence in the mean in the LMS algorithm, the choice for the step size parameter must be in the range given by [HAY02]:

$$0 < \mu < \frac{2}{\lambda_{\max}} \tag{8.3}$$

where $\lambda_{\max}$ is the largest eigenvalue of the correlation matrix $\boldsymbol{R}_{xx}$.

Also it is found that:

$$\lambda_{\max} < \sum_{k=0}^{L-1} \lambda_k = trace\, \boldsymbol{R}_{xx} = L \cdot E[x^2(n)] \tag{8.4}$$

where the estimate of $E[x^2(n)]$ is taken to be $\frac{1}{L}\sum_{i=0}^{L-1} x^2(n-i) = \frac{\|\boldsymbol{X}(n)\|^2}{L}$, which corresponds to the input power of $x(n)$.

Therefore, from the relation found in 8.3 and 8.4, the step size should not exceed:

$$\mu_{\max} = \frac{2}{\lambda_{\max}} \leq \frac{2}{\|\boldsymbol{X}(n)\|^2}$$

However, in a practical situation, the input power is not always known in advance or perhaps it can vary if the system changes such as in a non-stationary environment. Therefore, the solution of the adaptive algorithm could diverge or be unstable if the step size is chosen too high during initialization, or to exceed the maximum allowed at a certain time during the adaptive process. However, in the NLMS algorithm, the convergence (stability) condition is considered in the algorithm. The parameter μ in 8.2 is replaced by $\alpha \cdot \mu_{\max}$ where α varies between 0 and 1.

$$\boldsymbol{W}(n+1) = \boldsymbol{W}(n) + \alpha \cdot \frac{2}{\|\boldsymbol{X}(n)\|^2} \cdot \boldsymbol{X}(n) \cdot e(n) \tag{8.5}$$

The value of the adaptation constant parameter, α, determines the speed of convergence. The closer it is to 1, the faster the convergence but the more the residual noise i.e. the adaptive filter coefficients will oscillate ($n \to \infty$) with higher magnitude around the optimum coefficients. The NLMS algorithm can be viewed as the LMS algorithm with a time-varying step-size parameter [HAY02]. The adjustment applied to the tap-weight

vector at iteration n+1 is "normalized" with respect to the squared Euclidean norm of the tap-input vector $\boldsymbol{X}(n)$ at iteration n, hence the term "normalized"[HAY02]. More importantly, the NLMS exhibits a rate of convergence that is potentially faster than the standard LMS. However, the rate of convergence for both the NLMS or the LMS is determined by the eigenvalue spread of the correlation matrix vector that is the ratio $\frac{\lambda_{max}}{\lambda_{min}}$ where λ_{min} is the smallest eigenvalue of R_{xx} [PRO88]. If the eigenvalue spread is small, the convergence will be rapid. On the other hand, if eigenvalue spread is large, the convergence of the algorithm is slow.

The NLMS algorithm is computationally very efficient with an order of complexity of 2L. The NLMS algorithm used is summarized in the following table.

Table 8-1: NLMS Algorithm

$\boldsymbol{X}(n) = L-by-1$ *tap input vector at time n*

$d(n)$ = *desired response at time step n*

$\tilde{\mu}$ = *adaptation constant*, $0 \le \tilde{\mu} < 2$

$\delta > 0$, *small constant*

Iteration: *For* $n = 0, 1, 2, \ldots$, *compute*

$$e(n) = d(n) - \boldsymbol{W}^{H}(n)\boldsymbol{X}(n)$$

$$\boldsymbol{W}(n+1) = \boldsymbol{W}(n) + \frac{\tilde{\mu}}{\delta + \|\boldsymbol{X}(n)\|^2} \cdot \boldsymbol{X}(n) \cdot e(n)$$

It should be noted that in Table 8-1, the variable parameter α and the factor coefficient of equation 8.5 has been replaced by $\tilde{\mu}$. Also, when the tap-input vector $\boldsymbol{X}(n)$ is small, numerical difficulties may arise by dividing by a small value for the squared Euclidean norm $\|\boldsymbol{X}(n)\|^2$, thus a small off-set parameter δ is inserted [HAY02].

8.2.2 Fast RLS Algorithm

The major advantage of the NLMS or the LMS algorithm lies in its computational simplicity. However, the drawback is slow convergence especially when the eigenvalues of the autocorrelation matrix R_{xx} have a large spread [PRO88]. Furthermore, from another point of view, the LMS algorithm has only a single adjustable parameter for controlling the convergence rate as discussed in the previous section, namely the step-size parameter. To obtain faster convergence, it is necessary to develop more complex algorithms, which involve additional parameters such as in the Recursive Least Squares (RLS) algorithm.

The previous algorithm has been developed by employing the concept of a search i.e. the available data have been used in attempts to move (via the estimation of the gradient) the current estimate of the filter coefficients to the optimum filter coefficients at each step [TRE01]. However, the RLS algorithm uses the input data in a way as to obtain optimality at each step. The RLS algorithm adopts the least squares criterion instead of the statistical approach based on the MSE criterion [PRO88].

The algorithm will be briefly described by only providing the main results since the complete procedure can be found in several literatures [HAY02][TRE01][PRO88]:

The RLS algorithm determines the filter coefficient vector that minimizes the weighted sum of the magnitude squared errors as follows:

$$J_{RLS}(n) = \sum_{i=0}^{n} \beta^{n-i} \mid e(i) \mid^2 = \sum_{i=0}^{n} \beta^{n-i} \mid d(i) - y(i) \mid^2$$

where β is the weighting factor in the range of $0 < \beta \leq 1$. The purpose of the exponential weighting factor is to weight the most recent data points more heavily and thus allowing the filter coefficients to adapt to time-varying statistical characteristics of the data [PRO88] (i.e. in a non-stationary environment) with an effective memory of $\frac{\beta}{1-\beta}$.

The minimization of $J_{RLS}(n)$ with respect to the filter coefficients $\boldsymbol{W}$ yields the set of L linear equations [PRO88]:

$$\boldsymbol{R}_{RLS}(n)\boldsymbol{W}(n) = \boldsymbol{D}_{RLS}(n)$$

where $\boldsymbol{R}_{RLS}(n)$ is the signal (estimated) correlation matrix similar to $\boldsymbol{R}_{xx}$ defined as:

$$\boldsymbol{R}_{RLS}(n) = \sum_{i=0}^{n} \beta^{n-i} \boldsymbol{X}^*(i)\boldsymbol{X}^T(i).$$

and $\boldsymbol{D}_{RLS}(n)$ is the signal (estimated) crosscorrelation vector similar to $\boldsymbol{P}_{xd}$ defined as:

$$\boldsymbol{D}_{RLS}(n) = \sum_{i=0}^{n} \beta^{n-i} \boldsymbol{X}^*(i)d(i)$$

The optimum solution (8.6) at time index n is then:

$$\boldsymbol{W}(n) = \boldsymbol{R}_{RLS}^{-1}(n)\boldsymbol{D}_{RLS}(n) \tag{8.6}$$

However, supposing that the optimum solution given by equation 8.6 is found for time index n -1 (i.e. $\boldsymbol{W}(n\text{-}1)$) and willing to compute $\boldsymbol{W}(n)$, it is impractical to solve again the set of L linear equations for each new signal component coming in during the adaptation process. Instead, to the reduce the computational requirement for the algorithm, it is possible to compute the matrix and vectors above recursively [PRO88] as:

$$\boldsymbol{R}_{RLS}(n) = \beta \cdot \boldsymbol{R}_{RLS}(n-1) + \boldsymbol{X}^*(n)\boldsymbol{X}^T(n)$$

$$\boldsymbol{D}_{RLS}(n) = \beta \cdot \boldsymbol{D}_{RLS}(n-1) + d(n)\boldsymbol{X}^*(n)$$

and by employing the matrix inversion lemma, $\boldsymbol{R}_{RLS}^{-1}(n)$ is found to be [PRO88]:

$$\boldsymbol{R}_{RLS}^{-1}(n) = \frac{1}{\beta} \cdot \left[\boldsymbol{R}_{RLS}^{-1}(n-1) - \boldsymbol{K}(n)\boldsymbol{X}^T{}_{RLS}(n)\boldsymbol{R}_{RLS}^{-1}(n-1)\right]$$

where $\boldsymbol{K}(n)$ is called the Kalman gain vector defined as:

$$\boldsymbol{K}(n) = \frac{\boldsymbol{R}_{RLS}^{-1}(n-1)\boldsymbol{X}^*(n)}{\beta + \left[\boldsymbol{X}^T(n)\boldsymbol{R}_{RLS}^{-1}(n-1)\boldsymbol{X}^*(n)\right]}$$

Also, it is not shown in here but a matrix $\delta \cdot \boldsymbol{I}$ is initially added to $\boldsymbol{R}_{RLS}(n)$ in order to make $\boldsymbol{R}_{RLS}^{-1}(n)$ invertible for small values of n. $\boldsymbol{I}$ is an L-*by*-L identity matrix and δ is a small positive constant. With exponential weighting into the past, the effect of adding $\delta \cdot \boldsymbol{I}$ is dissipated with time.

It should be noted that several steps have been purposely omitted to get to the final result but they can found in [PRO88].

The update of the filter coefficient vector is found to be:

$$\boldsymbol{W}(n) = \boldsymbol{W}(n-1) + \boldsymbol{K}(n)e(n)$$

It can be observed that the filter coefficients vary with time by an amount equal to the error $e(n)$ multiplied by the Kalman gain vector $\boldsymbol{K}(n)$. Since $\boldsymbol{K}(n)$ is an L dimensional vector, each coefficient is controlled by one of the elements of $\boldsymbol{K}(n)$ [PRO88]. An analogy to the NLMS algorithm is that the RLS algorithm defines just the right step size and the right direction to retain optimality over each time sample [TRE01]. As a result, rapid convergence can be obtained. Furthermore, the rate of convergence of the RLS algorithm is invariant to the eigenvalue spread of the ensemble-average correlation matrix $\boldsymbol{R}_{xx}$ of the input vector $x(n)$ [HAY02].

Regarding the complexity, the RLS algorithm presented above has a computational complexity proportional to L^2. However, when the input vector $\boldsymbol{X}(n)$ is a time-series, it is possible to obtain the time-update equations for the Kalman gain vector, and the resulting algorithms have a complexity that is proportional to L (multiplications and divisions) and hence they are called Fast RLS algorithms. One of the algorithms used for the simulation is presented in Table 8-2. It employs a transversal filter structure, which has an order of complexity of $9L + 3$. The complete algorithm description can be found in [PRO88].

Table 8-2: Fast RLS algorithm

Initialization

$$\boldsymbol{a}_{L-1}(-1) = \boldsymbol{b}_{L-1}(-1) = \boldsymbol{0}$$

$$\boldsymbol{K}_{L-1}(-1) = \boldsymbol{0}$$

$$\boldsymbol{W}_{L}(-1) = \boldsymbol{0}$$

$$E^{f}(-1) = \delta, \delta > 0$$

Iteration: For n = 0,1,2,..., *compute*

$$f(n) = x(n) + \boldsymbol{a}_{L-1}^{T}(n-1)\boldsymbol{X}_{L-1}(n-1)$$

$$g(n) = x(n-L+1) + \boldsymbol{b}_{L-1}^{T}(n-1)\boldsymbol{X}_{L-1}(n)$$

$$\boldsymbol{a}_{L-1}(n) = \boldsymbol{a}_{L-1}(n-1) - \boldsymbol{K}_{L-1}(n-1)x(n-L+1)f(n)$$

$$fp(n) = x(n) + \boldsymbol{a}_{L-1}^{T}(n)\boldsymbol{X}_{L-1}(n-1)$$

$$E^{f}(n) = \beta \cdot E^{f}(n-1) + f(n)fp^{*}(n)$$

$$\begin{bmatrix} \boldsymbol{C}_{L-1}(n) \\ c(n) \end{bmatrix} = \boldsymbol{K}_{L}(n) = \begin{bmatrix} 0 \\ \boldsymbol{K}_{L-1}(n-1) \end{bmatrix} + \frac{fp^{*}(n)}{E^{f}(n)} \begin{bmatrix} 1 \\ \boldsymbol{a}_{L-1}(n) \end{bmatrix}$$

$$\boldsymbol{K}_{L-1}(n) = \frac{\boldsymbol{C}_{L-1}(n) - c(n)\boldsymbol{b}_{L-1}(n-1)}{1 - c(n)g(n)}$$

$$\boldsymbol{b}_{L-1}(n) = \boldsymbol{b}_{L-1}(n-1) - \boldsymbol{K}_{L-1}(n)g(n)$$

$$y(n) = \hat{d}(n) = \boldsymbol{W}_{L}(n-1)\boldsymbol{X}_{L}(n)$$

$$e(n) = d(n) - \hat{d}(n)$$

$$\boldsymbol{W}_{L}(n) = \boldsymbol{W}_{L}(n-1) + \boldsymbol{K}_{L}(n)e(n)$$

Note that for clarity the subscripts for some variables are present to indicate their respective vector dimension.

8.2.3 Fast Affine Projection Algorithm

The third and last algorithm briefly presented is the Affine Projection algorithm (APA). It can be viewed as an intermediate between the normalized LMS and the recursive least-squares algorithms. By employing several input vectors, the APA provides faster convergence than the NLMS, and requires fewer computations than the RLS method. It is found that the affine projection algorithms or their low-computational implementations can produce a good tradeoff between convergence speed and computational complexity [BOU03].

The affine projection algorithm is a generalization of the normalized LMS algorithm. More specifically, the adjustment term $\frac{\tilde{\mu}}{\delta + \|\boldsymbol{X}(n)\|^2} \cdot \boldsymbol{X}(n) \cdot e(n)$ applied to the filter tap-weight vector in the NLMS algorithm as in Table 8-1 is replaced by the more elaborate term [HAY02]:

$$\tilde{\mu} \cdot \boldsymbol{A}(n) \cdot \left[\boldsymbol{A}^T(n) \cdot \boldsymbol{A}(n) + \delta \cdot \boldsymbol{I}\right]^{-1} \cdot \boldsymbol{e}(n)$$

where:

$$\boldsymbol{A}(n) = \left[\boldsymbol{X}(n), \boldsymbol{X}(n-1), \ldots, \boldsymbol{X}(n-N+1)\right]$$

$$\boldsymbol{e}(n) = \boldsymbol{d}(n) - \boldsymbol{A}^T(n) \cdot \boldsymbol{W}(n)$$

$$\boldsymbol{d}(n) = \left[d(n), d(n-1), \ldots, d(n-N+1)\right]^T$$

It can be observed that in the NLMS, the new adaptive filter weights have to best fit the last input vector $\boldsymbol{X}(n)$ to the corresponding desired signal $d(n)$. However, it can be seen that the affine projection algorithm uses (N-1) past values of both the tap-input vector $\boldsymbol{X}(n)$ and the desired response $d(n)$. N is the number of multiple constraints, which defines the projection order. For the special case where N=1, the APA algorithm reduces to the original NLMS algorithm. Similar to the NLMS algorithm, the inversion of the N-by-N

matrix product $A^T(n)\cdot A(n)$ may cause to numerical difficulties so $\delta\cdot I$ is added, where I is the identity matrix and δ is a small positive constant.

From a geometric point of view, in the NLMS algorithm, it can be observed that the direction of adjustment of the tap-weight vector is the same as that of the input vector $X(n)$ [HAY02]. Under this interpretation, the NLMS is viewed as a one dimensional affine projection. However, in APA the projections are made in multiple dimensions [GAY00]. As the projection dimension (order) increases (N), so does the convergence speed, but unfortunately the computational complexity increases as well. For the time series inputs, there are techniques that can reduce the computational load, giving as a result fast affine versions of APA (FAP). A fast affine algorithm is found in [GAY00] called FAP-RLS. Since APA requires an implicit inverse of the input matrix product defined as $R(n)=A^T(n)\cdot A(n)+\delta\cdot I$, the FAP algorithm in [GAY00] uses a sliding windowed RLS type approach based on the matrix inversion lemma to update the inverse covariance matrix to achieve faster computation. The order of complexity of FAP-RLS is about $2L + 3N^2+8N$. The FAP-RLS algorithm found in [GAY00] is shown in Table 8-3.

Table 8-3: FAP algorithm

Initialization

$r(0)=0,\quad \eta(0)=0,\quad P(0)=I/\delta,\quad W(0)=0$

$a(n)=R^{-1}(n-1)d(n)$

$\alpha(n)=\left[1+d'(n)a(k)\right]^{-1}$

$Q^{-1}(n)=R^{-1}(n-1)-\alpha(n)a(n)a'(n)$

$b(n)=Q^{-1}(n)d(n-L)$

$\beta(n)=\left[1+d'(n-L)b(k)\right]^{-1}$

$R^{-1}(n)=Q^{-1}(n)+\beta(n)b(k)b'(k)$

$r(n)=r(n-1)+x(k)\bar{d}(n-1)-x(n-L)\bar{d}(n-L-1)$

where $r(n)$ is a correlation vector of size N -1

$\bar{d}(n)$ is made up of the first (i.e top) N -1 entries of $d(n)$

$e(n)=y(n)-W'(n-1)X(n)-\tilde{\mu}\cdot\bar{\eta}'(n-1)r(n)$

$\varepsilon(n)=e(n)p(n)$ where $p(n)=$ 1st column of $R^{-1}(n)$

$\eta(n-1)=\varepsilon(n)+\left[0,\bar{\eta}'(n-1)'\right]'$

$W(n)=W(n-1)+\mu\cdot x(L-(N-1))\eta_{N-1}(n)$

Chapter 9

Simulations

This chapter evaluates the performance of the crosstalk canceller under different conditions. It starts by evaluating the complexity and the convergence speed of the crosstalk canceller with the three adaptive algorithms (briefly defined in Chapter 8) in a selected scenario. It continues by considering the conditions under which the simulations of the different scenarios have been performed and the measures that were used to evaluate the performance of the crosstalk canceller. It finishes by presenting the simulation results of the different scenarios.

9.1 Complexity and Convergence Speed Comparisons

In most DSL technologies, an initialization sequence is mandated where the training and synchronization of the two modems is performed, and also where the equalizers are trained. The time of training is limited, and therefore the convergence speed is evaluated because the training has to be done in this allotted time. The complexity of each algorithm is presented for reference and could be a decisive factor in determining the algorithm for a practical implementation.

Table 9-1 shows the order of complexity (i.e. the computational load) for the three considered algorithms, and a coarse estimation of the complexity with the number of adds and multiplies per iteration required by each algorithm.

Table 9-1: Order of complexity of the three considered adaptive algorithms for L=90 filter taps

Algorithm Type	Order of complexity (adds and multiplies/iteration)	Estimate for L = 90 filter Taps (adds and multiplies/iteration)
NLMS	2L	180
FAP (N=10)	$2L+N^2+8N$	360
Fast-RLS	9L + 3	813

Simulations have been performed to indicate the relative convergence speed of each adaptive algorithm for a selected scenario as shown in Figure 9-1.

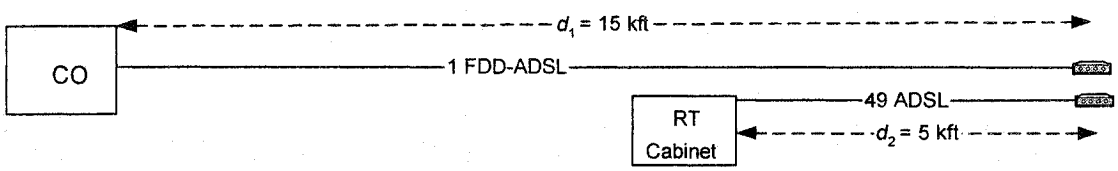

Figure 9-1: Selected scenario to evaluate the convergence speed

The selected scenario was undertaken for a d_1=15 kft 24-gauge transmission line deployed from the Central Office (CO-served line) with a 1.5 Mb/s downstream data rate. The Remote-Terminal (Cabinet) was located at d_2=5 kft from the considered customer of the CO-served line i.e. 10 kft from the central office. 49 ADSL crosstalkers (disturbers) were located at the Cabinet (i.e. 49 ADSL lines deployed from the Remote Terminal).

The crosstalk canceller was adapted using the three adaptive algorithms for the scenario above. Table 9-2 shows the training time required to adapt the filter coefficients to generate an output which closely resembles the differential crosstalk signal that corrupted the desired differential signal, from the reference common mode crosstalk signal (i.e. resulting NEXT/FEXT common crosstalk signal)

The target convergence was chosen to be 15 dB but only in the region of interest, which is over the frequencies where the desired signal has been transmitted. This convergence was calculated by taking the power ratio of the initial FEXT/NEXT differential level in the frequency band used to transmit the desired (useful) signal, over the remaining FEXT/NEXT component not removed by the canceller in the same frequency band (refer to section 9.2 for more details). A convergence of 15 dB is usually adequate to reduce the bit error rate (BER) on the useful differential signal, which will be discussed in the next section.

Table 9-2: Convergence speed comparisons for L=90 filter taps and 40 causality delays

Algorithm Type	Iterations for 15dB Convergence (Time in sec) (In the band of interest)	Overall Convergence (dB) (Across all frequencies)
NLMS	$3.1 \cdot 10^5$ (0.14 sec)	12.5
FAP (N=10)	$2.2 \cdot 10^5$ (0.09 sec)	18.4
Fast-RLS	$1.8 \cdot 10^5$ (0.08 sec)	21.7

It can be observed that the advantage of using a RLS-type algorithm (such as the Fast-RLS algorithm) over a more basic NLMS algorithm is a faster convergence speed, which can be significant if the number of samples available for training is limited. On the other hand, Table 9-2 shows that the complexity of the Fast-RLS is about 4.5 times the complexity of the NLMS. Therefore, there is the expected performance-cost tradeoff.

The target convergence in the considered frequency band was 15 dB for all three algorithms. The third column contains the overall convergence level. This is a measure to evaluate the performance of the crosstalk canceller with respect to the power of the remaining crosstalk signal across the entire frequency band instead of being limited to the frequency band where the desired (useful) signal is transmitted. When the FAST-RLS algorithm reached 15 dB over the desired frequency band, the overall convergence reached 21.7 dB as opposed to only 12.5 dB for the NLMS algorithm.

The FAP algorithm performs better than the NLMS but worse than the Fast-RLS algorithm, as expected. Its complexity is also found between the complexity of the other two algorithms.

It should be noted that since the hybrid circuit is not ideal, the upstream signal is not entirely removed. Therefore, some residual upstream signal still remains and would only affect the low frequency band (i.e. outside the frequency band of interest of the downstream FDD-ADSL signal) of the reference signal used by the crosstalk canceller. Consequently, the convergence speed is slowed down but the achievable convergence in the frequency band of interest is not affected.

Table 9-3 shows respectively the various received signal power level involved for the adaptive crosstalk canceller as shown in Figure 8-1 or reproduced again in Figure 9-3.

Table 9-3: Power received for NEXT/FEXT

	Power at receiver (of the CO-served line) in dBm	
	Over frequency band of interest	Over entire frequency band
Differential useful signal, $s_{Diff}(n)$	-31.7	-31.2
NEXT crosstalk differential signal, first component of $x_{Diff}(n)$	-72.4	-45.5
NEXT common mode signal, first component of $x(n)$	-26.4	1.5
FEXT crosstalk differential signal, second component of $x_{Diff}(n)$	-48.5	-44.9
FEXT common mode signal, second component of $x(n)$	-7.7	-5.9
AWGN	-84.7	-79.5

9.2 Crosstalk Canceller Performance

The convergence of the crosstalk canceller was calculated only in the frequency band where the useful differential signal was transmitted since this is the only region of interest. The frequency band of interest is taken to be from the lowest tone number allocated by the bitloading algorithm up to the highest tone number where bits were allocated, even though it is possible that the bitloading algorithm did not allocate bits to certain tones. This convergence was calculated by taking the power ratio of the sum of the original differential FEXT and NEXT components in the frequency band of interest, over the remaining differential FEXT and NEXT components not removed by the canceller in the same frequency band.

The performance of the crosstalk canceller was evaluated by measuring the BER before and after the Reed-Solomon Forward Error Correction (RS FEC). The goal of the crosstalk canceller is to reduce the BER to a value that can be corrected by the RS FEC. As mentioned in Chapter 3, the RS FEC is capable of correcting BER in the order of 10^{-3}. The subjective performance of the DSL applications is better evaluated at the upper protocol stack layers at the byte level after all error correction has been performed. As a result, the two performance evaluation parameters are the bit error rate (BER) before any error correction on the received data stream and the byte error rate after all error correction has been performed. A value of 0% is indicated in the results of the column of the byte error rate after error correction when the BER after correction is below 10^{-7}.

The crosstalk canceller was trained until it had reached predetermined convergence levels in the frequency band of interest. The performance was evaluated at each convergence level with different data samples than those used to train the canceller. The number of bits used to evaluate the performance ranged from $4 \cdot 10^5$ to $2 \cdot 10^6$.

9.3 Simulation Environment

The implemented crosstalk canceller has 90 filter taps and the causality delay Z^{-D} as shown in figures 8-1 and 8-10 was chosen to be 40. A delay of 40 samples is sufficient to compensate mainly for the propagation delay difference between the common and differential mode signals from the Remote Terminal located at d_2=5 kft from the customer. Since the delay is adequate for a distance of 5kft, it will be more than sufficient for Remote Terminals located at distances below 5kft from the customer. The number of filter taps and the delay have been kept constant for all the simulations in order to minimize the number of variable parameters and to simplify the comparisons between different scenarios.

The scenarios presented are divided in three major sections corresponding to the type of disturbers (interference) involved in the CO-RT architecture, and is illustrated in Figure 9-2. In the first section, the only type of technology deployed from the Remote Terminal is full rate FDD-ADSL. In the second section, only VDSL technology is deployed and finally in the third section, both VDSL and ADSL are deployed from the Remote Terminal.

Each section presents different cases where the distance of the Remote Terminal from the customer (d_2) are 5 kft, 3 kft and 1 kft and the number of disturbers can be 12, 24 or 49. The bundle used for the simulations contains fifty twisted pairs but not all the lines have to be active.

The bit rate for the reference line (i.e. the line deployed from the central office (CO-served line) was selected to be a downstream 1.5 Mb/s for a 15kft transmission line (i.e. d_1=15kft). This data rate for the long line cannot be maintained when a Remote Terminal is present (CO-RT architecture)[SON02]. Most documents evaluating the

performance of the CO-RT architecture use 1.5 Mb/s [SON02][KER02b][TSA01] as a reference.

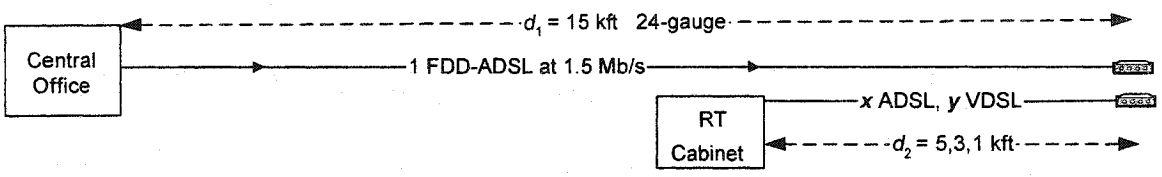

Figure 9-2: Simulated scenarios

Operators will want to preserve their current DSL deployment from the Central Office when a Remote Terminal is overlaid. The addition of the Remote Terminal will degrade the performance of the currently installed DSL services, therefore a solution must be provided to maintain the quality of service of the existing DSL services deployed from the Central Office. The simulations are performed with this in mind, by forcing the data rate of 1.5 Mb/s without regard for what can actually be transmitted without errors, which is generally significantly lower [STA02]. The crosstalk cancellation is then performed and the resulting performance is compared to see if 1.5 Mb/s is possible to maintain. Thus, it is providing a possible solution to the severe crosstalk problem emerged by the addition of a Remote Terminal.

Throughout all the simulations, the power density level of the background noise in differential mode was selected to be –140 dBm/Hz (AWGN), and was injected at the receiver as shown in Figure 8.1. For a frequency bandwidth of 0 to 1.104MHz, the noise power is -79.5 dBm.

Before performing any simulations for this thesis, the validity of the differential crosstalk signal power levels were verified by comparing with known data rate simulation results contained in [STA99] for the same type of scenario where d_1=15 kft and d_2=5 kft. The simulation results of [STA02] claims that the reference ADSL line can only operate at a maximum downstream data rate of 300 kb/s in the presence of one ADSL disturber located at the RT. In this work, the simulation's bitloading algorithm determined that a

maximum data rate of 325 kb/s was attainable. This small verification permitted to evaluate the degree of validity of the crosstalk levels, the line attenuation and the bitloading algorithm, which all seem to concord with actual simulations.

This first scenario is presented in detail to illustrate the important elements of the recorded data. The following scenarios will present only the pertinent information to avoid redundancy. Also, for convenience, the general structure of the adaptive crosstalk canceller of Figure 9-3 is shown again to illustrate the considered signals.

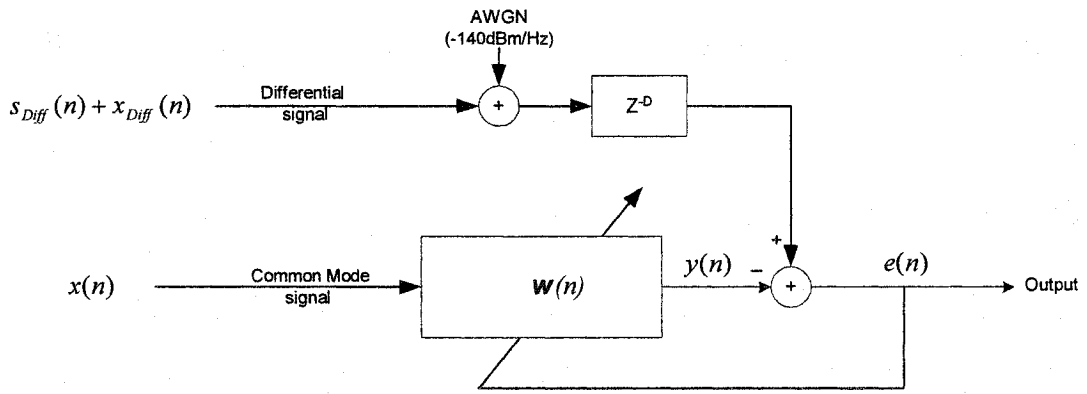

Figure 9-3: General structure of the crosstalk canceller

9.4 Results for Only ADSL Type Disturbers in the Remote Terminal

Three cases will be presented where the location of the remote terminal (d_2) is located at 5 kft, 3 kft and 1 kft from the RT-served customers and the number of FDD-ADSL disturbers can be 12, 24, 49.

9.4.1 Remote Terminal at d_2 = 5kft

The following are the comprehensive simulation results obtained (Figure 9-4 to 9-8) for x = 49 FDD-ADSL disturbers located at the Remote Terminal DSLAM at a distance of d_2 = 5kft. The performance of the crosstalk canceller obtained is shown in Table 9-5.

The SNR per tone and the corresponding bitloading allocation per tone for the above scenario are shown in Figure 9-4.

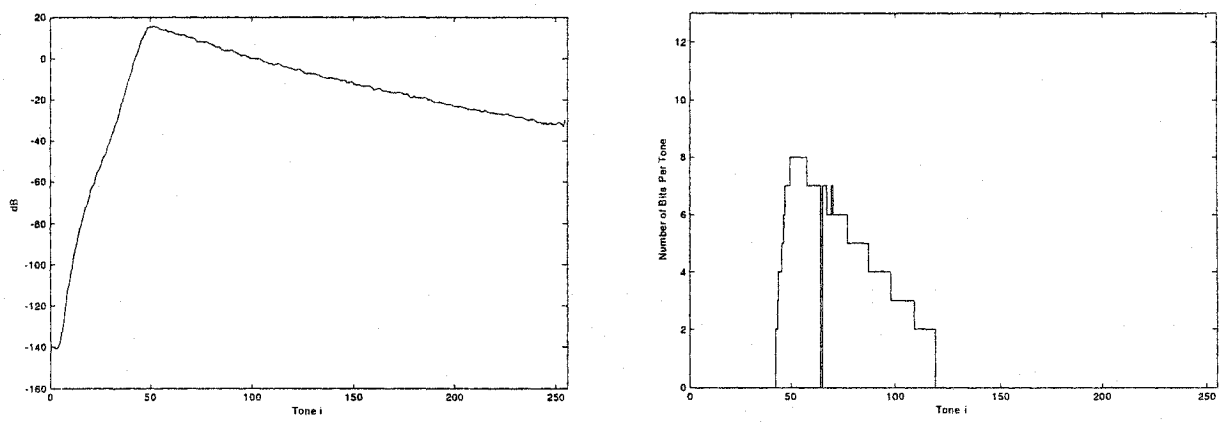

Figure 9-4: SNR per tone (left) and corresponding bitloading allocation results for each tone (right)

Figure 9-5 illustrates the PSDs of the crosstalk in differential mode (differential NEXT and FEXT) present at the CO-served customer receiver from the 49 FDD-ADSL transmitters at the Remote Terminal. Figure 9-5 also shows the corresponding PSDs of the crosstalk in common mode that will be used by the crosstalk canceller as an input reference signal. However, only the aggregated common mode crosstalk signal is available as the reference input signal for the canceller.

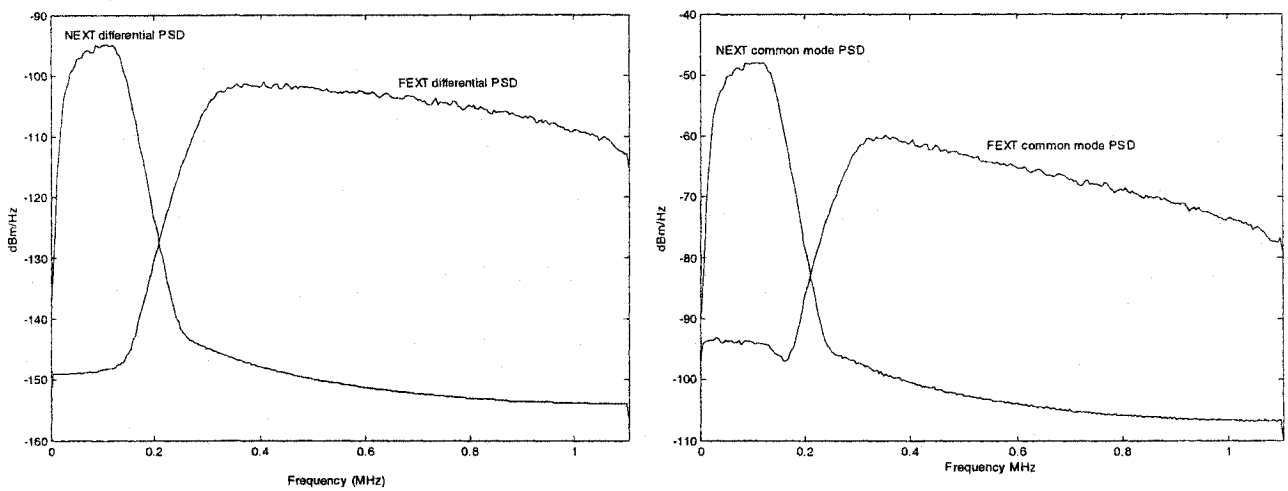

Figure 9-5: Differential crosstalk PSDs (left) and Common mode crosstalk PSDs (right)

Figure 9-6 demonstrates the maximum achievable convergence level at each frequency represented by the maximum convergence curve. The maximum convergence level at each frequency is constrained by the common mode PSDs levels of NEXT and FEXT of Figure 9-5 as explained in Chapter 8. It should be noticed that from Figure 9-6, in this scenario, at about 215 kHz, the NEXT and FEXT PSD levels of the common mode reference are approximately the same, so the canceller typically cannot converge at that frequency. It is easily noticed in Figure 9-6, where the convergence level is about 1 dB. However, looking at Figure 9-4, the SNR at about 215 kHz (corresponding to tone number 50 (50*4.3125 kHz/Tone)) is quite high thus the crosstalk component would be much weaker than the desired useful signal component in that tone. Therefore, the consequence of a low level convergence as to remove the crosstalk efficiently is then diminished at the considered frequency.

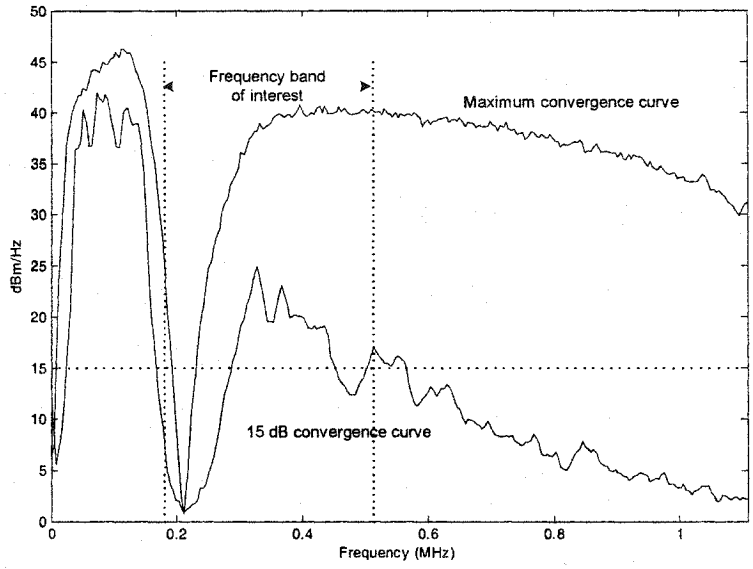

Figure 9-6: Crosstalk canceller convergence vs frequency shown for 15 dB convergence over the frequency band of interest and the maximum convergence achievable curve.

The NEXT differential signal caused by the upstream FDD-ADSL transmission should not affect the downstream desired (useful) signal for the CO-served customer since the frequency range of the NEXT signal does not overlap the desired signal frequency band (i.e. the frequency band of interest) due to the frequency duplexing transmissions (FDD-ADSL) in the CO-RT architecture. The frequency band of interest has been defined by the bitloading allocation of Figure 9-4. However, the NEXT differential signal and more specifically the common mode NEXT signal is still an important consideration for the convergence of the adaptive filter as explained above.

Also, in Figure 9-6, the 15 dB convergence curve represents the convergence for each frequency when a 15 dB convergence over the frequency band of interest was achieved (that is 15 dB convergence obtained by taking the power ratio of the sum of the original differential FEXT and NEXT components in the frequency band of interest, over the remaining differential FEXT and NEXT components not removed by the canceller in the same frequency band).

The adaptive filter was trained to only 15 dB of convergence in this example since as shown in Table 5-1, 15 db of convergence is enough to bring the BER below 10^{-3} where the Reed-Solomon FEC can correct the residual errors.

For reference, the resulting power levels at the CO-served receiver are presented again in Table 9-4.

Table 9-4: Power levels at CO-served customer receiver for 49 FDD-ADSL disturbers with d_2 = 5kft

Power at receiver (of the CO-served line) in dBm		
	Over frequency band of interest	Over entire frequency band
Differential useful signal, $s_{Diff}(n)$	-31.7	-31.2
NEXT differential signal, first component of $x_{Diff}(n)$	-72.4	-45.5
NEXT common mode signal, first component of $x(n)$	-26.4	1.53
FEXT differential signal, second component of $x_{Diff}(n)$	-48.5	-44.9
FEXT common mode signal, second component of $x(n)$	-7.7	-5.84

Table 9-5: Results with d_2 = 5 kft and the considered crosstalk is Self-NEXT and Self-FEXT from x= 49 FDD-ADSL at the Remote Terminal DSLAM

Convergence over Desired frequency band	BER (without FEC)	Byte error rate (with FEC)
Off (Reference)	1.2e-1	74 %
10	5.4e-3	3.8 %
15	4e-4	0 %

Figure 9-7 illustrates as an example where the received QAM samples are for tone number 95 with no crosstalk cancellation performed and with a 15 dB crosstalk

cancellation. Figure 9-8 shows finally the corresponding adaptive filter obtained with 15 dB convergence.

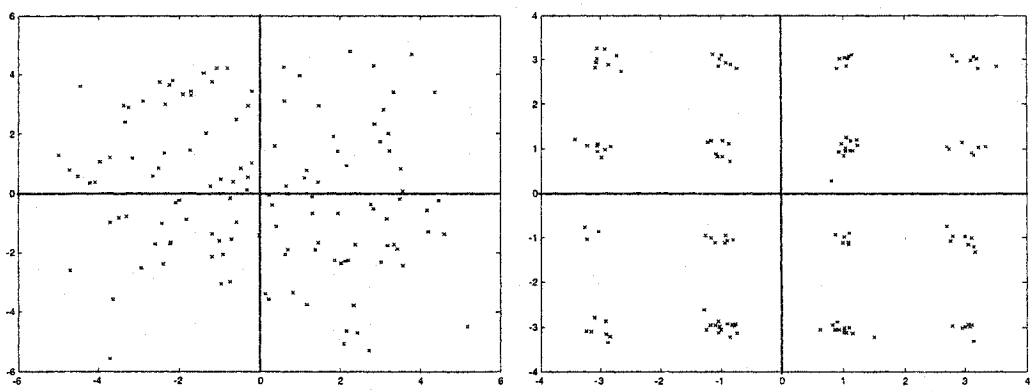

Figure 9-7: QAM data samples received for the tone number 95 (representing a constellation size of *M*=16) with the crosstalk canceller OFF (left) and the improved QAM data samples with the crosstalk canceller ON at 15 dB of convergence (right)

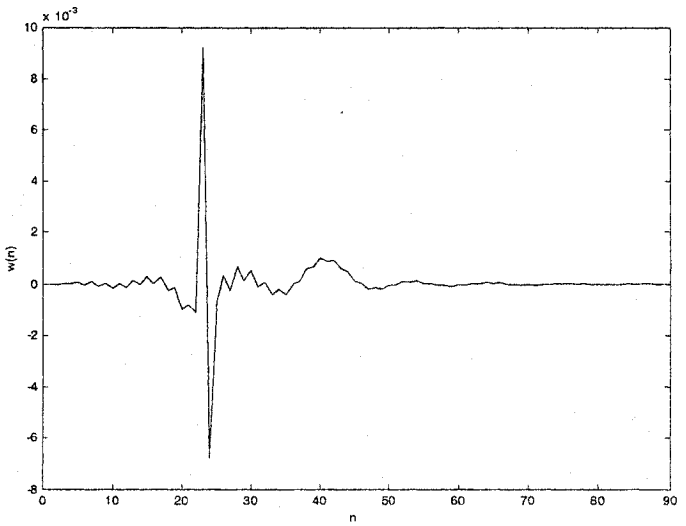

Figure 9-8: Adaptive crosstalk canceller impulse response obtained with 15 dB of convergence

The following table illustrates the crosstalk canceller performance where the number of ADSL disturbers has been reduced to 12. The power levels at the CO-served customer receiver is also shown in Table 9-7.

Table 9-6: Results with d_2 = 5 kft and the considered crosstalk is NEXT and FEXT from 12 FDD-ADSL at the Remote Terminal DSLAM

Convergence over Desired frequency band	BER (without FEC)	Byte error rate (with FEC)
Off (Reference)	5.3e-2	49 %
10	6.3e-4	0 %

Table 9-7: Power levels at CO-served customer receiver for 12 FDD-ADSL disturbers with d_2 = 5kft

Power at receiver (of the CO-served line) in dBm		
	Over frequency band of interest	Over entire frequency band
Differential useful signal, $s_{Diff}(n)$	-31.7	-31.2
NEXT differential signal, first component of $x_{Diff}(n)$	-76.2	-49.25
NEXT common mode signal, first component of $x(n)$	-30.2	-2.26
FEXT differential signal, second component of $x_{Diff}(n)$	-52.3	-48.6
FEXT common mode signal, second component of $x(n)$	-11.5	-9.56

Compared to the previous scenario where the number of FDD-ADSL disturbers was 49, this scenario with only 12 disturbers shows that the power levels of NEXT and FEXT in the frequency band of interest are lower therefore causing a lower BER and a 10 dB convergence instead of 15 dB is sufficient to bring the BER to a level where the Reed-Solomon FEC is able to correct the remaining errors.

9.4.2 Remote Terminal at d_2 = 3kft

The following case is identical to the case presented in Table 9-5, with the exception that d_2 is now 3kft instead of 5kft, which permits a comparison to see the effect of varying the location of the remote terminal.

Table 9-8: Results with d_2 = 3 kft and the considered crosstalk is Self-NEXT and Self-FEXT from x= 49 FDD-ADSL at the Remote Terminal DSLAM

Convergence over Desired frequency band	BER (without FEC)	Byte error rate (with FEC)
Off (Reference)	2.4e-1	90 %
15	2.6e-2	25 %
20	3.6e-3	2 %
25	<1e-5	0 %

Table 9-9: Power levels at CO-served customer receiver for 49 FDD-ADSL disturbers with d_2 = 3kft

	Power at receiver (of the CO-served line) in dBm	
	Over frequency band of interest	Over entire frequency band
Differential useful signal, $s_{Diff}(n)$	-31.1	-30.7
NEXT crosstalk differential signal, first component of $x_{Diff}(n)$	-68.6	-45.5
NEXT common mode signal, first component of $x(n)$	-22.4	1.43
FEXT crosstalk differential signal, second component of $x_{Diff}(n)$	-43.4	-38
FEXT common mode signal, second component of $x(n)$	-2.6	0.70

By comparing tables 9-5 and 9-8, when the remote terminal is closer to the CO-served customer, it creates a higher level of FEXT since the level of FEXT is dependent on the

distance traveled, that is a power of – 45 dBm at d_2 = 5 kft and increased to –38 dBm at d_2 = 3kft.

It should be noted that the NEXT power levels do not depend on the channel, therefore the power levels remains approximately the same over the entire frequency band (i.e. – 45.5 dBm in both cases). The level of FEXT increases inversely proportionally to the distance of the remote terminal, therefore the FEXT power level in shorter distance will cause a higher BER (i.e. a BER of 2.4e-1 at d_2=3kft as in Table 9-8 and a BER of 1.2e-1 at d_2=5kft as in Table 9-5). Also, in this case, the convergence level of the crosstalk canceller is higher than in Table 9-5 where 15 dB was sufficient; in contrast, this case requires 25 dB convergence in order to eliminate the residual errors after Reed- Solomon FEC. The same conclusions can be drawn for the case with x =12 FDD-ADSL disturbers at the remote terminal, therefore it is not presented here. The results can be found in Appendix A.

9.4.3 Remote Terminal at d_2 = 1kft

The following case is identical to the case presented in Table 9-5 and Table 9-8, with the exception that d_2 is now 1kft.

Table 9-10: Results with d_2 = 1 kft and the considered crosstalk is Self-NEXT and Self-FEXT from x=49 FDD-ADSL at the Remote Terminal DSLAM

Convergence over Desired frequency band	BER (without FEC)	Byte error rate (with FEC)
Off (Reference)	3.2e-1	97 %
20	8.6e-3	4.8 %
25	7.4e-4	0 %
30	3.3e-5	0 %

Table 9-11: Power levels at CO-served customer receiver for 49 FDD-ADSL disturbers with d_2 = 1kft

Power at receiver (of the CO-served line) in dBm		
	Over frequency band of interest	Over entire frequency band
Differential useful signal, $s_{Diff}(n)$	-31.1	-30.6
NEXT crosstalk differential signal, first component of $x_{Diff}(n)$	-68.6	-45.5
NEXT common mode signal, first component of $x(n)$	-22.3	1.5
FEXT crosstalk differential signal, second component of $x_{Diff}(n)$	-41.0	-32.2
FEXT common mode signal, second component of $x(n)$	0.07	5.3

The tendency is preserved when d_2 is reduced from 5kft to 3kft to 1 kft. The level of FEXT in differential mode is increased from – 45 dBm for the 5 kft case to -38 dBm for the 3kft case and to -32 dBm for the 1kft case. Furthermore, for the 1kft case, the

convergence level has to be increased to 30 dB as shown in Table 9-10 (25 dB is still somewhat adequate in this case as well). Appendix B shows the results obtained with d_2 = 1kft and when only 12 FDD-ADSL disturbers are present at the remote terminal where 25 dB of convergence is sufficient to eliminate the residual errors after RS-FEC.

9.5 Results for Only VDSL Type Disturbers in the Remote Terminal

Three cases will be presented where the location of the remote terminal (d_2) is located at 5 kft, 3 kft and 1 kft from the RT-served customers and the number of VDSL disturbers can be 12 or 49. Compared to FDD-ADSL disturbers located in the remote terminal, VDSL disturbers are expected to cause less problems to the ADSL reference line (CO-served line) because the PSD mask of the downstream VDSL transmission in the frequency band of 138kHz and 1.104 MHz is lower (-60dBm/Hz) than the ADSL PSD mask in the same frequency band (-38 dBm/Hz).

9.5.1 Remote Terminal at d_2 = 5kft

At d_2=5kft, with 49 VDSL disturbers located in the remote terminal, the differential FEXT level is not strong enough (-63dBm as in Table 9-13) to cause significant problems to the CO-served line. Therefore, this case is presented to show that the use of a crosstalk canceller is not required as shown in Table 9-12.

Furthermore, the NEXT differential signal caused by the upstream VDSL transmission does not overlap the desired useful downstream FDD-ADSL signal, therefore it is not expected to cause more (or less) problems than the NEXT differential signal caused by the upstream FDD-ADSL transmission since both the upstream PSD VDSL and the upstream PSD FDD-ADSL masks are approximately identical.

Table 9-12: Results with d_2 = 5 kft and the considered crosstalk is NEXT and FEXT from y=49 VDSL at the Remote Terminal DSLAM

Convergence over Desired frequency band	BER (without FEC)	Byte error rate (with FEC)
Off (Reference)	<1e-5	0 %

Table 9-13: Power levels at CO-served customer receiver for 49 VDSL disturbers with d_2 = 5kft

Power at receiver (of the CO-served line) in dBm		
	Over frequency band of interest	Over entire frequency band
Differential useful signal, $s_{Diff}(n)$	-35.8	-35.0
NEXT crosstalk differential signal, first component of $x_{Diff}(n)$	-72.6	-42.2
NEXT common mode signal, first component of $x(n)$	-27.5	4.7
FEXT crosstalk differential signal, second component of $x_{Diff}(n)$	-66.7	-63.4
FEXT common mode signal, second component of $x(n)$	-26.3	-24.6

9.5.2 Remote Terminal at d_2 = 3kft

At d_2 = 3kft, with 49 VDSL disturbers located in the remote terminal, the differential FEXT level is stronger than in the previous case.

Table 9-14: Results with d_2 = 3 kft and the considered crosstalk is NEXT and FEXT from y=49 VDSL at the Remote Terminal DSLAM

Convergence over Desired frequency band	BER (without FEC)	Byte error rate (with FEC)
Off (Reference)	2.5e-3	1.3 %
10	<1e-5	0 %

Table 9-15: Power levels at CO-served customer receiver for 49 VDSL disturbers with d_2 = 3kft

Power at receiver (of the CO-served line) in dBm		
	Over frequency band of interest	Over entire frequency band
Differential useful signal, $s_{Diff}(n)$	-35.2	-34.5
NEXT crosstalk differential signal, first component of $x_{Diff}(n)$	-70.7	-42.4
NEXT common mode signal, first component of $x(n)$	-25.5	4.5
FEXT crosstalk differential signal, second component of $x_{Diff}(n)$	-61.4	-55.7
FEXT common mode signal, second component of $x(n)$	-21.0	-17.9

Reducing the distance to 3 kft, the FEXT power level in differential mode increases and starts causing problems to the CO-served line. However, since this case was presented with 49 VDSL disturbers, this number is higher that is normally expected in the bundle. A more realistic number of VDSL disturbers in the bundle would be 12 or 24 and a fewer

number of disturbers do not cause significant problems at d_2 = 3kft. Refer to Appendix C for the scenario with only 24 VDSL disturbers.

9.5.3 Remote Terminal at d_2 = 1kft

In this case at d_2 = 1kft, with a reasonable number of disturbers, that is 12 VDSL disturbers located in the remote terminal, the differential FEXT power level is strong enough to cause problems and it is the only case presented in this section. The case with 49 VDSL disturbers can be found in Appendix D.

Table 9-16: Results with d_2 = 1 kft and the considered crosstalk is NEXT and FEXT from y=12 VDSL at the Remote Terminal DSLAM

Convergence over Desired frequency band	BER (without FEC)	Byte error rate (with FEC)
Off (Reference)	2.4e-3	0.9 %
10	<1e-5	0 %

Table 9-17: Power levels at CO-served customer receiver for 12 VDSL disturbers with d_2 = 1kft

	Power at receiver (of the CO-served line) in dBm	
	Over frequency band of interest	Over entire frequency band
Differential useful signal, $s_{Diff}(n)$	-34.4	-33.8
NEXT crosstalk differential signal, first component of $x_{Diff}(n)$	-71.8	-45.9
NEXT common mode signal, first component of $x(n)$	-26.7	0.98
FEXT crosstalk differential signal, second component of $x_{Diff}(n)$	-62.2	-53.4
FEXT common mode signal, second component of $x(n)$	-21.8	-16.6

From Table 9-16, 10dB convergence is appropriate to reduce the BER to a level where the Reed-Solomon FEC is able to correct the remaining errors. It can be noticed that the FEXT differential power level in the frequency band of interest of Table 9-17 and Table 9-15, are approximately the same. Table 9-14 had 49 disturbers at d_2 =3kft and Table 9-16 had 12 disturbers at d_2 = 1kft. Those two scenarios had approximately the same BER prior to cancellation.

9.6 Results for Both ADSL and VDSL Disturbers in the Remote Terminal

Only the case where the location of the remote terminal (d_2) is located at 1 kft from the RT-served customers and the number of disturbers is 24 FDD-ADSL and 24 VDSL was considered. This case is presented to illustrate the worst-case situation (distance-wise) causing a strong differential FEXT signal.

Table 9-18: Results with d_2 = 1 kft and the considered crosstalk is NEXT and FEXT from x=24 VDSL and y=24 ADSL at the Remote Terminal DSLAM

Convergence over Desired frequency band	BER (without FEC)	Byte error rate (with FEC)
Off (Reference)	2.7e-1	96 %
20	4.2e-3	2.4 %
25	4.1e-4	0 %

Table 9-19: Power levels at CO-served customer receiver for 24 VDSL and 24 ADSL disturbers with d_2 = 1kft

	Power at receiver (of the CO-served line) in dBm	
	Over frequency band of interest	Over entire frequency band
Differential useful signal, $s_{Diff}(n)$	-32.2	-31.7
NEXT crosstalk differential signal, first component of $x_{Diff}(n)$	-61.6	-42.5
NEXT common mode differential signal, first component of $x(n)$	-15.8	4.4
FEXT crosstalk differential signal, second component of $x_{Diff}(n)$	-43.1	-35.1
FEXT common mode differential signal, second component of $x(n)$	-1.4	-3.4

The reference BER of Table 9-18 is lower than the reference BER of Table 9-10. This is because the 24 VDSL disturbers have a lower level downstream PSD mask than the corresponding downstream ADSL disturbers. It can be concluded that the worst case is when only ADSL disturbers are located in the remote terminal.

Chapter 10

Conclusion

10.1 Primary Conclusion

When shorter lines deployed from the Fiber to the Cabinet (referred also in this thesis as CO-RT architecture) are combined with longer lines in the same bundle, the crosstalk impairments can become severe for the long lines deployed from the Central Office (CO-served lines).

In this thesis, an adaptive wideband crosstalk canceller using the common mode signal as an input reference was proposed to reduce the crosstalk in the desired differential signal of a CO-served line and was simulated for an FDD-ADSL link. The goal of the canceller is to produce an output that closely resembles the differential crosstalk signal originating from the shorter lines (i.e. serviced by the remote terminal) that corrupted the desired differential signal. The proposed crosstalk canceller was simulated for FDD-ADSL with a CO-RT architecture, but it is not limited to this specific implementation of ADSL on the CO-served line. The simulations show that the technique is beneficial to the differential signal quality, and consequently the error rates were lowered which translates into the possibility of having DSL services deployed from a Remote Terminal sharing the same bundle as the lines carrying DSL services deployed from the Central Office.

10.2 Secondary Conclusions

For the considered architecture, having a long line deployed from the central office sharing a bundle with shorter lines deployed from a remote terminal, the downstream

signals transmitted from the remote terminal will cause severe interference to the attenuated signal of CO-served customer's receiver. By varying the distance of the remote terminal, that is the length of the lines deployed from the remote terminal, the significant power level of the FEXT differential signal originating from the remote terminal transmitters causes potentially severe interference problems. Since the power level of the FEXT is inversely proportional to the distance between the remote terminal and the customer, then the severity of the interference is increased as this distance decreases. ADSL disturbers deployed from the remote terminal cause much more FEXT problems than VDSL disturbers. Therefore, the crosstalk canceller is more valuable in the case where ADSL is deployed from the remote terminal as opposed to VDSL. It was shown through simulations that the crosstalk canceller was able to reduce the BER, which allows the coexistence of CO-served lines and RT-served lines in the same bundle.

The addition of a crosstalk canceller module to a practical implementation requires an additional training period on top of the current required training period for the equalizers in the ADSL standard. It is assumed that the training period should fall within the time reserved for training the channel equalizers. To avoid modifying the standard, the time required to adapt the crosstalk canceller must be kept very short. Three distinct algorithms have been compared in terms of convergence speed and complexity to determine the adequacy of each for the task of crosstalk cancellation in ADSL. The simulations show that all three adaptive algorithms used were able to achieve 15 dB convergence over the frequency band of interest in less than 0.2 seconds. It is interesting to note that the total time available to train the channel equalizers is typically 8 seconds, therefore training the crosstalk canceller to an adequate convergence level (15-25dB) does not seem to be an important constraint. Thus, since the required training time for the crosstalk canceller using all three algorithms is not significant, the NLMS algorithm seems to be the most suitable because of its low complexity.

In the case of ADSL or VDSL disturbers, NEXT and FEXT have different power distributions in the frequency domain. The convergence of the crosstalk canceller is

constrained by the respective power ratio of each crosstalk source at individual frequencies. The crosstalk canceller will converge in the frequency domain to a level defined by the ratio of the PSDs of both crosstalk sources at each particular frequency.

Also, the delay in the general structure of the adaptive crosstalk canceller is mainly required to compensate for the lag between the FEXT common signal and the FEXT differential signal from the remote terminal. Heuristically, the delay should be around 10-15 samples per kilo feet (i.e. proportional to the length of the RT-served lines) to be sufficient for the propagation delay difference.

10.3 Future Work

Since the crosstalk canceller is able to reduce the crosstalk level in the useful differential signal, it thus seems to be an interesting option to mitigate crosstalk problems in practical implementations of future generations of DSL, improving the number of data services supported by a bundle, extended loop reach or increased data rates.

As the next step, experimental measurements of the common mode signals (i.e. common mode coherence with differential mode, crosstalk levels, group delay differences) should be performed to validate the performance of the proposed canceller.

The performance of the crosstalk canceller could be evaluated with other types of DSL technologies, namely echo cancelled technologies instead of frequency division duplexed technologies, and wider bandwidth technologies (such as VDSL).

In a non-stationary environment, as might be expected in practice, the crosstalk canceller filter solution would have to change over time. The efficiency of the crosstalk canceller could be analyzed if it is permitted to adapt continuously as opposed to a static solution. In the case of continuous adaptation, it would be primordial that the algorithms be

compared for stability. The robustness of the algorithms to quantization effects should also be evaluated.

Appendix A: Results for d_2 = 3 kft, x=12

Simulation results with d_2 = 3 kft and the considered crosstalk is Self-NEXT and Self-FEXT from x=12 FDD-ADSL at the Remote Terminal DSLAM

Convergence over Desired frequency band	BER (without FEC)	Byte error rate (with FEC)
Off (Reference)	1.6e-1	82 %
10	1.9e-2	20 %
15	3e-3	1.4 %
20	1.3e-4	0 %

Power at receiver (of the CO-served line) in dBm		
	Frequency band of interest	Entire frequency band
Differential useful signal, $s_{Diff}(n)$	-31.3	-30.9
NEXT crosstalk differential signal, first component of $x_{Diff}(n)$	-74.1	-49.1
NEXT common mode signal, first component of $x(n)$	-27.97	-2.13
FEXT crosstalk differential signal, second component of $x_{Diff}(n)$	-46.89	-41.2
FEXT common mode signal, second component of $x(n)$	-6.11	-2.87

Appendix B: Results for d_2 = 1 kft, x=12

Simulation results with d_2 = 1 kft and the considered crosstalk is Self-NEXT and Self-FEXT from x=12 FDD-ADSL at the Remote Terminal DSLAM

Convergence over Desired frequency band	BER (without FEC)	Byte error rate (with FEC)
Off (Reference)	2.1e-1	89 %
20	2.2e-3	0.4 %
25	1e-4	0 %

Power at receiver (of the CO-served line) in dBm		
	Frequency band of interest	Entire frequency band
Differential useful signal, $s_{Diff}(n)$	-31.1	-30.6
NEXT crosstalk differential signal, first component of $x_{Diff}(n)$	-72.6	-49.1
NEXT common mode signal, first component of $x(n)$	-26.4	-2.2
FEXT crosstalk differential signal, second component of $x_{Diff}(n)$	-44.8	-35.9
FEXT common mode signal, second component of $x(n)$	-3.7	1.53

Appendix C: Results for d_2 = 3 kft, y=24

Simulation results with d_2 = 3 kft and the considered crosstalk is NEXT and FEXT from y=24 VDSL at the Remote Terminal DSLAM

Convergence over Desired frequency band	BER (without FEC)	Byte error rate (with FEC)
Off (Reference)	2e-4	0 %
10	<1e-5	0 %

Power at receiver (of the CO-served line) in dBm		
	Over frequency band of interest	Over entire frequency band
Differential useful signal, $s_{Diff}(n)$	-34.9	-34.2
NEXT crosstalk differential signal, first component of $x_{Diff}(n)$	-71.1	-44.2
NEXT common mode signal, first component of $x(n)$	-25.8	2.7
FEXT crosstalk differential signal, second component of $x_{Diff}(n)$	-63.2	-57.6
FEXT common mode signal, second component of $x(n)$	-22.8	-19.8

Appendix D: Results for d_2 = 1 kft, y=49

Simulation results with d_2 = 1 kft and the considered crosstalk is NEXT and FEXT from y=49 VDSL at the Remote Terminal DSLAM

Convergence over Desired frequency band	BER (without FEC)	Byte error rate (with FEC)
Off (Reference)	1.7e-2	25 %
10	7.4e-5	0 %

Power at receiver (of the CO-served line) in dBm		
	Over frequency band of interest	Over entire frequency band
Differential useful signal, $s_{Diff}(n)$	-34.4	-33.8
NEXT crosstalk differential signal, first component of $x_{Diff}(n)$	-68.2	-42.2
NEXT common mode signal, first component of $x(n)$	-22.9	4.7
FEXT crosstalk differential signal, second component of $x_{Diff}(n)$	-58.9	-49.8
FEXT common mode signal, second component of $x(n)$	-18.3	-12.9

References

[BIN00] John A. C. Bingham, *ADSL, VDSL, and Multicarrier Modulation,* Wiley Series in Telecommunications and Signal Processing, 2000

[BOU03] Martin Bouchard, "Multichannel Affine and Fast Affine Projection Algorithms for Active Noise Control and Acoustic Equalization Systems", *IEEE Transactions on Speech and Audio Processing*, Vol. 11, No. 1, January 2003, pp. 54 - 60

[BRO03] Jim Brown and Bill Whitlock, "Common-Mode to Differential-Mode Conversion in Shielded Twisted pair Cables (Shield-Current-Induced Noise)", *Audio Engineering Society*, Convention Paper 5747, March 2003

[CIO91] John M. Cioffi, "A Multicarrier Primer", *ANSI Contribution TIE1.4/91-157*, November 1991

[COM98] Richard Combellack, "Improving Range and Bandwidth of Telco Loop Plant", Proceedings of the *International Wire and Cable Symposium*, 1998, pp. 176 - 183

[COO93] J. W. Cook, "Wideband Impulsive Noise Survey of the Access Network", *BT Technology Journal*, Vol. 11, No. 3, July 1993, pp. 155 - 162

[CRT02] "Technical and Deployment Issues and Solutions Regarding Access to Sub-loops at Remotes", CRTC Industry Steering Committee (CISC), Network Working Group, March 28, 2002

[CAM99] Jorge Campello, "Practical Bit Loading for DMT ", *IEEE International Conference On Communications*, Vancouver, Canada, 1999, pp. 801 – 805

[CHE92] David K. Cheng, *Field and Wave Electromagnetics*, Second Edition, Addison-Wesley, November 1992

[FEN99] D. K. Fenton, "Digital Noise Cancellation for xDSL", Master's Thesis, Ottawa University, School of Information Technology and Engineering, August 1999

[FER97] Dennis Ferguson, Ravi Cherukuri, "Self-Synchronous Scramblers for PPP Over Sonet/SDH: Some Analysis", *PPP Extensions Working Group*, November 1997

[GAL02] Stefano Galli, Kenneth J. Kerpez, "Methods of Summing Crosstalk from Mixed Sources – Part I: Theoretical Analysis", *IEEE Transactions on Communications*, Vol. 50, No. 3, March 2002, pp 453 - 461

[GAY00] Steven L. Gaa, Jacob Benesty, *Acoustic Signal Processing for Telecommunication*, Kluwer International Series in Engineering and Computer Science, 2000

[GAL01] Stefano Galli, Graig Valenti, "A Frequency-Domain Approach to Crosstalk Identification in xDSL Systems", *IEEE Journal on Selected Areas in Communications*, Vol. 19, No. 8, August 2001, pp. 1497 - 1506

[GIN02] George Ginis, John M. Cioffi, "Vectored Transmission for Digital Susbcriber Line Systems", *IEEE Journal on Selected Areas in Communications*, Vol. 20, No. 5, June 2002, pp. 1085 – 1094

[HAY94] Simon Haykin, *Communication Systems*, Third Edition, Wiley, 1994

[HAY02] Simon Haykin, *Adaptive Filter Theory*, Fourth Edition, Prentice-Hall, 2002

[ITU99] "ITU-T Recommendation G.992.1", ITU-T ADSL metallic interface standard, June 1999

[ITU02] "ITU-T Recommendation G.996.1", Test procedures for digital subscriber line (DSL) transceivers, February 2002

[ITU03] "ITU-T Recommendation", ITU-T Very-high-bit-rate Digital Subscriber Line (VDSL) Metallic Interface, *T1E1.4/2003-210R2*, Montreal, Canada, August 2003

[JAC99] Krista S. Jacobsen, "VDSL: The Next Step in the DSL Progression", Texas Instruments, Broadband Access Group, San Jose, CA, August 1999

[KER93] K. J. Kerpez, "Near End Crosstalk is Almost Gaussian", *IEEE Transactions in Communications*, Vol. 41, May 1993, pp. 670 - 672

[KER02a] Kenneth J. Kerpez, Stefano Galli, "Methods of Summing Crosstalk from Mixed Sources – Part II: Performance Results", *IEEE Transactions on Communications*, Vol. 50, No. 4, April 2002, pp. 600 - 607

[KER02b] K. Kerpez, J. Cioffi, S.T. Chung, J. Lee, W. Yu, "Response to 2001-273R1 using Telcordia DSL Analysis", *T1E1.4/2002-063*, February 2002

[KOU99] S. Kourtis, "Optimum bit allocation algorithm fro DMT-based systems under minimum transmitted power constraints", *Electronics Letters*, December 9th 1999, Vol. 35 No. 25, pp. 2181 - 2182

[LAO02] Richard Lao, "The Twisted pair Telephone Transmission Line", *High Frequency Electronics*, November 2002, pp. 20 - 30

[LEF00] Pierre D. Lefebvre, "Adaptive Multiple Sub-band Common Mode RFI Suppression", Master's Thesis, Ottawa University, School of Information Technology and Engineering, April 2000

[LEO94] Alberto Leon-Garcia, *Probability and Random Processes for Electrical Engineering,* Second Edition, Addison Wesley, 1994

[PRO88] John G. Proakis and Dimitris G. Manolakis, *Introduction to Digital Signal Processing,* Macmillan, 1988

[PRO01] John G. Proakis, *Digital Communications,* Fourth Edition, McGraw Hill, 2001

[RIC03] Keith Richardson, "DSL Deployment From Remotes", RTC INC, *Ref. # NTTF008*, February 11, 2003

[SHE03] Jim Sherwin, "Understanding common-mode signals", *Electronic Design News Magazine* (*EDN*), April 17, 2003

[SML01] "Spectrum Management for Loop Transmission Systems", ANSI Standard T1.417-2001, January 2001.

[SON02] Kee Bong Song and Seong Taek Chung, George Ginis, John M. Cioffi, "Dynamic Spectrum Management for Next-Generation DSL Systems", *IEEE Communications Magazine*, October 2002, pp. 101 – 109

[SONG02] Ranjan Sonalkar, "Bit and Power Allocation Algorithm for Symmetric Operation of DMT-Based DSL Modems", *IEEE Transactions on Communications*, Vol. 50, No. 6, June 2002, pp. 902- 906

[STA02] Thomas Starr, Massimo Sorbara, John M. Cioffi and Peter J. Silverman, *DSL Advances*, Prentice Hall, December, 2002

[STA99] Thomas Starr, John M. Cioffi and Peter J Silverman, *Understanding Digital Subscriber Line Technology*, Prentice Hall, December 1998

[TRE01] John R. Treichler, C. Richard Johnson, Jr. and Michael G. Larimore, *Theory and Design of Adaptive Filters,* Prentice Hall, 2001

[TSA01] M. Tsatsanis, I. Kanellakopoulos, J. Cioffi, "Identification of crosstalk couplings using MIB-reported data", *T1E1.4/2001-278*, Greensboro, NC, November 5, 2001

[VAL97] C. Valenti, "Cable Crosstalk Parameters and Models", *ANSI Contribution T1E1.4/97-302*, Bellcore, Minneapolis, MN, September 1997

[WID85] Bernard Widrow and Samuel D. Stearns, *Adaptive Signal Processing*, Prentice Hall, 1985

[YEA03] T.H. Yeap, D.K. Fenton and P.D. Lefebvre, "A novel common mode noise cancellation technique for VDSL applications", *IEEE Transactions on Instrumentation and Measurement*, Vol. 52, August 2003, pp. 1325 -1334

[YEA] T. H. Yeap and P. Lefebvre, "Adaptive Multiple-Subband Common-mode RFI Suppression", U.S. Patent Number 6052420

[YU01] Wei Yu, George Ginis and John M. Cioffi, " An Adaptive Multiuser Power Control Algorithm for VDSL", *Proceedings of IEEE Globecom 2001*, Vol. 1, San Antonio, TX, pp. 394-398, November 2001, pp. 394 - 398

[ZEN02] Chaohuang Zeng and John M. Cioffi, "Near-End Crosstalk Mitigation in ADSL Systems", *IEEE Journal on Selected Areas in Communications*, Vol. 20, No. 5, June 2002, pp. 949 - 958

[ZHA01] L. Zhang, A. Yongacoglu, "Turbo Coding in ADSL DMT Systems", *International Conference on Communications* (*ICC2001*), Helsinki, Finland, June 2001